ABSTRACT

Title of Document:	SMALL-SCALE TESTING TO STUDY MITIGATION OF ACCELERATION ON SIMULATED VEHICLES
	Jarrod Mark Bonsmann, Ph.D., 2013
Directed By:	Professor William Fourney, Department of Mechanical Engineering

This dissertation investigates various means for mitigating acceleration experienced

by passengers on vehicles subjected to blast loading. In order to complete this study,

small-scale testing of simulated vehicles was used. The explosives designated for this

research are exclusively buried in saturated sand, which will act as the loading media

for the simulated vehicles. In addition to explosive testing, various tests were

performed dynamically using a high-pressure gas gun. Initially, tests were performed

to better understand the effects of vehicle mass and stand-off distance on vehicle

acceleration due to blast loads; after which, studies were conducted to mitigate the

acceleration. Test plates used in this study vary in both size and geometry. When

necessary, simple plate geometries are employed to investigate various mitigation

parameters. Ultimately, much of the testing was conducted on simplified scaled

versions of vehicles likely to be subjected to attack. This paper focuses mainly on

mitigation through crushing of thin-walled cylinders, but also investigates the

advantages of applying polymeric coatings to dynamically loaded structures. Piezoelectric accelerometers are used in conjunction with high speed videography to collect test data. In addition to acceleration, impulse and kinetic energy of each test plate is examined. This research, though funded by the US Army, will be of use to all branches of the armed forces utilizing Mine-Resistant Ambush-Protected vehicles. The ultimate goal of this research is to help create a vehicle that will increase the probability that the passengers will survive a blast event with minimal long-term damage to the brain.

SMALL-SCALE TESTING TO STUDY MITIGATION OF ACCELERATION ON
SIMULATED VEHICLES

By

Jarrod Mark Bonsmann

Dissertation submitted to the Faculty of the Graduate School of the
University of Maryland, College Park, in partial fulfillment
of the requirements for the degree of
Doctor of Philosophy
2013

Advisory Committee:
Professor William Fourney, Chair
Professor Amr Baz
Professor Hugh Bruck
Professor Teng Li
Professor Charles Schwartz

Dedication

This work is dedicated to my parents: David Bonsmann – for instilling in me an unfailing work ethic and insisting impossible wasn't a word to be found in my personal dictionary, and Phyllis Bonsmann – for teaching me humility should coexist with my dad's message.

Acknowledgements

Primarily, I would like to give my deep and many thanks to my advisor and mentor Professor William L. Fourney. His personal brand of genius along with his unwavering support constantly challenged me to make my work better, and I literally could not have done it without him.

I would also express much gratitude to the members of the committee: Professor Amr Baz, Professor Hugh Bruck, Professor Teng Li, and Professor Charles Schwartz. Again, their input and support has made this possible.

I would like to take a few words to thank Dr. Uli Leiste and Leslie Taylor for their expert help day in and day out working in the Dynamic Effects Lab. Their massive amounts of knowledge helped pave the way for my research.

Additionally, I am eternally grateful to the Luthor Davis, my high school physics professor, who is 100% responsible for instilling in me the love of science. Also thanks are due to Dr. Peter Ifju, who filled that mentorship role during my stay at the University of Florida. Not only did these two brilliant educators develop me into the student that I am today, but they were role models in how to work hard while having fun, a skill which I highly value to this very day.

Finally, I would like to thank the undergraduate research team without whose tireless labor and assistance in test preparation this work would not have been possible – Tyler Duff, Max Kinsey, Zac Plitt, and Brad Weber.

Table of Contents

List of Tables

List of Figures

viii

x

Chapter 1 - Introduction

1.1 Introduction

Over the past decade, the increase in fatalities due to use of buried explosives has created a demand for expanded knowledge in the field of target response to blast loading. When a vehicle experiences a blast load from a buried explosive, it is speculated that the damage mechanisms for a passenger in the vehicle result from rapid accelerations [1] and large changes in momentum [2]. Blast loading results in traumatic brain injury (TBI) and violent injuries such as broken limbs due to rapid accelerations and large changes in momentum respectively. In recent years a growing number of people involved in buried explosive attacks have been diagnosed with TBI in what is speculated to have resulted from the rapid acceleration of the targeted vehicle. This research aims to help design vehicles that will minimize the amount of damage to a passenger traveling in a vehicle that undergoes explosive loading.

In order to accomplish the goals of the research, the primary experimental testing technique employed is small-scale explosive testing. This testing method is used to investigate means of acceleration mitigation including tube buckling and, in more depth, crushing of thin-walled cylinders. A number of geometric properties of thin-walled cylinders, such as height, wall thickness and outer diameter are all studied. In addition to geometric properties, the number of cylinders and to a minor degree, the cylinder material is also studied. The majority of the aforementioned tests were conducted on plates fabricated to be simplified scaled down versions of vehicles likely to undergo blast scenarios.

On top of using explosive testing to study mitigation properties of buckling tubes and crushing of thin-walled cylinders, the mitigation properties of polymeric coatings of structures are also examined. Steel and aluminum bars coated with polyurea were tested dynamically using a pressurized gas gun to determine the effect of increasing the thickness of polymeric coatings on acceleration. Thin-walled cylinders were also coated in polyurea and crushed by explosively loaded plates to determine the benefits of adding polyurea to the previously tested mitigation technique.

At the conclusion of the research it was determined that there are great benefits to using thin-walled cylinders to mitigate the acceleration of a passenger travelling in an explosively loaded vehicle. In addition to this, polymeric coatings were determined to be of use in the crushing of thin-walled cylinders and coated beams but the effects depend greatly on the amount of polyurea applied to the metallic structure. Finally, other areas of interest that might have an effect on vehicle acceleration, such as hull flexibility, were identified for further research.

1.2 Background

In answer to the demand for knowledge pertaining to vehicle response under blast loading, the Dynamic Effects Lab at the University of Maryland has spent much time and many resources investigating this event. Research has been conducted to better understand the mechanisms of the vehicle loading [3] and to determine various methods of reducing impulse and acceleration on these structures [4, 5]. The main mechanism of the vehicle loading for a buried charge is the impact on the vehicle bottom by the soil that is thrown up by the detonated charge. This soil has been

shown to be traveling in excess of Mach one, and when it is brought to rest on the bottom of the vehicle very large pressures develop [6].

As a result of the increased understanding of vehicle response to blast loading, the number of injuries and deaths as a consequence of buried explosive attacks has steeply declined as seen in Figure 1.1 [7]. The most important development in vehicle design has been the utilization of Mine-Resistant Ambush-Protected vehicles which have angled bottoms that deflect the ejected soil in a sidewise direction as seen in Figure 1.2.
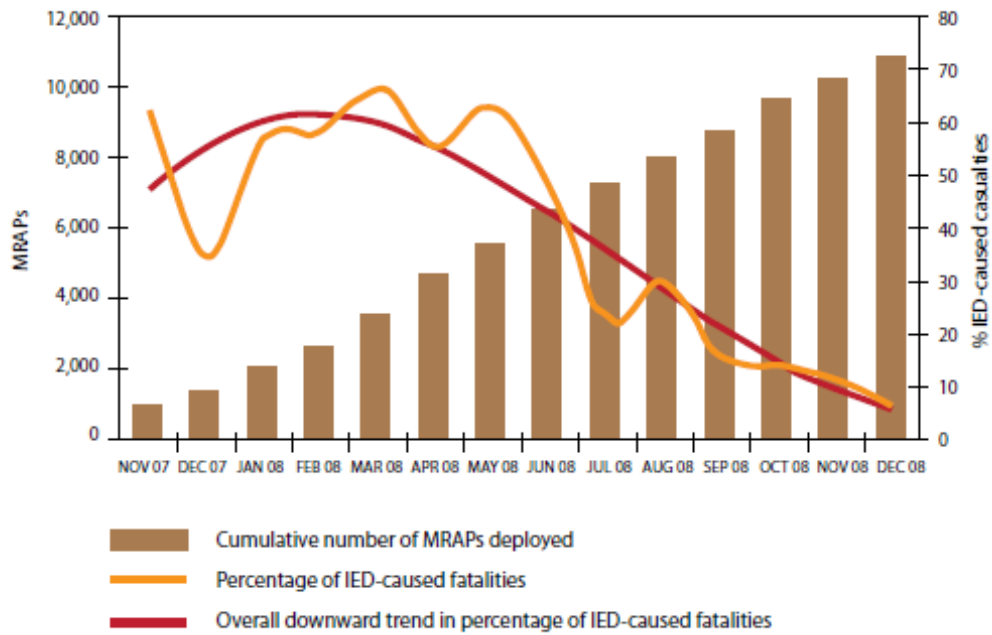
Figure 1.1: MRAPs deployed in the field versus IED casualties

Figure 1.2: Example of a V-Shaped bottom as tested by the Dynamic Effects Lab [6]

By shaping the bottom of the blast loaded vehicles, violent injuries and deaths due to the change in the impulse have steeply declined. However, since the passenger of the vehicle is surviving beyond the initial blast, the incidences of TBI have risen. For this reason, further knowledge is needed in the area of acceleration mitigation on blast loaded vehicles.

The studies mentioned above place a good deal of emphasis on blast mitigation due to vehicle shaping. One of the primary focuses in this paper is to study the acceleration mitigation effects of localized buckling (crushing) of thin-walled cylinders. Thin-walled cylinders have long been studied in the field of energy absorption. There exists a plethora of research detailing the benefits of adding tubes to structures to absorb impact energy. For lower speed impacts both Alghamdi and Yuen et al. give an overview of a multitude of collapsible structures for use as energy

absorbers [8, 9]. A number of studies have been performed characterizing the benefits of crushing tubes laterally for impact protection [10, 11]. Quite a few studies have been conducted to classify the energy absorption of composite tubes [12, 13, 14]. Additionally there have even been some studies, both numerical and experimental, where tubes or thin-walled structures of multiple geometries made of various materials (both metallic and composite) have been studied for use as sacrificial claddings for structures that undergo blast loading [15, 16, 17]. All of this research points to the fact that thin-walled structures, in a variety of geometrical patterns made of all kinds of materials, have numerous benefits to offer when it comes to protecting structures from blast loads. There is a dearth of information, however, involving the benefits of using thin-walled cylinders as a technique for mitigating acceleration.

Much effort has been spent [18, 19] in researching the mechanical behavior of polymeric materials used for coatings in blast applications, especially the material polyurea. It has been found that under very high strain rates the polymer loses its "rubbery" mechanical behavior and begins acting more like leather. This characteristic allows the polymer to increase toughness under high strain rates, making it more effective at absorbing blast loads. In addition to characterizing the high strain rate mechanical properties of polyurea, the polymeric coating has been applied to panels that undergo blast loading in order to determine what benefits it has as a protective layer to prevent deformation and damage to structures. Major benefits in protection of structures due to polymeric or elastomeric coatings have been found when applied to composite structures [20]. On the contrary, when applied to steel

plates, keeping the areal density constant, it was found that plain steel plates absorb the blast more efficiently than those coated with polyurea [21]. Finally, some preliminary work has been performed in previous years in the Dynamic Effects Lab that shows that coating the hull of a vehicle that undergoes blast loading is an effective means for acceleration mitigation, though it should be noted that the areal density of the plate was not kept constant in this study [22].

1.3 Small-Scale Testing

The testing facilities at the University of Maryland are equipped to perform small-scale explosive testing. Small-scale testing has a number of advantages over large-scale testing, costing less in both time and money to perform. In addition to these advantages, it has been shown [23, 24] that small-scale testing can accurately represent the response of a target to an explosion.

Figure 1.3 shows a comparison of results from small-scale tests and results obtained in full-scale tests at the Army Research Lab (ARL) in Aberdeen, Md. The full-scale testing used 2.27 to 4.54 kilogram TNT charges with a variety of depths of burial and stand-off distances while the small-scale testing used a maximum charge size of 3.3 grams of explosive. Tests 1 and Test 6 were a repeat of one another as were 4 and 4a. The full-scale tests as well as the small-scale tests were very repeatable. At the Dynamic Effects Lab the results were scaled up to the full-scale charge sizes and show very good agreement.
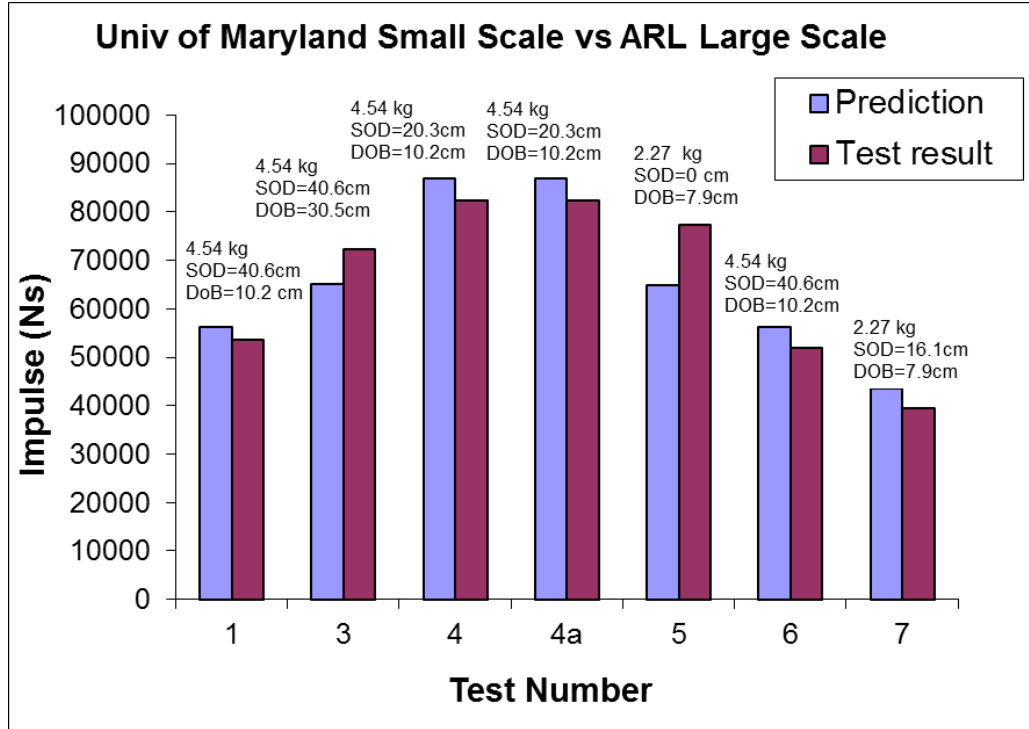
Figure 1.3: Comparison of full-scale and small-scale test results [3]

The scaling factor is determined by taking the cubed root of the ratio of the full-scale mass of the explosive over the small-scale mass of the explosive.

$$SF = \left(\frac{mass_{full-scale}}{mass_{small-scale}}\right)^{\frac{1}{3}}$$

In this work a geometry that will scale to 4.536 kilograms of explosive was used. In the majority of the research in this thesis, the small-scale tests use an explosive mass of 4.4 grams, resulting in a scaling factor of approximately ten. All length and time scales are scaled using this scale factor. The small-scale lengths and times are determined by dividing the full-scale values by this factor while the small-scale accelerations are determined by multiplying the full-scale values by this factor.

Chapter 2 - Experimental Set-Up

2.1 Test Equipment

In order to perform a successful explosive experiment, a wide array of equipment is needed. Instrumentation to obtain measurements of acceleration, displacement, and time are all required to generate the data necessary for proper analysis. On top of that, equipment is needed for the blasting itself. In addition to the blasting apparatus, equipment necessary for conducting dynamic testing using a pressurized gas gun is also required.

2.1.1 Data Acquisition Equipment

The accelerometers used in this research are manufactured by PCB Piezotronics Inc. The specific model chosen is 350B04 with a measurement range of ±5000g's. Each accelerometer is capable of producing 10000 samples per second. In certain tests where the acceleration levels were too high to read in the linear portion of the ±5000g range, the 350C02 model with a range of ±50000g's was used. This accelerometer is also capable of producing 10000 samples per second [25]. Each accelerometer is capable of being threaded directly into the test plates as seen in Figure 2.1.

Figure 2.1: Accelerometers used for dynamic testing. Note the 50000g accelerometer (left) has the cable integrated into the system and the 5000g accelerometer (right) does not. The upper scale is in inches.

To acquire a meaningful acceleration signal a PCB Piezotronics Inc. signal conditioner, model 483A, is employed. This piece of equipment supplies the proper excitation power for the PCB accelerometers and helps prepare the signal for recording. Each accelerometer is hardwired to a specific channel in the signal conditioner. Similarly each channel from the signal conditioner is then split and connected to a channel in one of two oscilloscopes manufactured by LeCroy, model numbers 9314AM and 9315AM, which are employed for data acquisition. Each scope is set to record anywhere from one mega-sample per second to five mega-samples per second, which is far above the production capacity of the accelerometers. In addition to setting the recording speed, each scope can be set to record a specific voltage range. Before each test, the voltage range corresponding to the acceleration level expected from each test was set in each scope, often with a couple of channels in one scope designated as safety channels to capture the reading if it turned out to be higher

than expected. Two scopes will be used for the purpose of ensuring that data is collected for each test, although only the data from one scope will be used. This is done to prevent loss of data due to improper scope settings or malfunction. The signal conditioner along with the oscilloscopes can be seen in **Error! Reference ource not found.** and Figure 2.2.

Figure 2.2: Front of the PCB signal conditioner

Figure 2.3: LeCroy oscilloscopes used for data acquisition

For obtaining displacement and time data from the blast tests, a Phantom v12.1 high speed camera equipped with a Tamron 28-75mm variable focus lens was used. Each camera was set on a standard tripod to help adjust the distance from the target to most accurately capture the test event. The v12.1 is rated to capture up to one million frames per second at reduced resolution and has its highest resolution of 1280 x 800 pixels. The resolution is adjusted before each test to obtain the best picture coupled with the highest recording speed possible for the blast testing. For every test it is necessary to attach the high speed camera to a laptop computer. The laptop computer must have the Phantom software installed on it to adjust camera resolution, frame rate, exposure, and trigger settings. The connection is made through an Ethernet cable. A picture of the Phantom v12.1 camera with the Tamron lens can be seen in Figure 2.4.

Figure 2.4: Phantom v12.1 on the tripod

Once collected, the data from the accelerometers and high speed camera can be processed and analyzed using two separate programs. For the accelerometer signal, the UERD Tools program developed by NSWC – Carderock Division was used for the analysis. This program interface allows the user to perform common mathematical functions on the signal as well as obtain the Fourier Spectra and filter specific frequencies out of the original signal.

To obtain useful information from the high speed camera video, the Phantom Camera Control program supplied with the camera is used. This program allows the user to collect points and writes the displacement in two dimensions of a given point and the corresponding time to a report file. This file can then be opened in Excel for further analysis.

2.1.2 Blast Testing Equipment

To create the blast, plastic explosive sheet (Deta Sheet from Omni Explosives) was used in conjunction with an Exploding Bridge Wire (EBW) Detonator manufactured by Teledyne RISI. The Deta sheet plastic explosive contains 63% of the high explosive PETN and the remaining 37% of the weight consists of plasticizer. The detonator used (RP-501 EBW) contains 227 milligrams of RDX and 136 milligrams of PETN high explosive that, when combined with the plastic Deta sheet, sums to the total explosive weight that will be reported for each test. A schematic of the detonator can be seen in Figure 2.5.

RP-501 Explosive Train

0.295" Dia. Max.

5.5" — 0.825" Max.

1. Plastic molded head
2. Bridgewire (Gold)
3. Aluminum cup 0.007" thick
4. Initiating explosive: 136 mg PETN
5. Output explosive: 227 mg RDX with binder
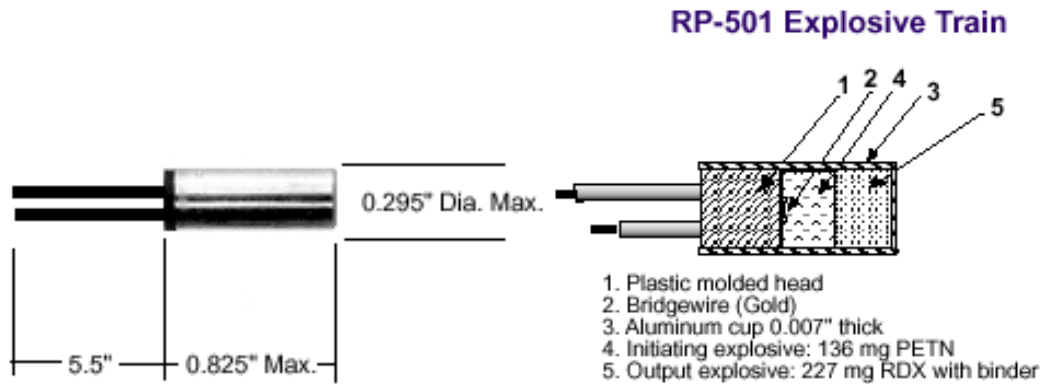
Figure 2.5: External (left) and internal (right) schematic of the RP-501 EBW Detonator [26]

The plastic explosive charge is formed and placed in a delrin plastic sleeve to ensure repeatability in charge geometry from test to test. An epoxy is used to hold the detonator (pressed one-third of its length into the deta sheet cylinder) in place during charge burial. Thin wooden rods are attached to the outer edge of the plastic casing which ensures the charge remains at a fixed depth throughout the test set-up process. For a visual of the final charge set-up refer to Figure 2.6. Two charge sizes were used throughout the course of this research. The dimensions of each charge casing can be seen in Table 2-1.
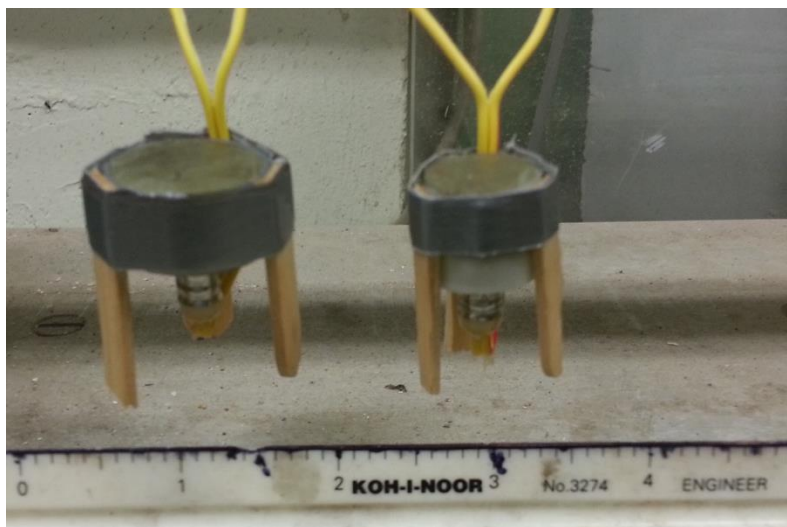
Figure 2.6: The final form of a 4.4g (left) and a 2.2g (right) charge

13

Table 2-1: Dimensions of cylindrical charges

Charge Mass (g)	Outer Diameter (mm)	Wall Thickness (mm)	Height (mm)
4.4	25.4	0.75	12.6
2.2	17.7	0.75	15.3

To detonate the detonator/charge system, the FS-17 firing system, manufactured by Reynolds Industries Incorporated and seen in Figure 2.7, is used. This module has an internal battery and electronics which are capable of delivering a 4000 volt charge to the detonator. This firing system is connected to the charge, high speed camera, and oscilloscopes so that when the firing system is discharged each of the recording devices trigger, recording the explosive event simultaneously.

Figure 2.7: FS-17 Firing Module by Reynolds Industries Inc.

The actual test takes place in a steel tank constructed to outer dimensions of 1.5 meters long by 1.5 meters wide by 0.6 meters deep. At the bottom of the tank, a pipe is fitted which connects to a water cylinder that is filled to add water to the tank. The bottom portion of the tank is layered with rocks covered by a very fine mesh net

which allows the water to saturate the bed but keeps the sand out of the water pipe. On top of the mesh net sits the sand in which the charge is buried.

Above the test bed, a high strength net is hung to ensure the plate, with the attached accelerometers, does not fly up and hit the ceiling or out of the test bed. Also above the test bed, four chains are hung from the ceiling. Each chain is fitted with a double turn-buckle eye-hook. The chain height is able to be roughly adjusted by changing the chain-link which is attached to the ceiling and fine adjusted by rotating the turn-buckle. At the end of each chain, an S-hook is attached. The chains allow for the test plate to hang from the ceiling at a specified stand-off distance. For a visual of the blast tank see Figure 2.8, and for a schematic of the final test set-up used for blast testing see Figure 2.9.

Figure 2.8: Blast tank used for explosive testing
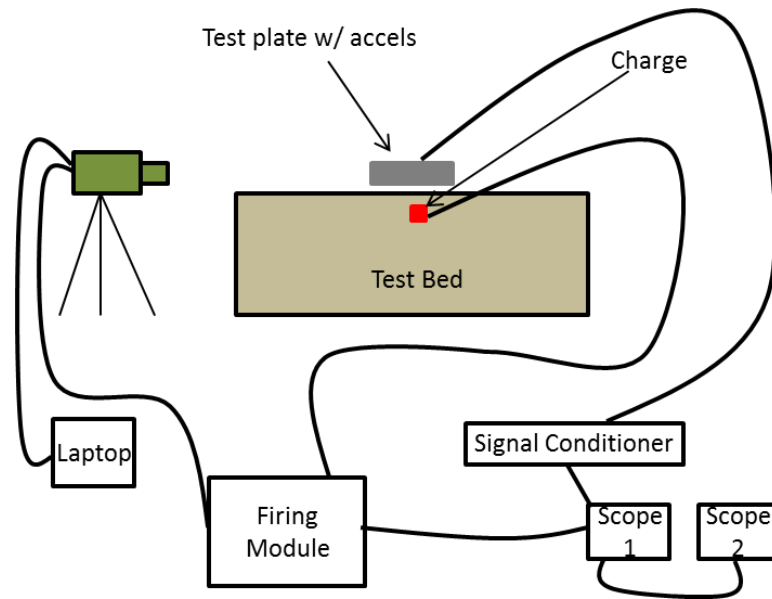
Figure 2.9: Schematic detailing blast test equipment set-up

2.1.3 Gas Gun Testing Equipment

Though not as extensive as the equipment needed for blast testing, there are a number of pieces of specific equipment necessary for dynamic testing using a pressurized gas gun. The gas gun is used for two primary testing purposes; each described at length in later chapters. Initially, the gun is used to locate the nodes of test plates. The gas gun is then used extensively for the dynamic testing of cantilevered polyurea coated bars. For the nodal testing, only a gas gun is needed. For the cantilever beam testing, the gas gun is needed in addition to a support used to supply the cantilever boundary condition to the beam.

The gas gun used consists of three valves controlling the pressure state of separate parts of the gas gun. The first valve allows for pressurized gas to enter into the "trigger chamber", the second controls the pressure in the chamber responsible for launching the projectile, and the third valve triggers the release of the pressures

16

resulting in the high speed ejection of the projectile. These valves and chambers are all attached to a 1.22 meter long barrel with an outer diameter of 4.3 centimeters and an inner diameter of 12 millimeters. Figure 2.10 is a picture labeling all of the different components of the gas gun.
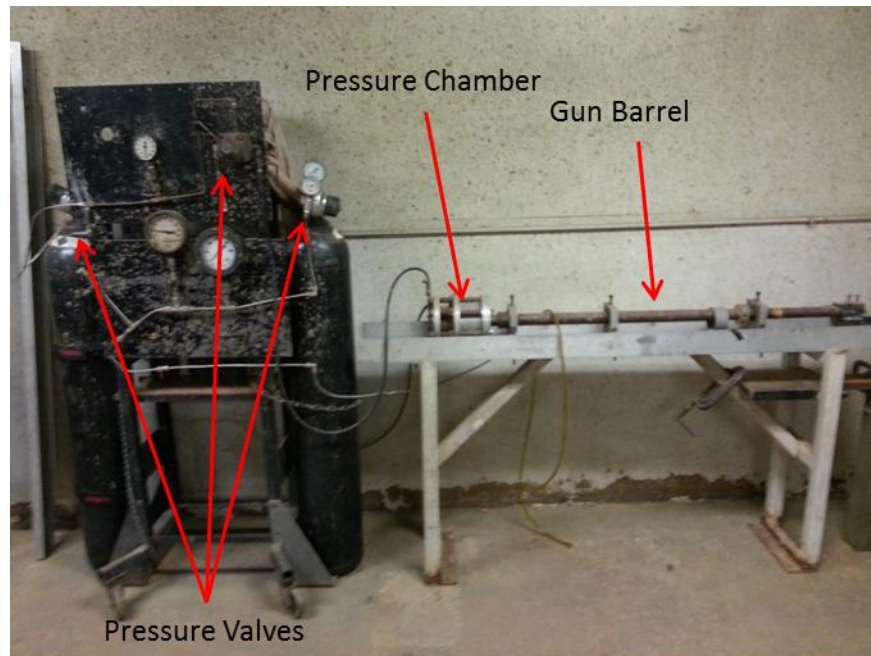
Figure 2.10: High-pressure gas gun for dynamic testing

The projectile used for the dynamic testing is a 44.4 gram steel cylinder. The projectile has a length of 5.13 centimeters with an outer diameter of 11.9 millimeters. There are visual targets mounted to the steel projectile so that it might be tracked using the Phantom software to determine its velocity. A picture of the projectile can be seen in Figure 2.11.
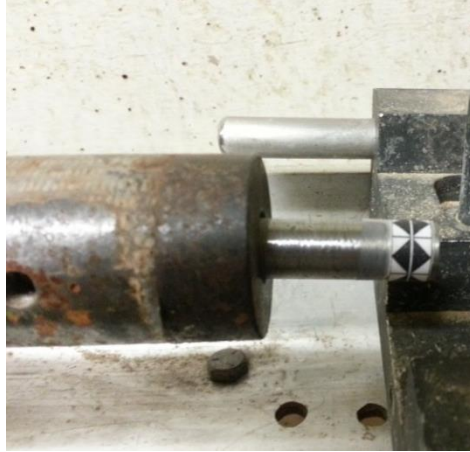
Figure 2.11: Steel projectile exiting gas gun

The last piece of equipment for the dynamic testing using the gas gun is the cantilever support. In order to create a cantilevered boundary condition for a bar to be shot by the gas gun, a cantilever mount was created. This mount consists of a 2.54 centimeter thick aluminum rectangle with a 2.54 centimeter by 2.54 centimeter square hole cut out of its center. This block is attached to a steel shelf extending from the frame of the gas gun using Hysol 9430 high strength epoxy, in addition to C-clamps for back-up. There are four holes drilled and tapped into the aluminum cantilever fixture to accommodate 9.53 millimeter bolts in each side. Two aluminum tabs are inserted into the front and the rear of the square hole so even pressure is applied from the bolts to the base of the cantilever beam. Each bolt can be tightened resulting in a very secure hold on a bar placed into the support. Finally, a wooden post with cross-sectional dimensions of 10.16 centimeters by 10.16 centimeters is placed under the steel shelf preventing any downward deflection. A picture of the cantilever support can be seen in Figure 2.12.

Figure 2.12: Cantilever support used for dynamic testing of polyurea coated beams

2.2 Blast Test Set-Up

There are a number of steps that must be taken in order to prepare for each blast test. Because the small-scale nature of the test, test preparation is performed with the utmost care as a small variation in any value may result in large variation in the test data. Each of the steps outlined below are taken before every blast test, with the sand bed platform (subsequently described) being cleared then reformed each time. For a view of the cleared sand bed refer to Figure 2.8.

2.2.1 Preparing the Saturated Sand Bed

The initial sand bed preparation consists of creating a 1.2 meter by 1.2 meter elevated sand platform in the center of the test bed. By locating the sand platform in the center of the bed any effects caused by boundaries are minimized. The sand is put into place layer by layer. Sand is piled in the middle of the bed to be leveled and shaped by hand to the 1.2 meter square. A cinder block is used to compact the top of

19

the sand bed as well as the sides of the platform; for each test care is taken to impact

the sand the same number of times with the cinder block. After the first layer of sand

is compressed, the surface of the sand is roughed (to ensure meshing between layers),

and another level of sand is added to the top surface of the platform. This level is, in

turn, compacted using the same cinder block method.

After the sides and top of the sand have been compressed to a satisfactory

level, an aluminum scraper, seen in Figure 2.13, is used to push sand off of the top of

the platform until a uniform and level surface is developed. By using the scraper, the

height of the sand will be controlled. Once the level surface is created, a piece of

wood is lightly brushed over the surface fixing any defects in the surface of the

platform resulting in a smooth and level sand bed.

Figure 2.13: Prepared test bed with aluminum scraper resting along the backside

2.2.2 Burying the Charge

Once the sand bed has been prepared the next task is to locate and bury the charge. Depending on plate geometry, there exists a method for the placement of the charge in the exact center of where the plate will rest in the test bed. For tests involving circular target plates – plates that are identical to the test plate are prepared with a hole in the exact center. For tests involving rectangular target plates – the outline of the plate is drawn in the sand on which the diagonals are connected thus locating the center of the plate.

Upon determining the specific location for the explosive, the charge is buried to the specified depth of burial (DOB). To bury the charge, a hollow cylinder with the same outer dimensions as the prescribed charge is pushed into the surface of the sand at the location identified as resting below the center of the plate. The tube is pressed into the sand a specified depth and then lifted out of the sand creating a hole in which the charge is buried. For all of the tests in this study a DOB corresponding to ten centimeters large-scale is used. The small-scale DOB is ten millimeters since, as previously mentioned, the scaling factor for this series of tests was determined to be approximately ten. DOB is defined here as the distance between the top surface of the charge and the surface of the sand. The charge is pressed incrementally deeper into the hole by tapping on the top of the charge using a metal rod and a hammer. Calipers are used to ensure proper DOB.

After the charge is buried the lead wires used to deliver the voltage to detonate the charge are run along the surface of the sand, out of the test tank, and taped to the side of the tank. Loose sand from the side of the tank is used to fill the space in

between the top of the charge and the surface of the sand. A smooth wooden block is used to tap down on the sand a prescribed number of times creating a uniform compaction level between the top of the charge and the surrounding sand. The block is then used to smooth out the surface resulting in a smooth and level sand platform once more.

2.2.3 Setting the Stand-Off Distance and Final Preparation Stages

The next step is to locate the plate and set its stand-off distance (SOD). SOD is defined as the distance between the top of the sand and the bottom of the target plate. Again, depending on the plate characteristics, a number of methods may be used for setting the SOD. The first method, most commonly used with lighter plates, involves setting the plate on a set of blocks that are machined to have the exact height of the specified SOD, as seen in Figure 2.14. The plate is placed on the blocks with the center of the plate lining up with the center of the charge. The second method, used when the plate becomes too heavy and is in danger of pressing the blocks into the sand, is to hang the plate from the adjustable length chains mentioned in the section describing the blast test equipment. The chains are attached to the plate and incrementally lowered until, using a set of calipers to ensure accuracy, the proper SOD is obtained.

The final step in the test preparation is the saturation of the sand bed. As mentioned previously, a pipe is attached to the bottom of the tank through which water can flow into the bed to saturate the sand from the bottom up. Water flows into the tank until the water level reaches a water level indicator located on the back wall of the bed. The indicator allows for the level of water to be repeated exactly from one

22

test to another. After the water reaches the level indicator and is shut off, the bed saturates for 30 minutes (the period of time believed to be necessary for full saturation to occur) allowing the water to permeate from channels surrounding the elevated sand platform to the center of the bed where the charge is buried. The final test set-up for a blast test is shown in Figure 2.14.

Figure 2.14: Fully prepared blast test sand bed

Once the bed has saturated fully, the accelerometer cables are connected to each accelerometer on the plate. The high speed camera is set-up and the image adjusted, following which a dummy charge is fired to make sure all data acquisition systems are functioning properly. After the dummy round, the charge lead wires are connected to the firing module and the charge is detonated. Upon detonation the video is examined and saved using the Phantom software. The acceleration signal is downloaded from the scopes and viewed in the UERDTools program to ensure proper recording; the signals are then saved and analyzed.

2.3 Gas Gun Test Set-Up

The test set-up for the dynamic testing of cantilevered beams and nodal testing of circular plates is significantly less arduous and consists of three primary steps outlined here and explained in depth in later paragraphs. The initial step is to place the plate/beam in the designated holder. Following the placement of the test object, the projectile is loaded into the gas gun. The final step is priming the gas gun and firing the projectile at the target.

The step requiring the most explanation in the set-up process of the gas gun is the placement of each test piece. In order to perform nodal testing, the circular plates are hung from the ceiling using adjustable length chains (similar to those used to set the SOD). The height of each chain is adjusted so that the center of the plate lines up with the center of the gun barrel. By setting the plate up in this fashion, its distance from the gas gun and the location the projectile hits can be precisely set. Hanging the plates also allows them to vibrate freely. For a picture of this test set-up refer to Figure 2.15.
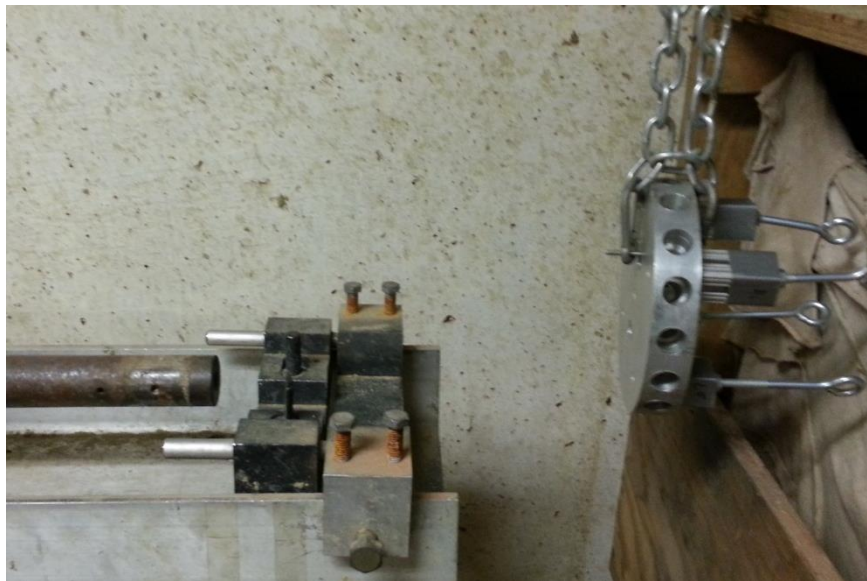
Figure 2.15: Hanging plate for nodal testing with the pressurized gas gun

The cantilever beam tests are set-up in a similar fashion. Instead of hanging the plate from the ceiling, the beam is placed in the cantilever support mentioned in the section on gas gun test equipment. Care is taken to place the center of the beam in line with the striker projectile path. The bolts are tightened using an Allen wrench so that the beam cannot move in the support. For a visual of this set-up see Figure 2.12.

Once the beam/plate has been placed in the respective testing position, the gas gun projectile is loaded and the pressure chambers primed. This task is accomplished by using a flexible rubber tube to press the projectile back into the barrel as far as possible. Once loaded, the pressure chamber is primed by first pressurizing the trigger chamber. The trigger chamber pressure is kept constant at its maximum allowable pressure of 380 kilopascals. Immediately following the pressurization of the trigger chamber, the pressure chamber responsible for launching the projectile is filled. For the nodal testing the pressure is kept constant for each test. The pressure that the projectile is fired at is not particularly important; the only essential aspects of the pressure are that it is high enough to launch the projectile at a velocity substantial enough to cause adequate plate vibrations (able to be read by the accelerometer), and that the pressure is the same from one test to another. For the beam testing the pressure is in the neighborhood of 75 kilopascals, and will be described in more detail later.

Once the gun is pressurized, the oscilloscopes are set to trigger off of the accelerometer signal excitation. For the cantilevered beam tests, the high speed camera trigger is readied and triggered at the same time that the pressure in the gas

gun is released in the gun, firing the projectile at the target. The data is then

downloaded from the oscilloscopes and saved for processing using the Phantom high

speed camera software.

Chapter 3 – Preliminary Tests

The first series of tests run in this research were designed to fulfill a number of objectives. First and foremost, it was necessary that greater familiarity be obtained with the test set-up and equipment. In addition, two studies needed to be conducted to better understand the effect of mass and SOD on a plate undergoing blast loading. During the mitigation study it was decided that certain design characteristics of the simulated vehicles might be changed, effectively changing the mass and SOD of the test plate. To this end, it was essential to develop a method for taking into account the effect of these changes on the test results.

3.1 Mechanical Filtering/Nodal Tests

3.1.1 Using Piezoelectric Accelerometers for Blast Testing

During early testing using a piezoelectric accelerometer to measure rigid body accelerations of a steel plate, numerous difficulties were encountered. One of the greatest challenges was getting a signal that accurately portrayed the acceleration envelope of the target resulting from the blast load. When a piezoelectric accelerometer is mounted by threading the device directly into the blast loaded target plate, the output is so noisy that it does not make intuitive sense. To prevent this, a mounting technique utilizing mechanical filtering is employed to reduce the noise on the signal. This results in an acceleration pulse more indicative of the rigid body motion of the target.

As mentioned previously, in order to acquire a signal that represents the rigid body motion of the target from the instrumentation, a proper mechanical filter is

employed. If the sensor does not have a suitable filter, the signal from the

accelerometer appears as in Figure 3.1. Trying to determine the peak rigid body

acceleration of the target plate from the acceleration signal shown in Figure 3.1 is a

daunting task. Even with the use of computer filters to reduce the effect of the high

frequency noise, the acceleration signal will not appear clean enough to convince the

researcher that what he/she is reading reflects rigid body motion.
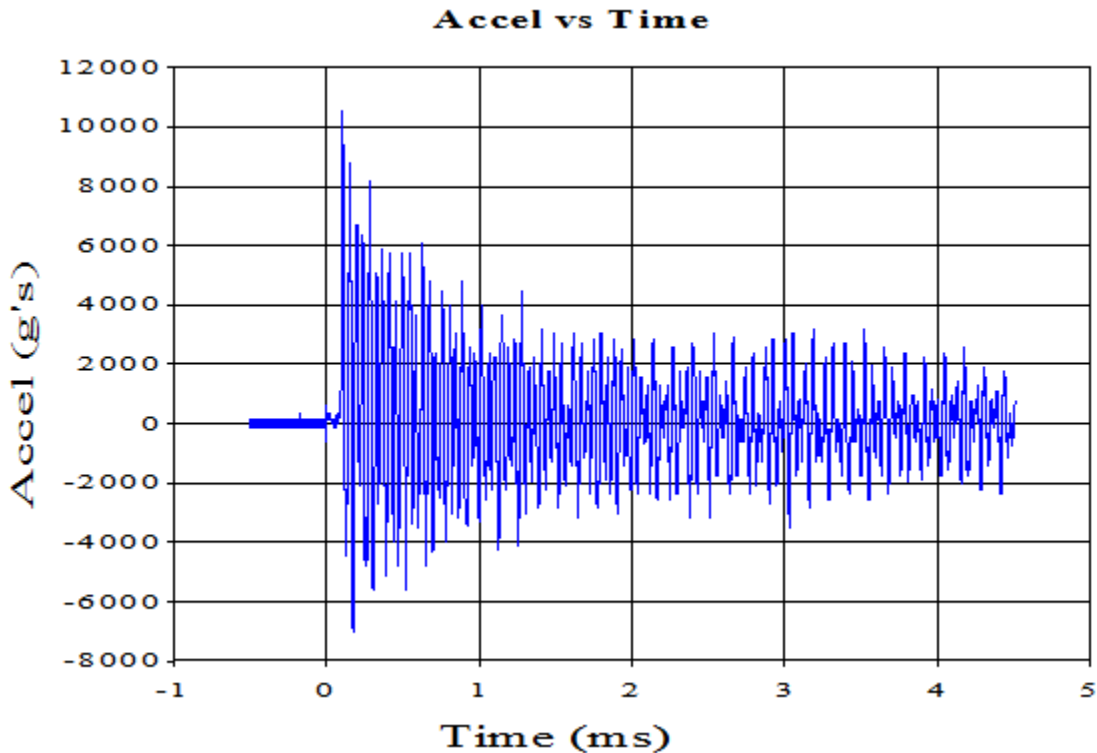
Figure 3.1: Typical acceleration reading from an accelerometer thread mounted directly into target plate

To solve this problem, a series of mounting pads were utilized under the same

test conditions employed in the test for which the data from Figure 3.1 was collected.

A range of materials including various types of foams, plastics, rubber, wood, and

carbon fiber composites were mounted on the target plate. The accelerometer was

then threaded into each material and underwent the blast load. At the end of this

series of tests, two materials were shown to adequately filter the data. The first was an X-Core material from Albany Engineered Composites. This material is a 3-D woven carbon fiber epoxy sandwich structure with a foam core and carbon fiber pins connecting the two outer layers. The second material was metal foam and can be seen in Figure 3.2 with the X-Core material. Figure 3.3 illustrates the signal obtained with a mechanical filter compared to no mechanical filter.
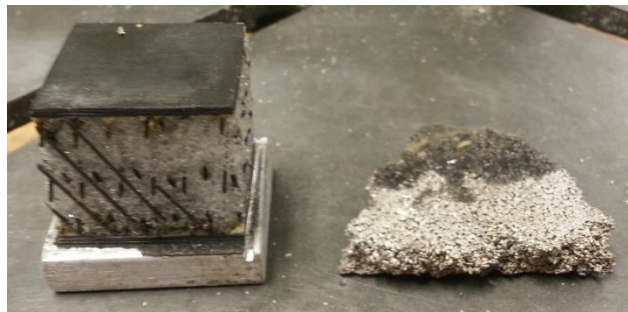
Figure 3.2: X-Core composite (left) and metal foam (right) used for mechanical filters
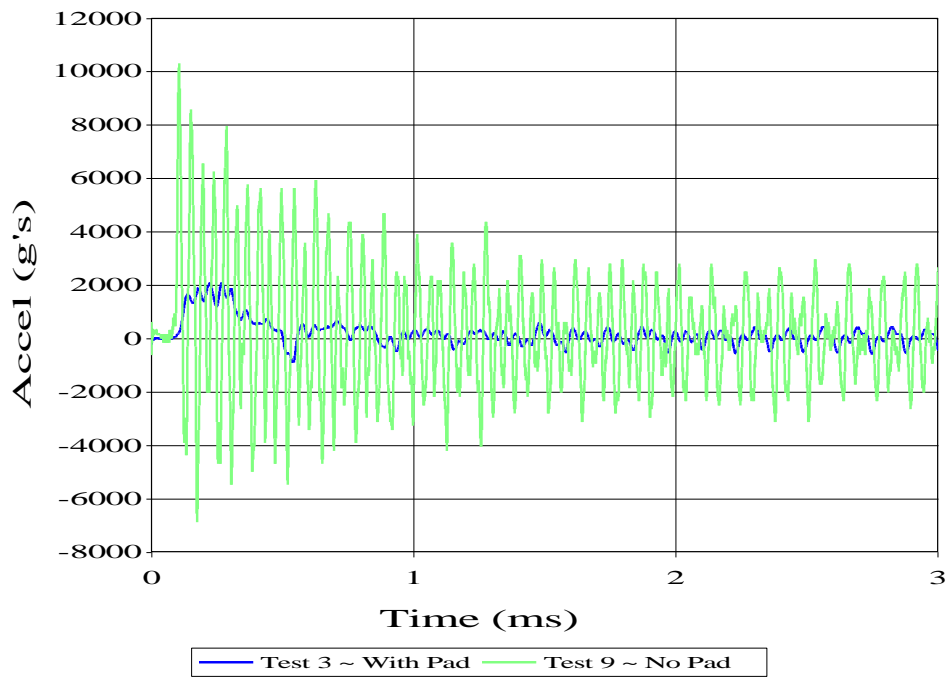
Figure 3.3: Effect of using a mechanical filter for blast testing

A prominent concern when choosing a mechanical filter for mounting an accelerometer is making sure the material chosen as a filter has enough compressive strength to resist crushing under the weight of the accelerometer during the loading scenario. It was noted in some of the earlier tests (namely the tests using foam as a filter) that the accelerometer would sink into the filter material when the plate accelerated. To address this concern a stress/strain curve for the materials under compression was developed for each of the two materials identified as an acceptable mechanical filter and compared with that of the target plate (steel). By comparing the slopes of the stress/strain curves shown in Figure 3.4 it is seen that though the X-Core pad might fail at a lower stress level, both of the materials are stiff enough to transmit the rigid body motion of the plate to the accelerometer. As assurance of the integrity of the data taken from an accelerometer with a mechanical filter, it was decided to use the metal foam so that material failure (of the pad) would not be an issue.
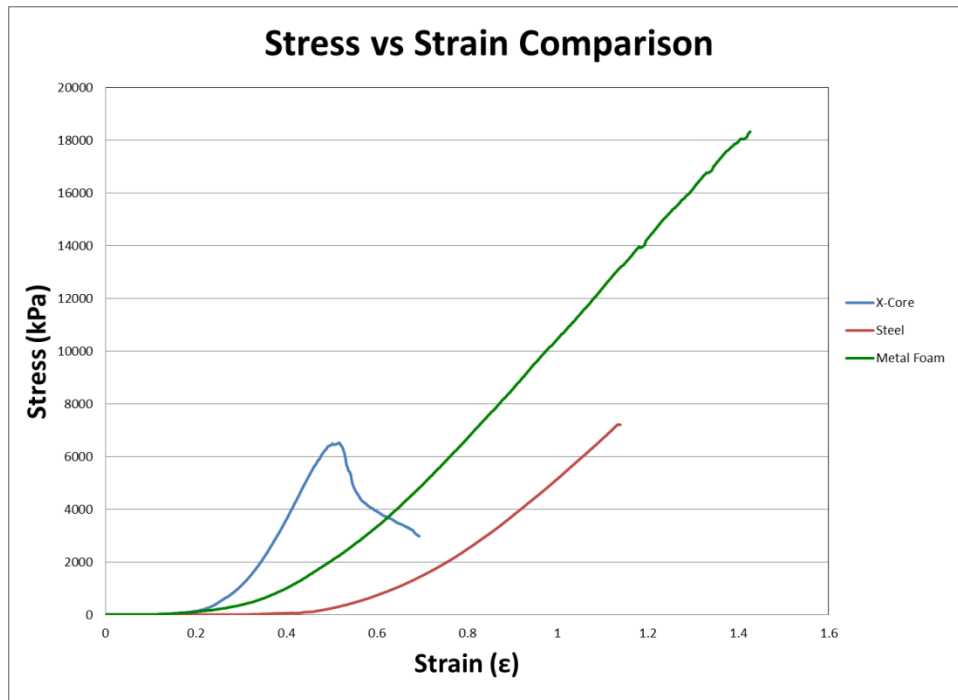
Figure 3.4: Stiffness comparison for mechanical filter materials and steel

3.1.2 Proper Mounting of Accelerometers on Plate Nodes

With a filtering material chosen, it was necessary to determine the best way to mount the filter pad and accelerometer to the plate. Though not visible to an observer, high frequency plate vibrations occur in the target when subjected to blast loads. These vibrations coupled with extraordinarily high acceleration values make it difficult to keep the metal foam pad on the target for the duration of the test. A variety of epoxies, silicones, glues, tapes, and even Velcro were tested not only for bond strength but also for compressibility to achieve a mounting technique that would supply a strong bond that compresses negligibly under high loads. After extensive testing it was found that the VHB tape from 3M was strong enough to hold the mounting pad, and also thin enough to have negligible amounts of compression. A small aluminum plug was machined into which the accelerometer can be threaded; the plug was then mounted onto the metal foam pad using the same VHB tape. This set-up can be seen in Figure 3.5.
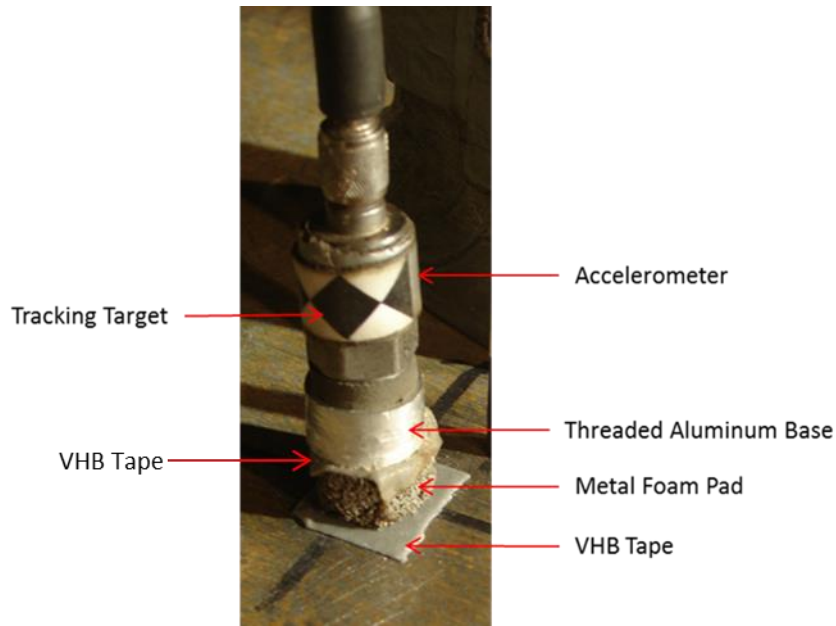
Figure 3.5: Mechanical filter set-up of accelerometer on target plate

A consideration when performing acceleration tests on a target plate is the need to place the accelerometer on the mode one vibrational node, if possible. If the accelerometer is not placed on a node it will pick up vibratory motions as well as rigid body motion of the plate. Though the amplitudes of plate vibrations are small enough to be invisible when viewing the plate motion with a high speed camera, it can be shown that even with a steel plate of 2.54 centimeters thickness, the vibrations can account for hundreds of g's of high frequency acceleration.

To illustrate this point, the gas gun mentioned in previous sections was employed to shoot each plate at its center. Ensuring equal pressures in the gas gun, each plate was shot on multiple occasions while the accelerometer position was varied along a line connecting the outer edge with the center of the plate. This effectively allowed the location for minimum plate vibration to be identified (the node). The difference between the accelerometer signal at the node and the center of the plate is shown in Figure 3.6.
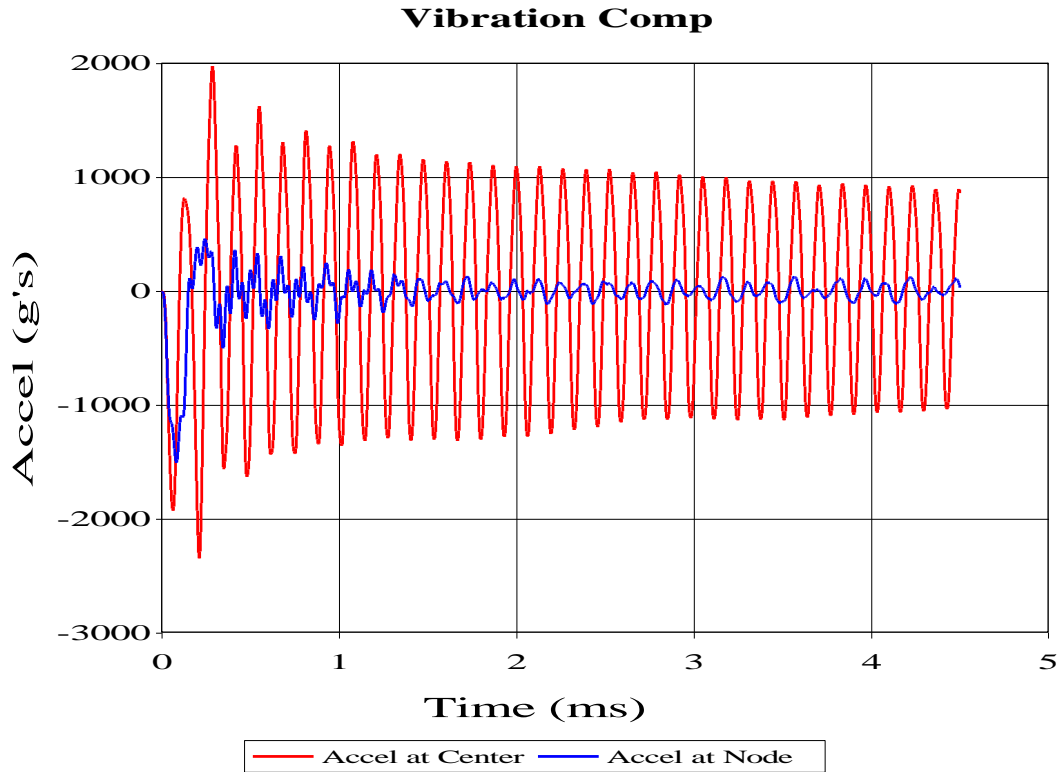
Figure 3.6: Acceleration signal comparison for a 9.12 kilogram steel plate shot with a gas gun with device at plate center compared to device at the plate node

3.2 Mass Study

3.2.1 Mass Study Test Outline

The first series of tests run to develop a greater understanding of target plate behavior under blast loads, involved varying only the mass of the target. To do this, five cylindrical steel plates of varying thickness but equal diameters were tested under the same SOD and DOB conditions. Each plate was tested twice to ensure test repeatability. The test matrix can be seen in Table 3-1.

Table 3-1: Matrix of test plate properties for the mass study

Test Number	Charge Mass (g)	SOD (mm)	DOB (mm)	Plate Diameter (cm)	Plate Thickness (mm)	Plate Mass (kg)
3	4.4	40	10	19.27	37.9	9.12
4	4.4	40	10	19.27	37.9	9.12
5	4.4	40	10	19.27	28.95	7.04
6	4.4	40	10	19.27	28.95	7.04
7	4.4	40	10	19.27	19.95	4.98
8	4.4	40	10	19.27	19.95	4.98
9	4.4	40	10	19.27	62.8	15.18
10	4.4	40	10	19.27	53.7	12.82
11	4.4	40	10	19.27	53.7	12.82
12	4.4	40	10	19.27	62.8	15.18

At the conclusion of each test the signal obtained from the accelerometer was analyzed. In addition to the analysis of the accelerometer data, the video of the test from the Phantom v12.1 was used to track targets located on the plate and on the accelerometers themselves. To ensure accuracy of the accelerometer data, the acceleration signal was integrated twice to obtain a displacement versus time curve which was then compared with the displacement versus time curve (obtained using high speed video) for the target on the accelerometer and for the target located closest to each accelerometer. The first integration of the accelerometer signal was also viewed in each scenario to make sure the velocity/time curve for each test was realistic.

Values for peak acceleration of each test were recorded and plotted to obtain a graph detailing how acceleration varies with plate mass. A sample of an acceleration signal along with its corresponding velocity/time and displacement/time curve can be viewed in Figure 3.7, Figure 3.8, and Figure 3.9 respectively. The red line in Figure 3.9 indicates the double integrated accelerometer signal, the blue line represents the displacement curve of the target closest to the accelerometer and the green line is the

displacement curve of the target on the accelerometer itself. Note that there is very

good agreement between the displacement/time curves obtained by high speed video

and the displacement/time curve obtained from double integration of the

accelerometer. This was the case for all of the tests being reported.
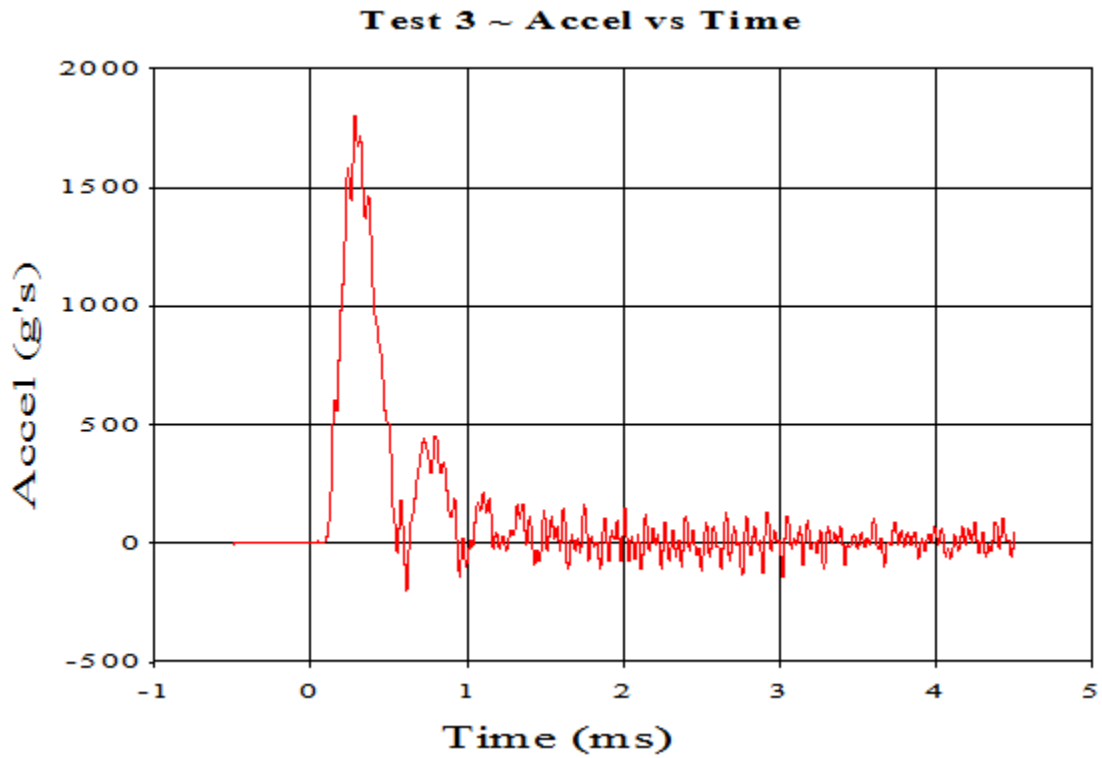
Figure 3.7: Acceleration versus time for a 9.12 kilogram steel plate
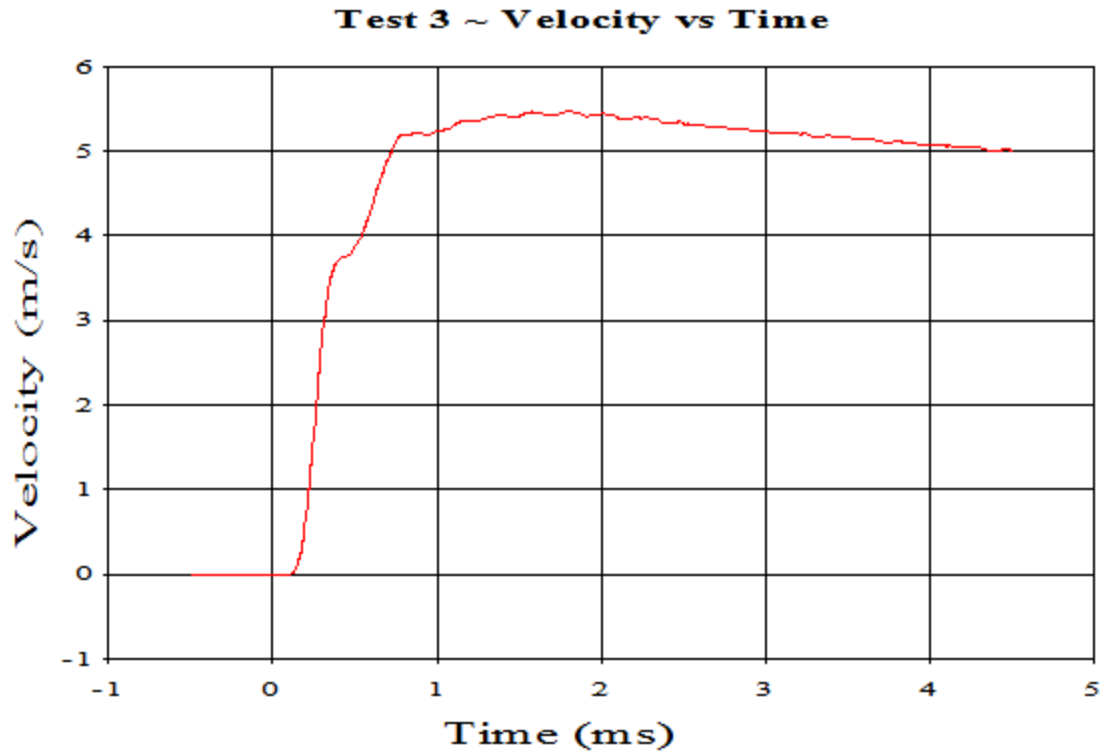
Figure 3.8: First integration of the acceleration signal obtained from blast test
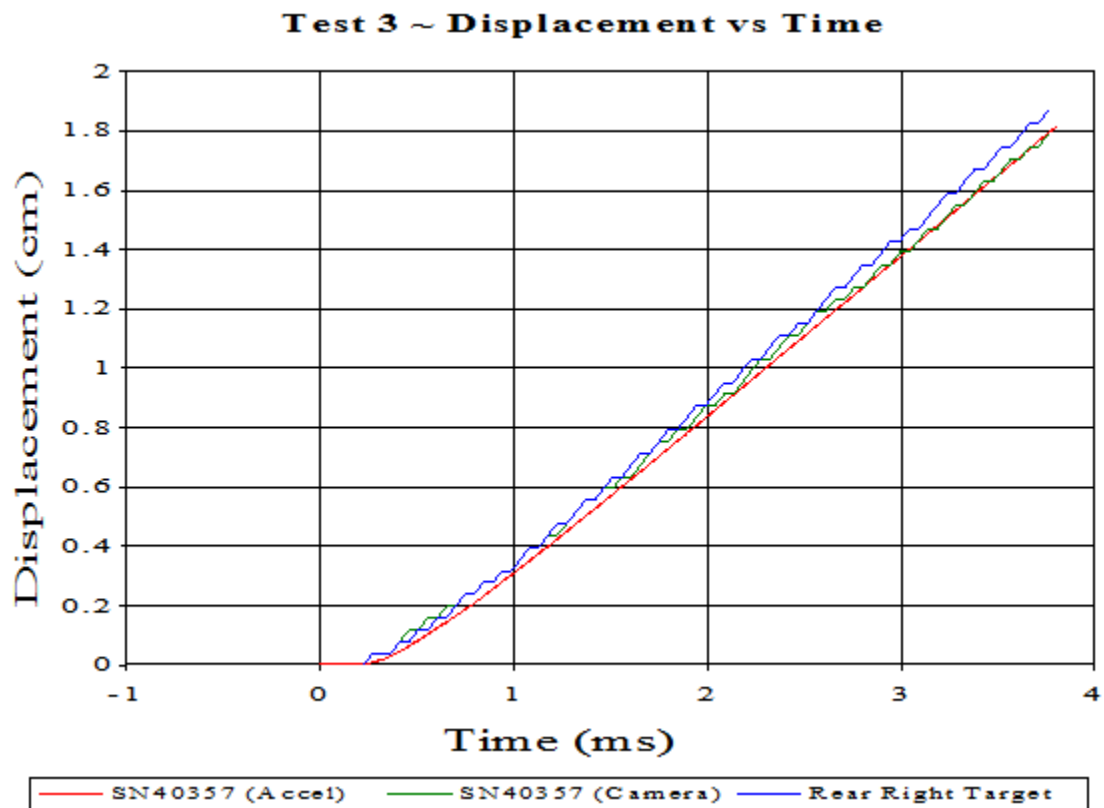
Figure 3.9: Second integration of the accelerometer signal compared to the targets tracked using high speed videography

36

3.2.2 Mass Study Test Results

In order to study the effects of plate mass on the kinetic energy and impulse imparted to the target plate, the displacement versus time curve from the high speed video along with the peak velocity obtained from the first integration of the accelerometer data was used. The slope of the high speed video displacement/time curve is the take-off velocity of the plate. The velocity was used along with the mass of the plate to obtain the change in linear momentum and kinetic energy of each plate. Figure 3.10, Figure 3.11, and Figure 3.12 present the acceleration, impulse, and kinetic energy of the blast loaded plate as the mass was varied. When reporting the impulse and kinetic energy of each test, the velocity values obtained from the camera as well as the first integration of the accelerometer are both reported.
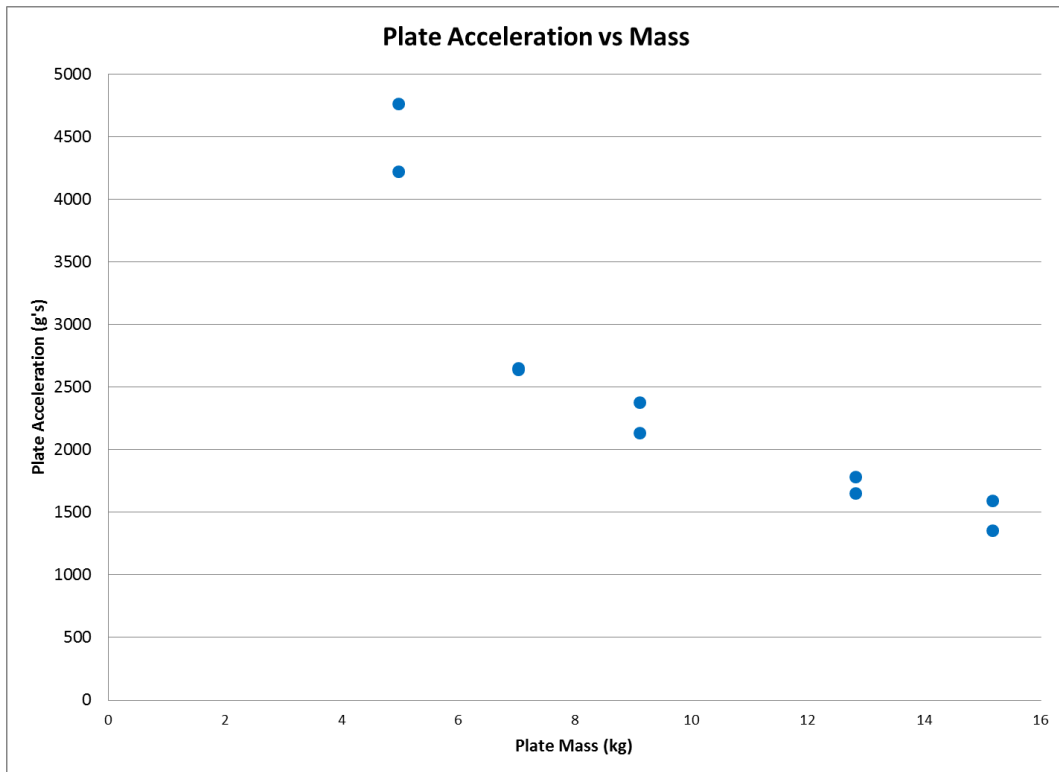
Figure 3.10: Plate acceleration as a function of mass
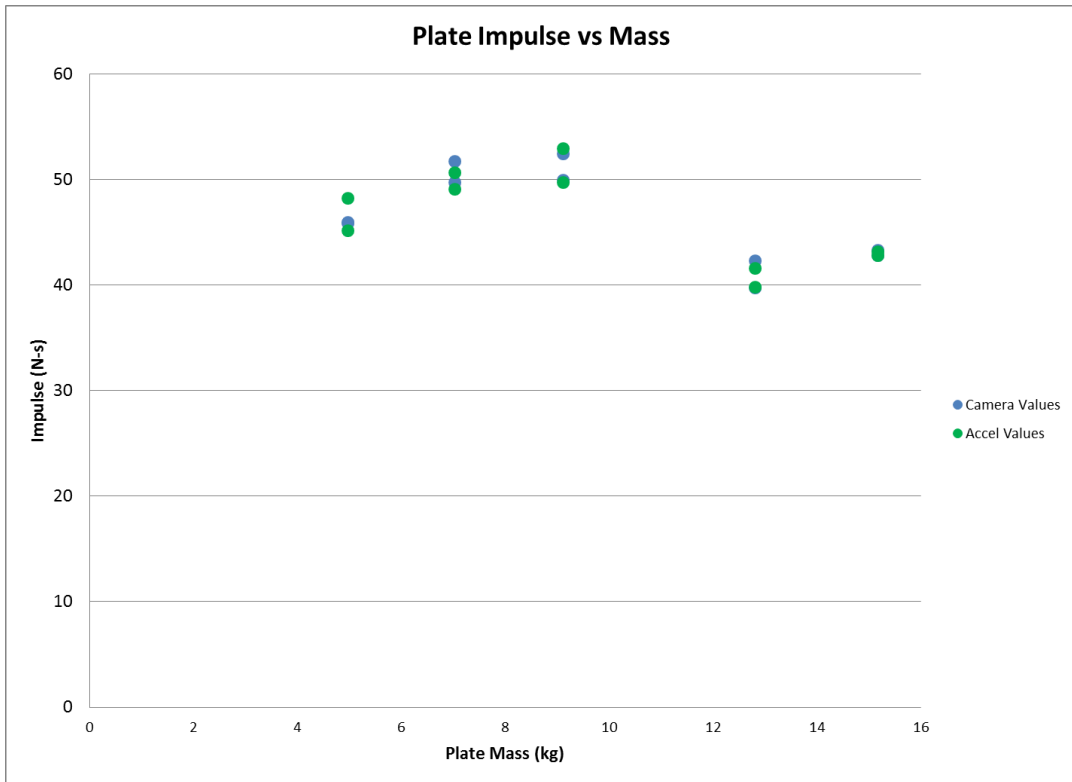
Figure 3.11: Plate impulse as a function of mass
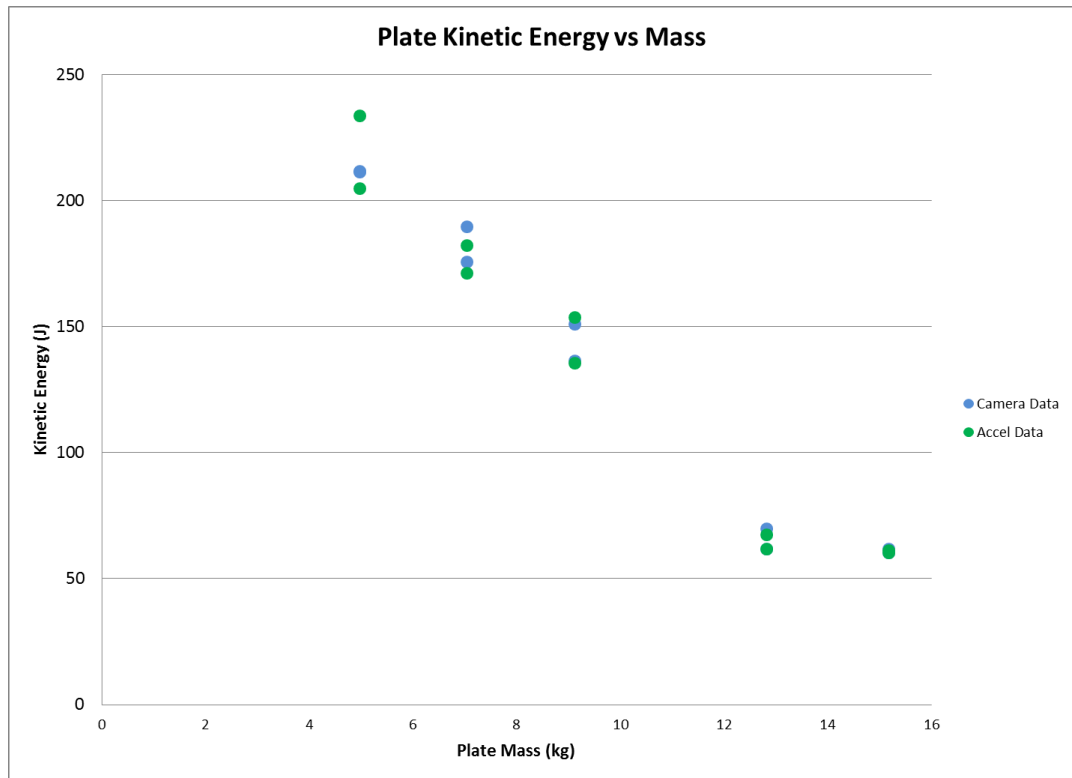
Figure 3.12: Plate kinetic energy as a function of mass

From Figure 3.10 note that after the initial rapid drop in acceleration as mass increases it appears as if the curve starts to level off a bit. This is encouraging in that if, in later tests, the mass of the test vehicle is increased by small amounts, large changes in acceleration due to the change in mass are not expected. Also of note is that the impulse supplied to the plates seems to peak around ten kilograms, and thereafter seems to fall off to a steady level. The kinetic energy on the other hand seems to follow an initially linear rapid drop with increasing mass up to the point of 12 kilograms at which point the kinetic energy imparted to the plate by the ejecta seems to begin to level off. The last take-away from Figure 3.11 and Figure 3.12 is that the peak velocity obtained by integrating the accelerometer data and the velocity obtained by differentiating the camera data are in very strong agreement. This provides further confidence in the validity of the accelerometer data collected in the harsh blasting environment.

3.3 Stand-off Distance Study

3.3.1 Stand-Off Distance Study Test Outline

Another relatively simple and controllable variable affecting acceleration of a vehicle due to blast loading is the stand-off distance (SOD). Using the same 9.12 kilogram steel plate as was used in the mass study series of tests, four different SODs were examined. For each of the SODs, the same parameters (acceleration, impulse, and kinetic energy) were studied as a function of the only test variable – SOD. A test matrix for the SOD study is shown in Table 3-2. It should be noted that the

repeatability of the tests was previously demonstrated in the mass study. As a result, after the first two tests in Table 3-2, each SOD was tested only once.

Table 3-2: Test matrix for SOD study

Test Number	Charge Mass (g)	DOB (mm)	SOD (mm)	Plate Diameter (cm)	Plate Thickness (mm)	Plate Mass (kg)
1	4.4	10	40	19.27	37.9	9.12
2	4.4	10	40	19.27	37.9	9.12
3	4.4	10	60	19.27	37.9	9.12
4	4.4	10	20	19.27	37.9	9.12
5	4.4	10	10	19.27	37.9	9.12

The same 5000g accelerometer was used in this series of tests as in the last. As in the mass study, each acceleration signal was developed by placing the instrumentation at the 9.12 kilogram plate's vibrational node. Each acceleration signal was also electronically filtered at the appropriate frequency to reduce the effect of the much diminished, but still present, plate vibration.

Finally, as in the previous study, each acceleration signal was double integrated to develop a displacement versus time curve which was then compared with the displacement of the plate as seen from the high speed camera. A signal and its corresponding displacement versus time curve are shown in Figure 3.13 and Figure 3.14. In Figure 3.14 the red line indicates the double integrated acceleration signal, the blue line represents the motion of the target nearest to the accelerometer, as recorded by the camera, and the green line shows the displacement of the target on the accelerometer itself, as recorded by the camera.
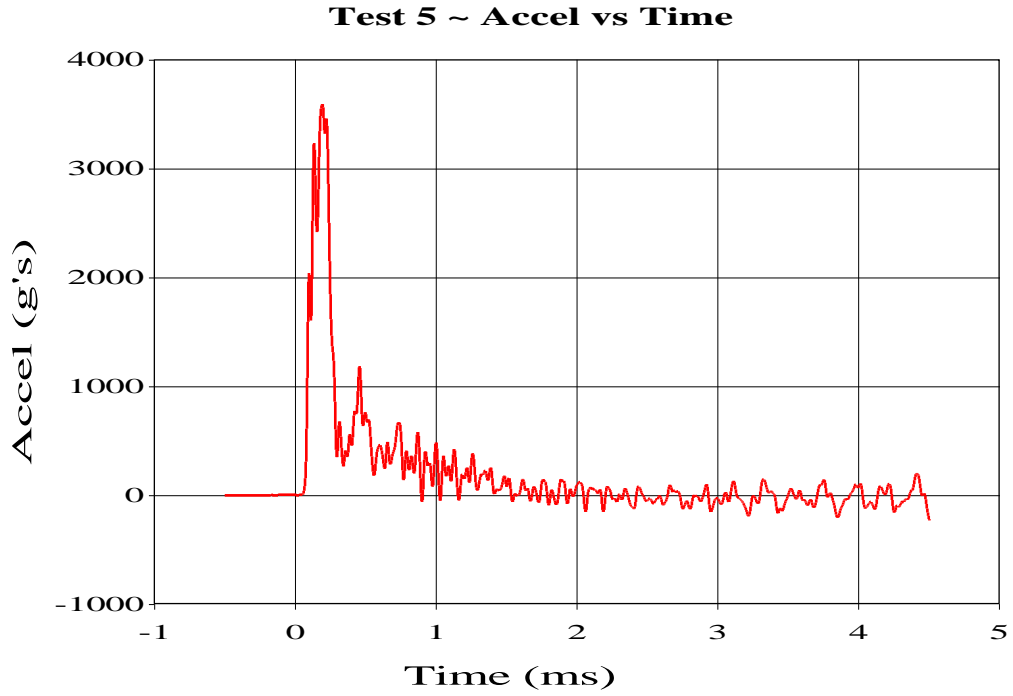
Figure 3.13: Acceleration versus time for a 9.12kg plate with a 10mm SOD
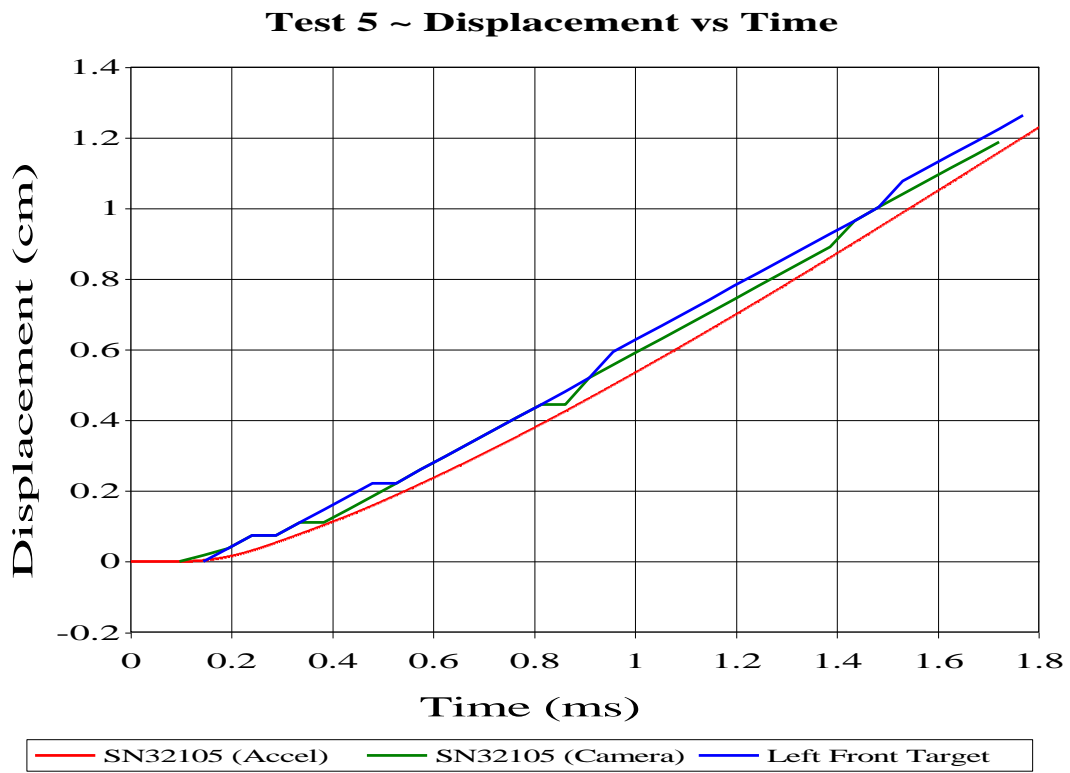
Figure 3.14: Displacement versus time for a 9.12kg plate with a 10mm SOD

41

3.3.2 Stand-Off Distance Study Test Results

Using the high speed camera to track targets located on the plate used for the SOD study, the take-off velocity of each plate was found. Both impulse and kinetic energy of these plates were plotted against SOD to illustrate the effect of target height. The results of these tests are shown in Figure 3.15, Figure 3.16, and Figure 3.17.
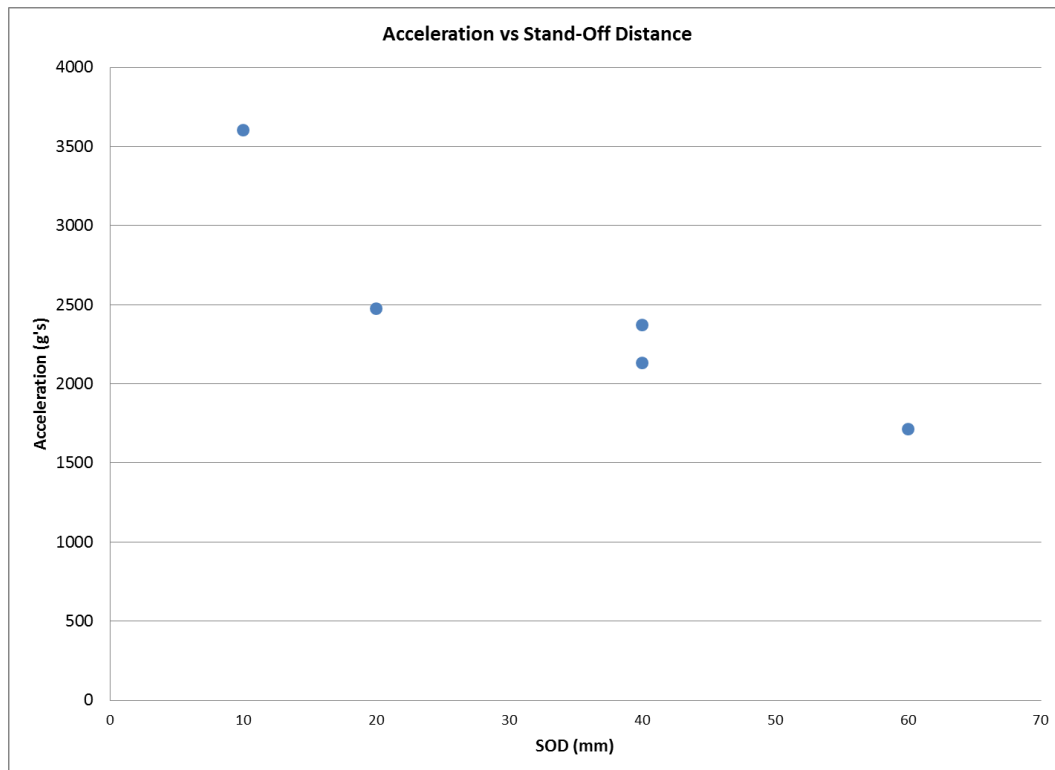
Figure 3.15: The effect of SOD on acceleration for a 9.12kg plate
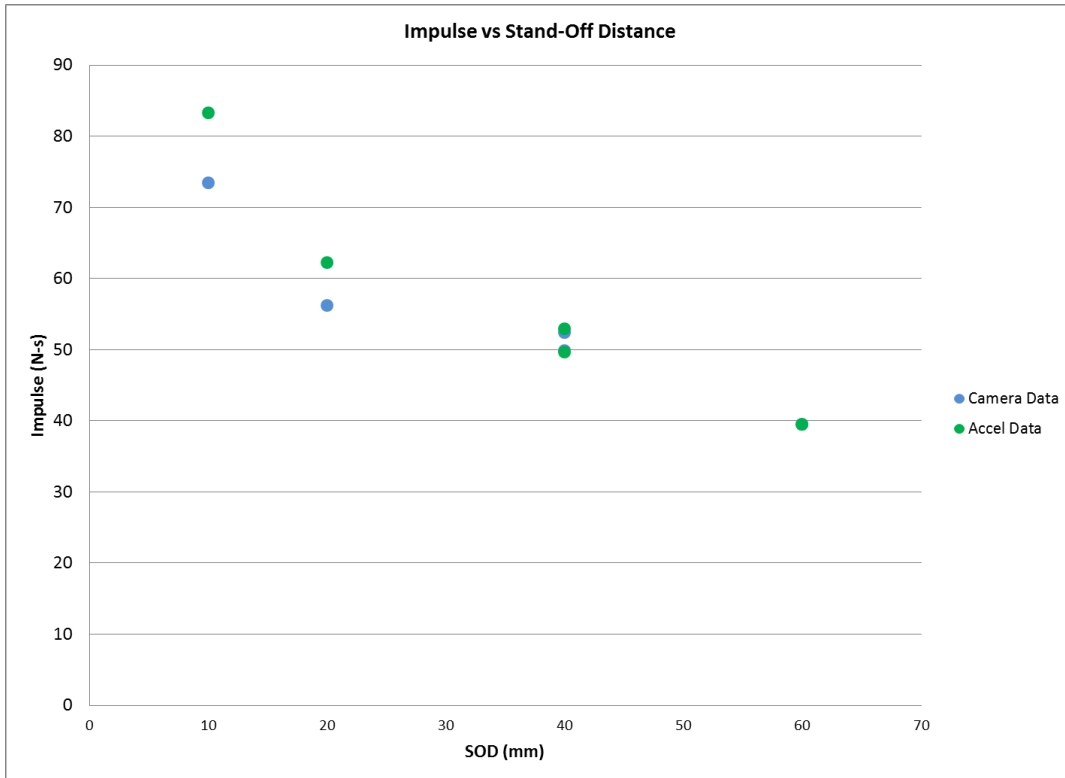
Figure 3.16: The effect of SOD on impulse for a 9.12kg plate
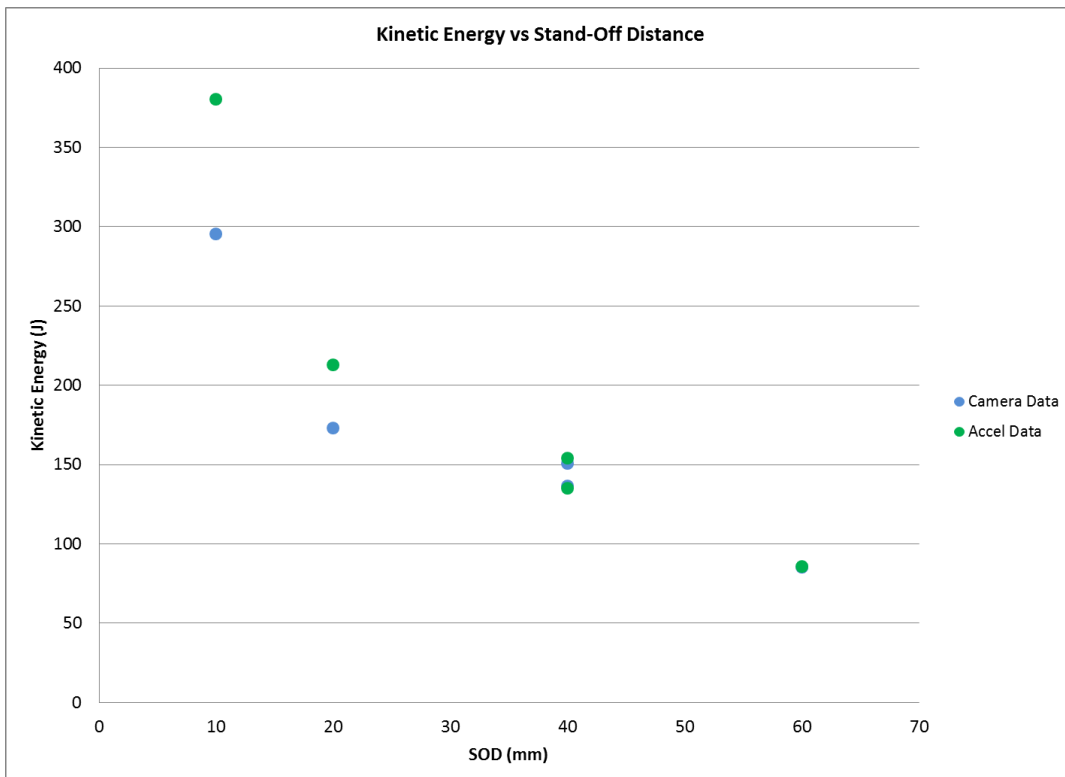
Figure 3.17: The effect of SOD on kinetic energy for a 9.12kg plate

Stand-off distance can affect acceleration, impulse, and kinetic energy very dramatically. The full scale SOD of interest is 40.64 centimeters. Scaled down to our model tests this would equate to 40 millimeters. In the range from 20 to 60 millimeters the decrease in acceleration, impulse, and kinetic energy is nearly linear. At very small SODs (10 millimeters), all three values jump to very high values. For a 4.54 kilogram explosive this would equate to a SOD of only 10.16 centimeters. For the values of interest an increase of SOD by 50 percent would result in a decrease in impulse, kinetic energy, and acceleration to about two-thirds of the value at the normal SOD. As in the mass study, the peak velocity was taken for both the data from the high speed camera as well as the integrated accelerometer signal and shows a strong correlation.

3.4 Early Mitigation Studies

3.4.1 Early Mitigation Study Test Outline

At the conclusion of both of the previously mentioned series of tests, an additional series of tests was run to develop ideas for effective means of acceleration mitigation. For this series of experiments, two of the circular plates used from the mass study (the 7 kilogram and 2 kilogram plates) were connected using a variety of structural elements meant to plastically deform during the blast loading. The hope here was to get a feel for how much acceleration could be reduced through plastic deformation of the connecting elements.

Amongst the plethora of tests run it was determined that a couple of methods for acceleration mitigation warranted further research – tube bucking and thin-walled cylinder crushing. Examples of two of the tests are seen in Figure 3.18. Each test

44

was conducted with a 4.4 gram charge buried at a ten millimeter DOB with the plate having a 40 millimeter SOD. As a control plate, eight 6.35 millimeter outer diameter steel rods were used to connect the two plates. No plastic deformation of the rods occurred resulting in an experiment with no mitigation.
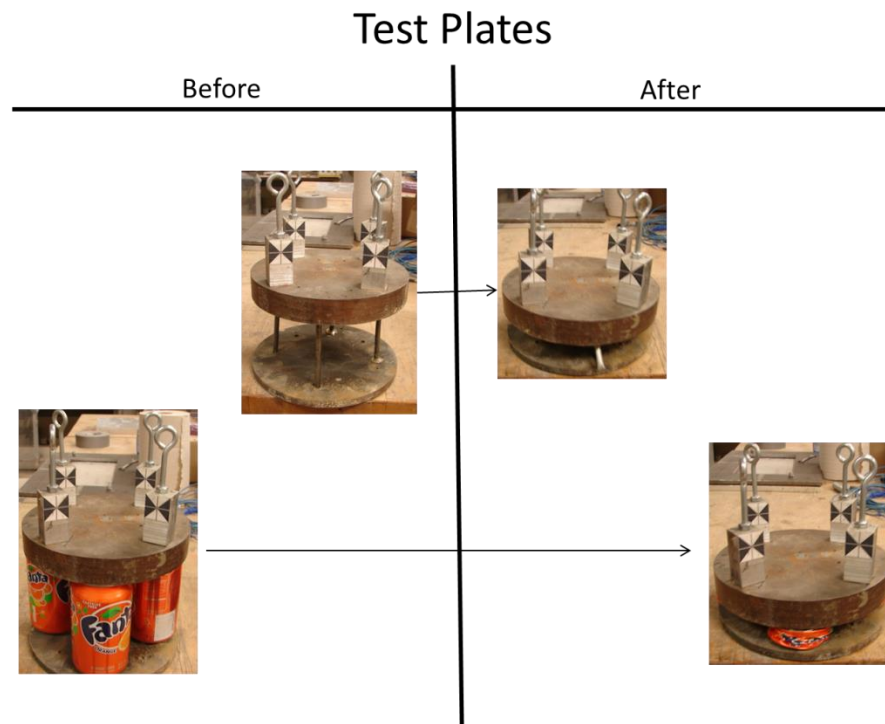
Figure 3.18: Early mitigation test set-up for two promising techniques

3.4.2 Early Mitigation Study Test Results

The first mitigation technique used was termed "tube buckling". This occurs when the wall thickness of the tube is of the same order of magnitude as the outer diameter. In the tube buckling mitigation technique each tube deformed by buckling at mid-span. The most promising result occurred using four 6.35 millimeter outer diameter and 4.6 millimeter inner diameter aluminum tubes to connect the plates. At this geometry the top plate begins to move slowly as the tubes begin to buckle and

speeds up slowly so that when the bottom plate reaches the top plate, no violent contact occurs between the two.

The second mitigation technique we have termed "tube crushing", which involves thin-walled large outer diameter tubes (for this series of tests, a number of beverage cans were used). Here the most promising result occurred with four 66 millimeter outer diameter, 65.8 millimeter inner diameter aluminum cans. The crushing of the cans is characterized by many areas of plastic deformation along the height of the cylinder, not following the typical buckling behavior of columns.

The resulting peak acceleration signals can be seen in Figure 3.19. It is easily seen how valuable plastic deformation can be in mitigating acceleration of targets that undergo explosive loading. In Figure 3.19 the green signal is for crushing and the blue signal is for tube buckling.
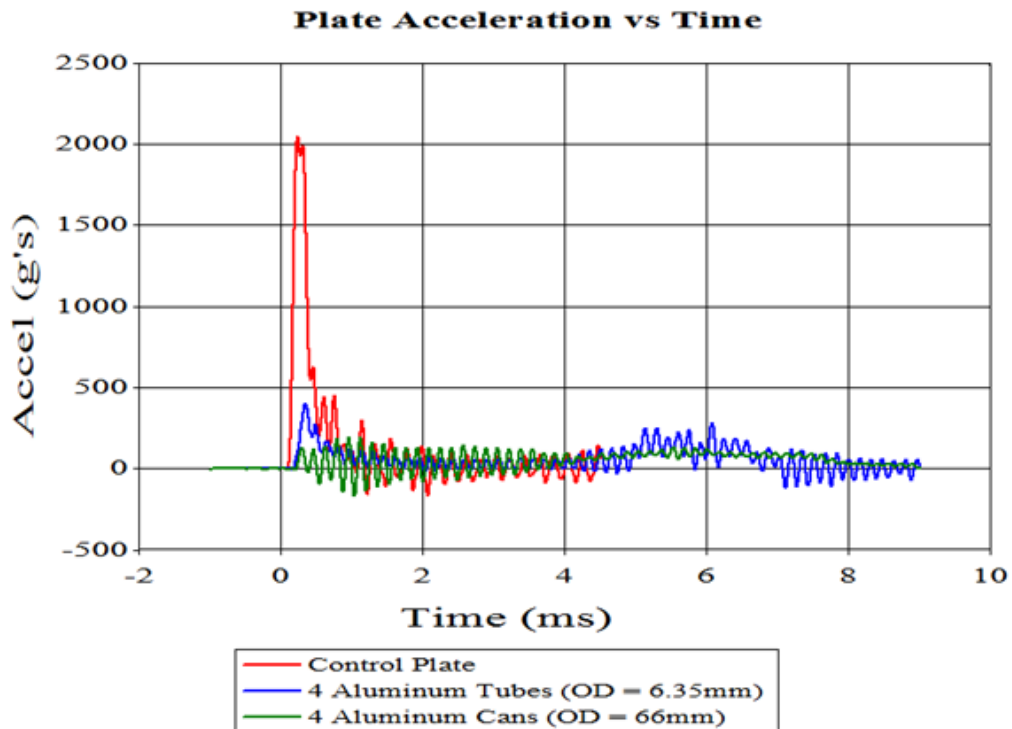
Figure 3.19: Acceleration signals for two of the early mitigation study tests

46

At the beginning of the chapter a number of goals were made. Initially it was desired that a deeper understanding be obtained for the use of accelerometers for blasting applications. The testing to develop an adequate means of mechanically filtering the data to eliminate high frequency frame vibrations, as well as the plate vibration nodal testing, allowed for this goal to be met.

After establishing familiarity with the testing procedure and data collection equipment, a series of tests was run to study the effect of changing the mass of the target plate on acceleration, impulse, and kinetic energy. In this series of tests it was found that as mass increases, there is a non-linear decrease in target plate acceleration. When increasing the plate mass from around five kilograms to the neighborhood of 15 kilograms a 66 percent decrease in acceleration was realized. The impulse of the target plate initially increases from the five kilogram plate to the nine kilogram plate, where it peaks. As the mass increases beyond nine kilograms it is found that the impulse decreases. The kinetic energy of the target plate was found to decrease in a more linear fashion as the target plate mass increased. This trend holds true up until the point where the plate mass reaches 15 kilograms, at which point the kinetic energy curve seems to level off.

The next series of tests run in this chapter involved changing the SOD of the target plate and measuring the accompanying change in acceleration, impulse, and kinetic energy. A steady decrease in acceleration was noted as the SOD increased. The maximum SOD of 60 millimeters resulted in a 50 percent decline in acceleration value over the minimum SOD of ten millimeters. The same trend was realized in the

impulse data. Though a steady decrease in the value of kinetic energy of the target

plate also resulted from increasing the SOD, the maximum SOD resulted in a 75

percent drop over the kinetic energy value of the minimum SOD of ten millimeters.

To conclude this chapter, two mitigation techniques showing promise were

identified. The first was the use of buckling tubes, which will only be identified as an

area of future study in this paper. The second promising technique came as the use of

thin-walled cylinder crushing to mitigate acceleration. This mitigation technique is

studied in much greater depth in the following chapters.

Chapter 4 – Mitigation Study on Small-Scale Vehicle Shapes

4.1 Introduction/Test Set-Up

Although valuable for highlighting promising areas for further research, the early mitigation studies left certain areas open for improvement. Namely, the small-scale testing done to study mitigation should be based more in reality. As such, this section of the research contains testing elements that are more realistic from a geometrical standpoint than those from the previous sections.

4.1.1 Testing Plate Components and Geometries

The first shortcoming of the early series of tests is the unrealistic nature of the geometry of the plates. Ideally, the plates under study should reflect the geometric properties of the vehicles that are regularly targeted by explosive devices. As such, for the upcoming portion of this research, rectangular plates having the scaled down dimensions of some of those vehicles are used. Specifically, each plate has outer dimensions of 45.72 centimeters by 30.48 centimeters.

Though somewhat captured in the early mitigation studies, this series of tests utilizes a hull/frame combination to represent the vehicle. The hull, or bottom, of the simulated vehicle is responsible for capturing all of the ejecta. The frame, or top, of the simulated vehicle represents where the passengers of an actual vehicle would sit; this is where the accelerometers and tracking targets are placed, as this is the portion of the vehicle for which the mitigation needs to have the most effect. The hull to frame mass ratio is kept close to one. If the mass of the hull is much greater than the

mass of the frame, it can be postulated that that the acceleration of the frame will be very high. On the other hand, if the frame is much more massive than the hull, this set-up might result in unrealistically low acceleration values.

4.1.2 Realism in Mitigation Techniques

Although promising, the first rounds of mitigation techniques were unrealistic. The distance between the bottom and top plate would have resulted in a full-sized vehicle with an absurdly high floor. As such, in this portion of the research the mitigation techniques employed keep realism in mind. For example, instead of using an eight or nine centimeter length tube, the tube length was cut to a maximum (and more realistic) value of five centimeters.

4.1.3 General Test Set-Up

Before going into any detail regarding the test series, it is necessary to describe the general test set-up used for the mitigation study. As previously mentioned, this series of tests employed a hull/frame combination small-scale vehicle. In between the hull and frame, there is at any given time either a series of thin-walled cylinders made from metal of various geometric properties, or air. The combination of the hull and frame resulted in a vehicle mass toward the upper end of the mass curve from the earlier conducted mass study.

It was mentioned previously that there are two methods for setting the SOD of a test plate – the stand-off blocks and hanging the plate from chains. The chains are normally used for heavier plates. For the mitigation tests, a combination of the two methods was used. The first portion of the mitigation study involved creating baseline data where the only air separates the hull and the frame. For these tests, the

hull rested on stand-off blocks and the frame hung on the chains a specific distance away from the hull. In later tests when mitigation was added in between the hull and the frame only one of two SOD scenarios is used.

The first and most common set-up involves attaching the thin-walled cylinders only to the hull. In this situation, as in the air gap tests, the hull rests on the blocks and the frame is lowered on the chains until the frame just makes contact with the thin-walled cylinders. This set-up prevents the stand-off block from supporting too much weight – causing them to sink in the saturated sand and changing the SOD. For a few tests, the thin-walled cylinders are attached to both the hull and the frame. These tests only require the use of the chains to set the SOD of the test plate. Pictures of the three different set-ups can be viewed in Figure 4.1, Figure 4.2, and Figure 4.3. The specifics of how each thin-walled cylinder is made will be given in the test outline portion for each study later in the chapter.
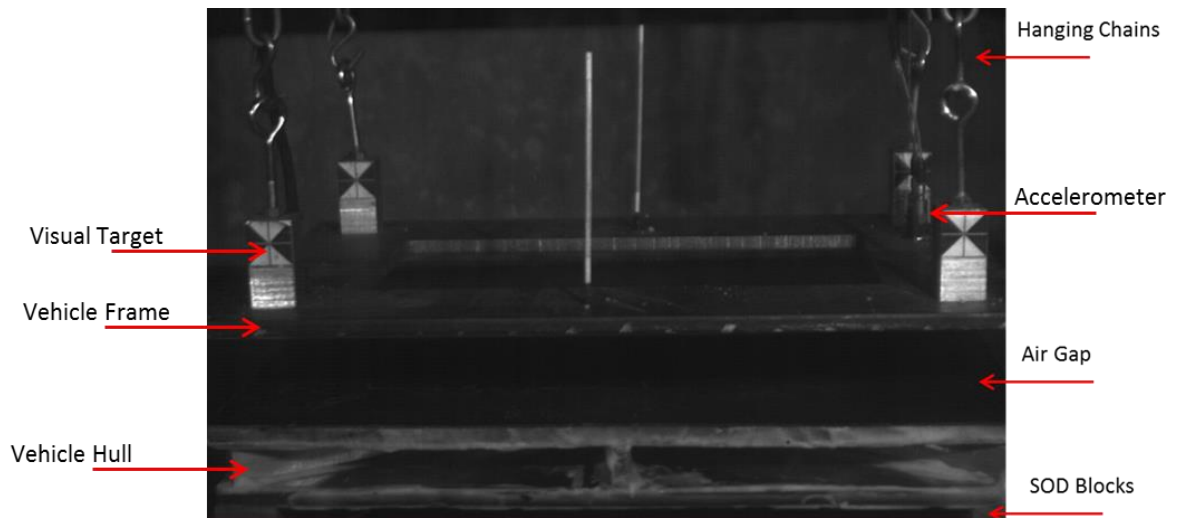
Figure 4.1: Test set-up for no mitigation tests
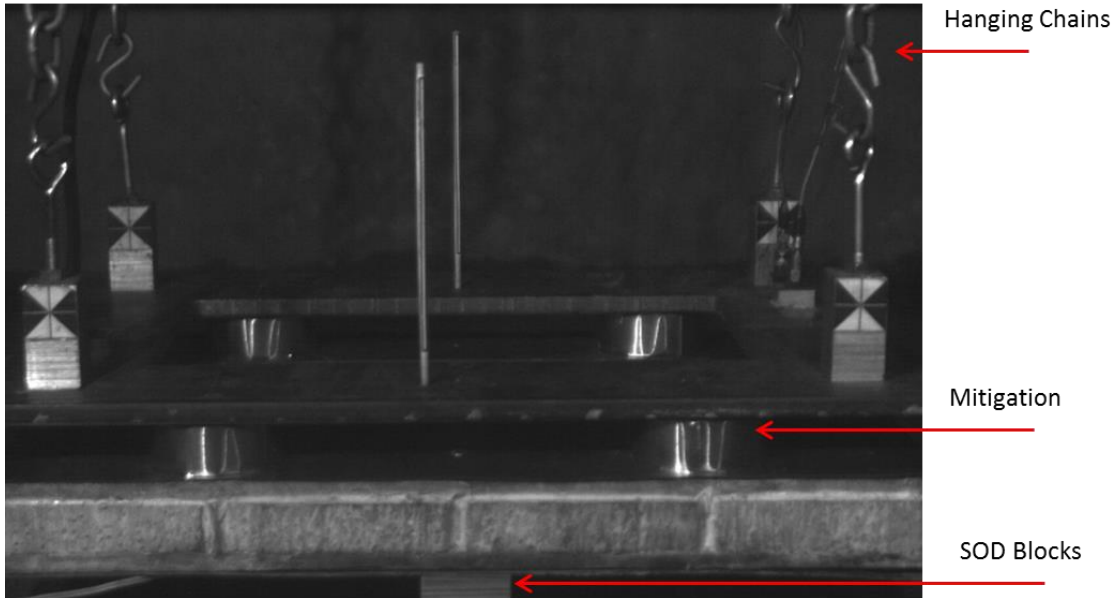
Figure 4.2: Test set-up with mitigation attached to hull only
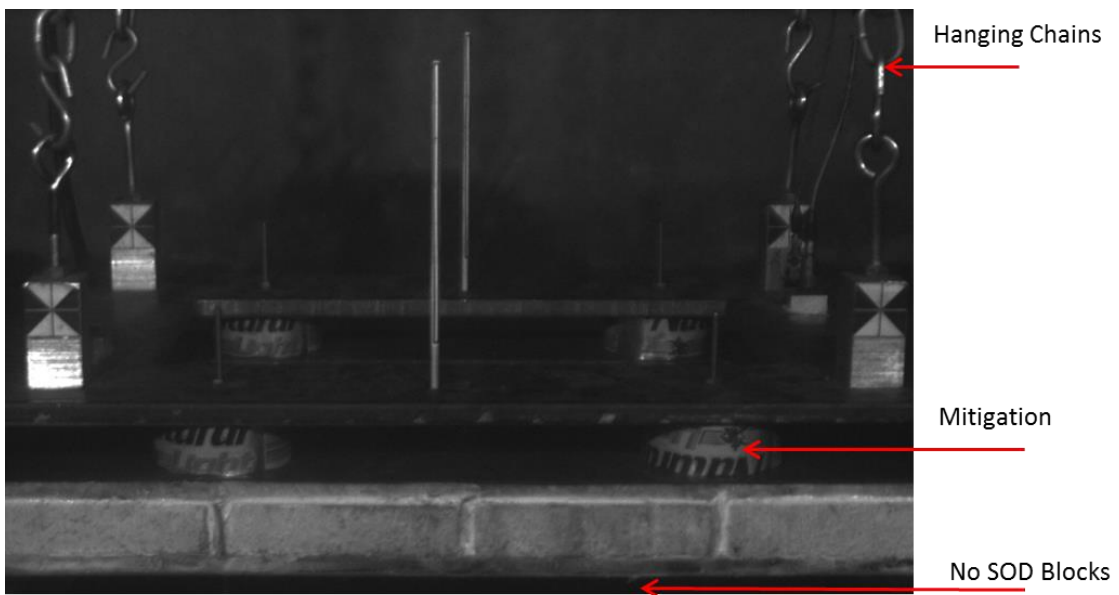
Figure 4.3: Test set-up with mitigation attached to hull and frame

A couple of minor things need to be mentioned in this section. The first is that each test plate will have four targets attached to the frame. One target will be located on each corner of the frame so that it may be tracked using the high speed camera. The second is that each test frame, much like those in the previous studies, will have two or three accelerometers located along a diagonal line connecting the left

front portion of the frame with the rear right portion. These acceleration signals are averaged to give the final readings reported in the results section. The accelerometers and the visual targets can all be seen in Figure 4.1, Figure 4.2, and Figure 4.3.

4.2 The Effect of Hull Vibration on Frame Acceleration

As with the early testing on circular plates, a number of difficulties were encountered at the onset of the mitigation test series. Although cumbersome, they were not without learning opportunities and each difficulty led to a change in the test method. The two primary changes made were a change to the hull construction and mechanical filtering mount for the accelerometers.

4.2.1 Vibrating Versus Non-Vibrating Hull Constructions

The first series of tests run in the mitigation study involved changing the height between the hull and the frame, which will be referred to in this paper at height of target (HOT), with only air separating the two plates. The idea was to determine how much the acceleration on the frame changes as it gets further away from the blast impacted hull. The hull for this initial set of tests was simply a 12.7 millimeter thick aluminum plate with the outer dimensions mentioned previously. It was hypothesized that the acceleration would either decrease marginally or remain the same as the distance between the hull and frame increased. Instead, the curve shown in Figure 4.4 resulted.
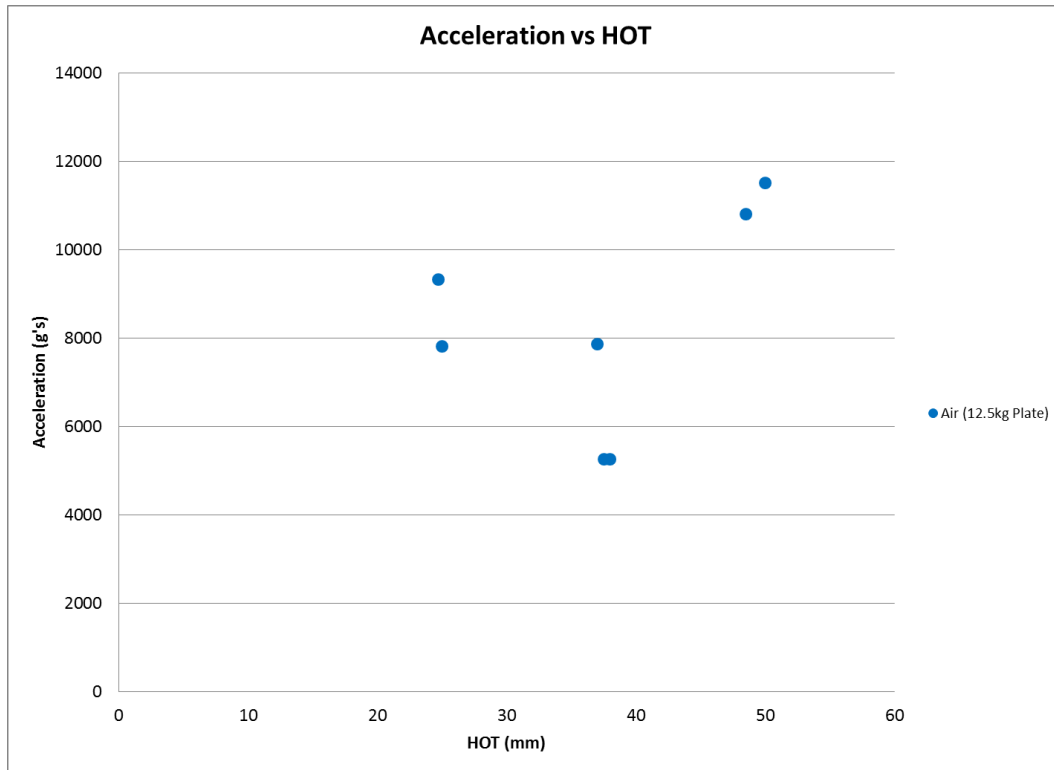
Figure 4.4: Acceleration versus height of target with no mitigation

At this point, and upon close examination of the high speed videos, it was determined that the hull was far too flexible for blast testing. Though plastic deformation of the hull was negligible from test to test, the plate had severe flapping characteristics immediately following the blast, up to the point when it contacted the frame. The same flapping characteristic held true when thin-walled cylinders were added in between the hull and the frame. An example of the flapping plate can be seen in Figure 4.5.

Figure 4.5: Severe flexing of the plain aluminum hull for mitigation tests

When watching the high speed video from a test performed at each HOT, it became clear that a major factor in the acceleration of the frame is at what point in the flapping behavior of the hull the two plates made contact. As such, a stiffer hull needed to be designed to eliminate this effect. Before designing this hull however, a series of tests was run to determine what the acceleration versus HOT should look like for a rigid hull. To this end, a 30.48 centimeter by 30.48 centimeter aluminum plate with a thickness of 5.08 centimeters was substituted for the thin aluminum hull. It was tested at three different HOT values and the true relationship between acceleration and HOT was determined and can be seen in Figure 4.6.
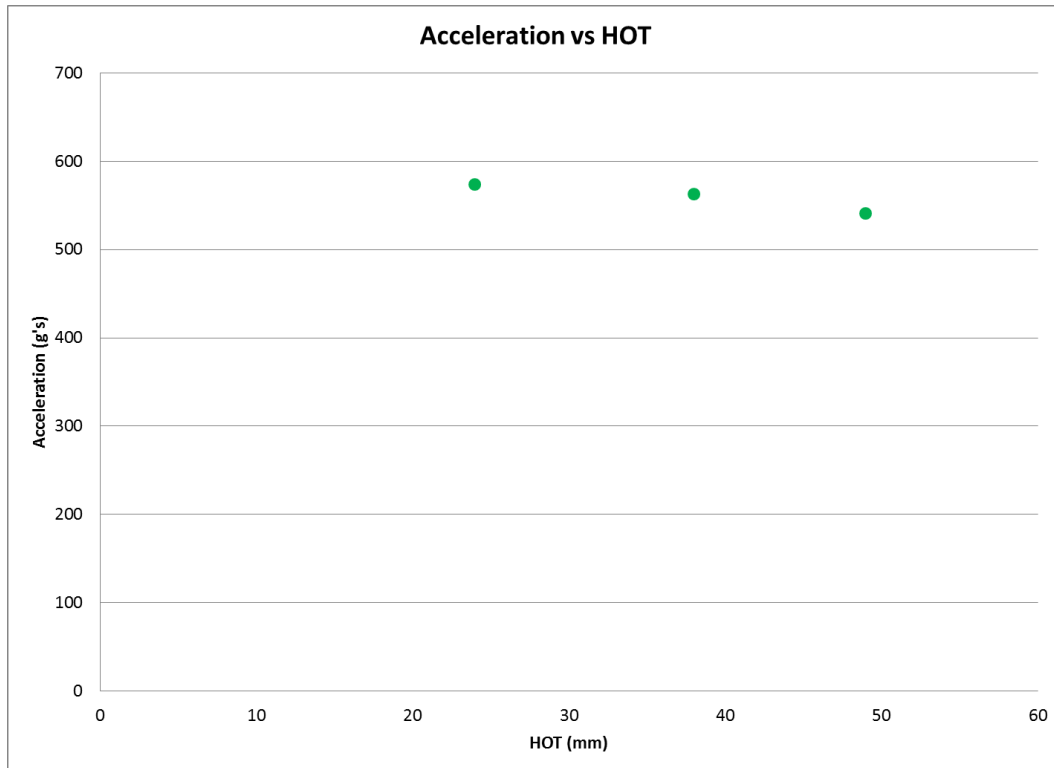
Figure 4.6: Acceleration versus HOT for a rigid hull

It should be noted at this point that the hull of this vehicle was extraordinarily heavy and thus, outside of observing the relationship between the HOT and acceleration, the acceleration values of Figure 4.6 cannot be used in determining frame acceleration on a realistic small-scale vehicle. For this reason they will not be reported as a comparison to studies performed with mitigation. From this figure it can also be noted that the original hypothesis of a slight decrease in acceleration with increasing HOT can be expected.

With this in mind, a number of plate designs were experimented with in hopes that at least a semi-rigid plate that maintained a reasonable mass could be developed. A few of the plates that were tested included aluminum plates separated by metal spars, aluminum/fiberglass composite plates, and carbon fiber composite plates. In the end, a plate was developed that consisted of two carbon fiber plates created by

layering 40 layers of plain-woven carbon fiber fabric with West Systems 105 epoxy as the matrix. To each of these plates, a 1.59 millimeter aluminum sheet was bonded using Hysol 9430 epoxy. These carbon fiber plates were attached to a 12 point star shaped bracing pattern created from 2.54 centimeter tall by 6.35 millimeter wide aluminum spars. The spars were attached to the aluminum sheets on each carbon fiber plate using Hysol 9430 epoxy. Each spar was long enough to travel from the center of the plate out to the edge. To cap it off, foam was placed in the gaps to prevent the plates from vibrating in the open air gaps. A photograph of the final plate is seen in Figure 4.7, although there is some foam missing in this photograph.
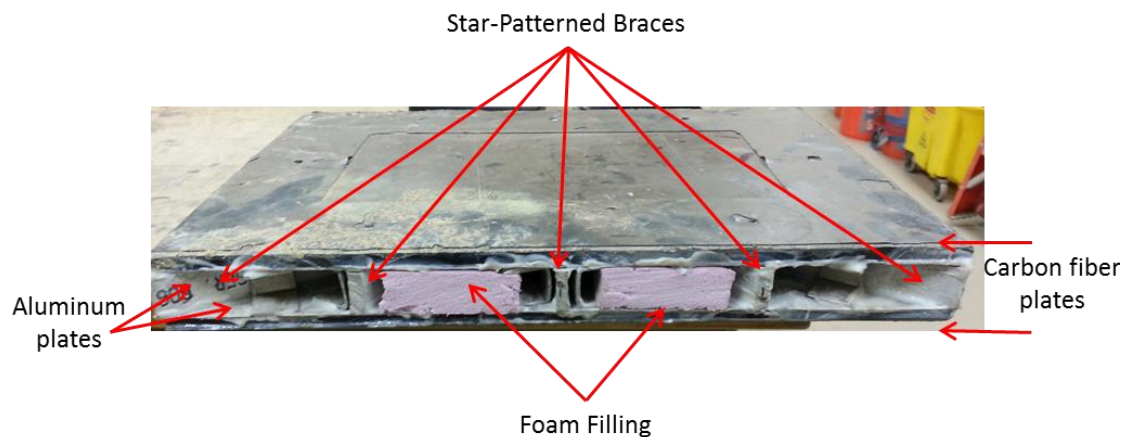
Figure 4.7: Picture of the final hull design

4.2.2 Mechanical Filtering for Accelerometers on Small-Scale Vehicles

The next challenge came as the need to develop a new mechanical filter material for the frame of the simulated vehicle. An effort was initially made to find the vibrational node of the frame, as was done previously with the round plate testing. Referring back to Figure 4.1, Figure 4.2, Figure 4.3, or Figure 4.5, it can be seen that the shape of the frame is a bit more complex. The complex shape of the frame resulted in a complex vibrational shape on which there were no easily identifiable

57

nodes. The acceleration signals obtained from using the metal foam mechanical

filtering pads were extremely noisy with many high frequency vibrations present.

To eliminate the higher frequency vibrations in the frame, a mechanical filter

made of a stiff rubber was developed. It was mentioned earlier that a reason rubber

was not used previously as a mechanical filter was that it visually compressed under

the weight of the accelerometer when experiencing high acceleration levels. To

ensure this was not an issue for the mitigation tests, an aluminum casing was

machined to surround the rubber pad, preventing it from expanding outward if the

accelerometer tried to press it down. This addition to the filter effectively increased

the stiffness in the vertical direction, preventing the rubber from deforming under the

weight of the accelerometer. High speed video was used to carefully examine the

rubber pad to make sure no visual deformation occurred during any of the tests. The

new mechanical filter can be viewed in Figure 4.8.
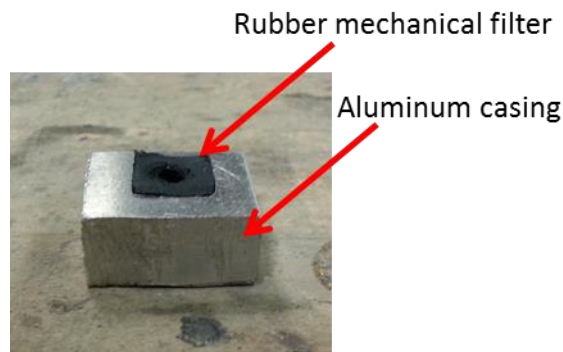
Figure 4.8: Mechanical filter used for mitigation testing

4.3 Height of Target Study

4.3.1 Height of Target Study Test Outline

The first series of complete tests run to study the effect of adding thin-walled

cylinders to mitigate acceleration was executed to determine how changing the height

of the cylinders changes the peak acceleration recorded on the frame. The initial tests in this series were conducted with no mitigation between hull and frame. Following this, four tests were run with standard aluminum beverage cans separating the hull and the frame by distances of 25, 38, and 50 millimeters.

The cylinders for the first round of mitigation tests were attached only to the hull. The second round of mitigation tests consisted of the same geometry cans tested with the cans attached to both the frame and the hull, resulting in an accordion type stretching following the initial crushing. One test was repeated to demonstrate test repeatability. The test matrix can be seen in Table 4-1.

Table 4-1: Test matrix for HOT test study

Test Number	Charge Mass (g)	DOB (mm)	SOD (mm)	# of Cylinders	Cylinder Material	Cylinder OD (mm)	Cylinder ID (mm)	Height of Target (mm)
1	4.4	10	40	-	-	-	-	50
2	4.4	10	40	-	-	-	-	25
3	4.4	10	40	-	-	-	-	38
4	4.4	10	40	4	Aluminum	66	65.8	50
5	4.4	10	40	4	Aluminum	66	65.8	25
6	4.4	10	40	4	Aluminum	66	65.8	38
7	4.4	10	40	4	Aluminum	66	65.8	25
8*	4.4	10	40	4	Aluminum	66	65.8	25
9*	4.4	10	40	4	Aluminum	66	65.8	38
10*	4.4	10	40	4	Aluminum	66	65.8	50
Note: Test numbers with an * were conducted with the cylinders attached to both frame and hull								

In order to create repeatable thin-walled cylinders for this portion of the test, rolls of masking tape were utilized. Each can was carefully taped circumferentially, ensuring the edges overlapped perfectly, with a length of tape having the exact the width of the final height of the can. Tabs were then cut into the exposed portion of the can resulting in crenellations that were later used to secure the can to the hull or frame.

Once the can is prepared, discs with the same outer diameter as the inner diameter of the can are machined out of 3.18 millimeter thick aluminum. These discs are attached via VHB tape to the crenellations of the can and then attached to the hull alone, or the hull and frame of the simulated vehicle. This process can be seen in Figure 4.9.
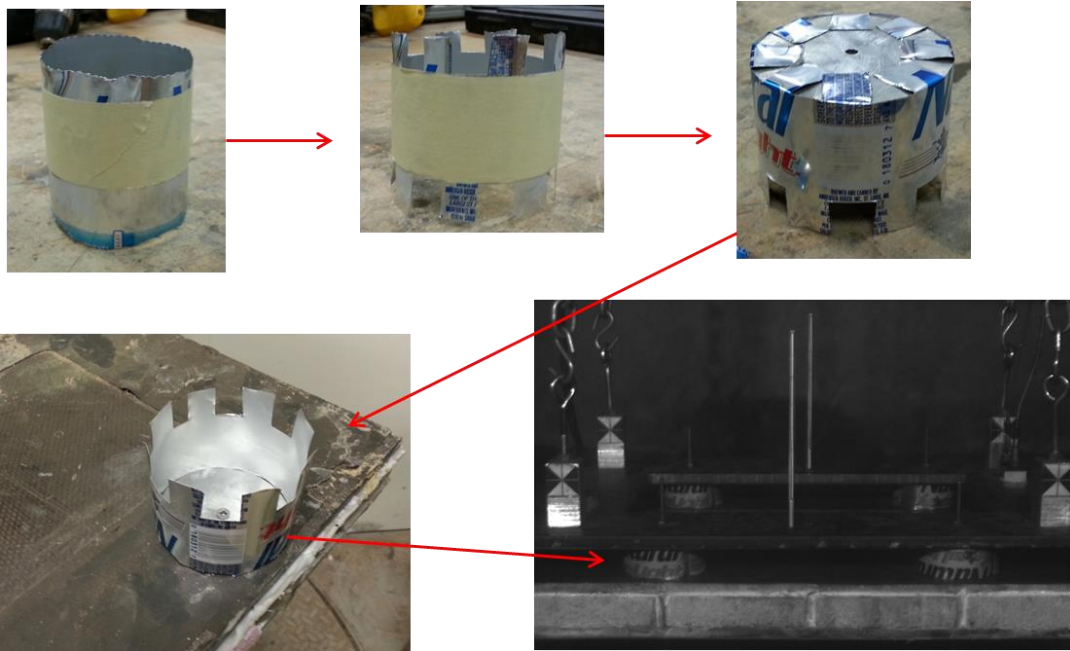
Figure 4.9: The creation and mounting of a thin-walled cylinder

4.3.2 Height of Target Study Test Results

At the end of the test series described in Table 4-1, the acceleration signals were analyzed and averaged for each test. It is of interest to view how the acceleration signal changes from a test with no mitigation, to mitigation attached the hull only, to mitigation attached to both the hull and the frame. A plot of this can be seen in Figure 4.10. This plot compares the signals from the accelerometers from the tests for each scenario at a HOT of 25 millimeters. Following this plot, a full summary is given of how the acceleration changes with HOT for the three different

test scenarios: No mitigation, mitigation attached to the hull, and mitigation attached

to the hull and the frame. This plot is presented in Figure 4.11. A zoomed in view of

the benefit of attaching the cylinders to the frame and the hull can be seen in Figure

4.12.
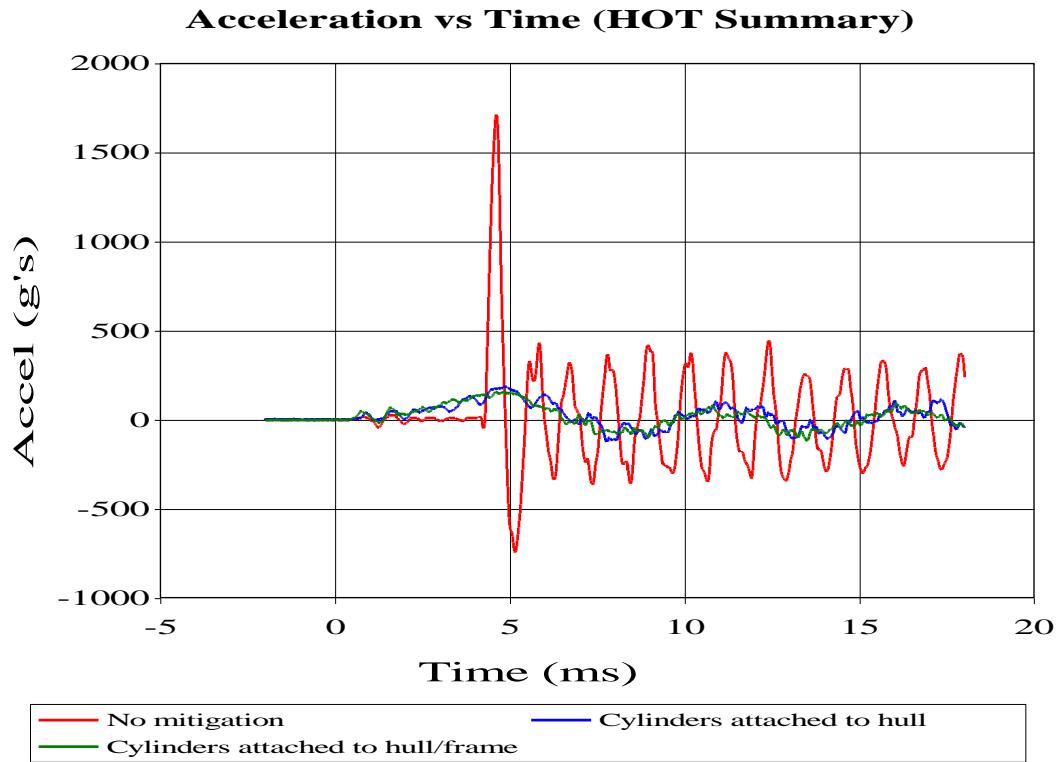
Figure 4.10: Comparison of acceleration signals for HOT study
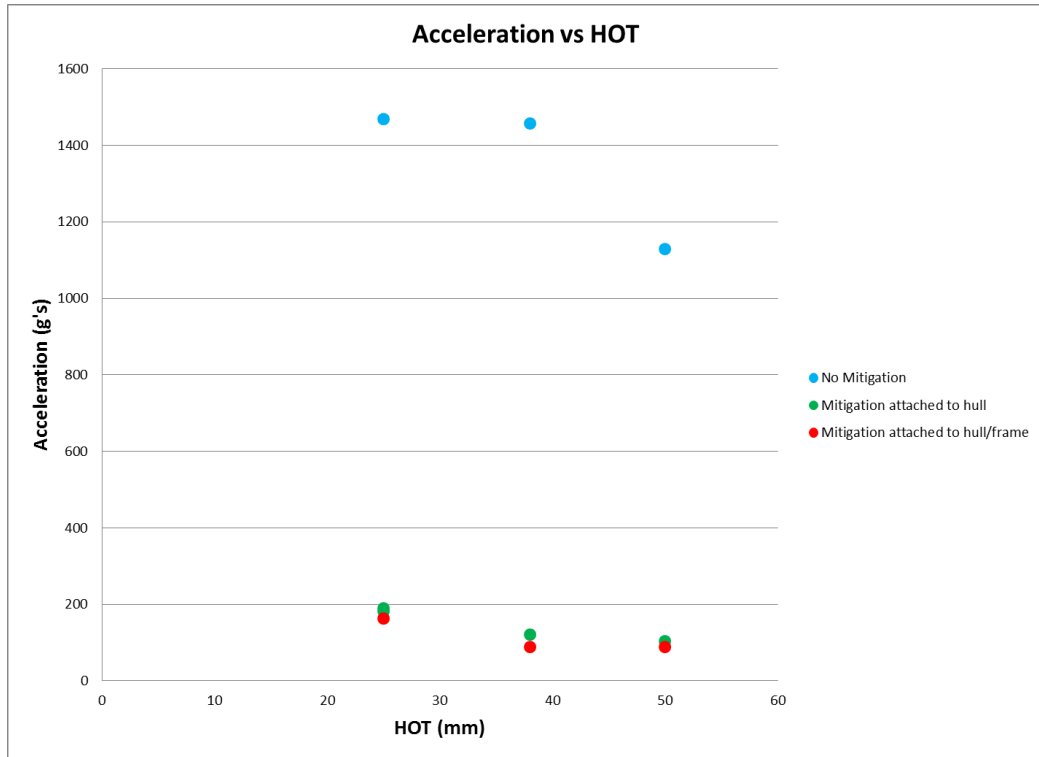
Figure 4.11: Acceleration versus height of target for no mitigation and mitigation
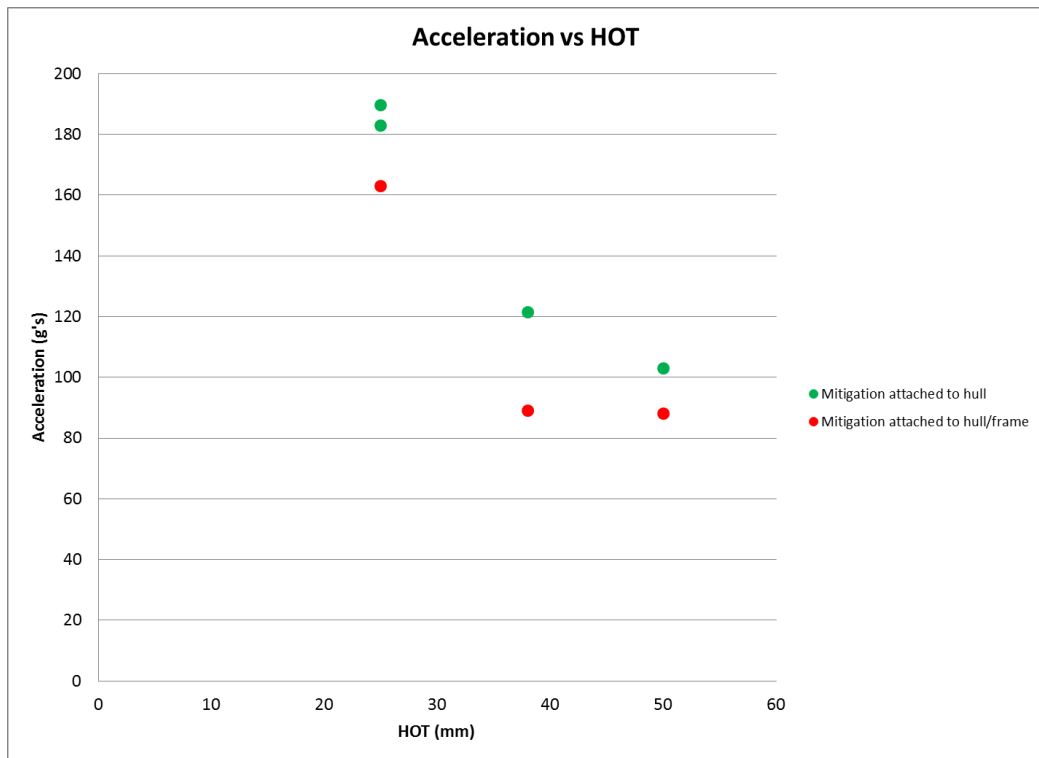
Figure 4.12: The effect of attaching cylinders to the hull and the frame

The next area of concern is how changing the HOT affects the impulse and kinetic energy delivered to the frame. Similar to the preliminary studies, the velocity can be obtained by either finding the slope of the displacement versus time curve developed from analysis of the high speed camera, or by taking the first integral of the acceleration signal. A quick comparison between the peak velocities as obtained by the high speed camera and the integrated accelerometer data can be seen in Figure 4.13.
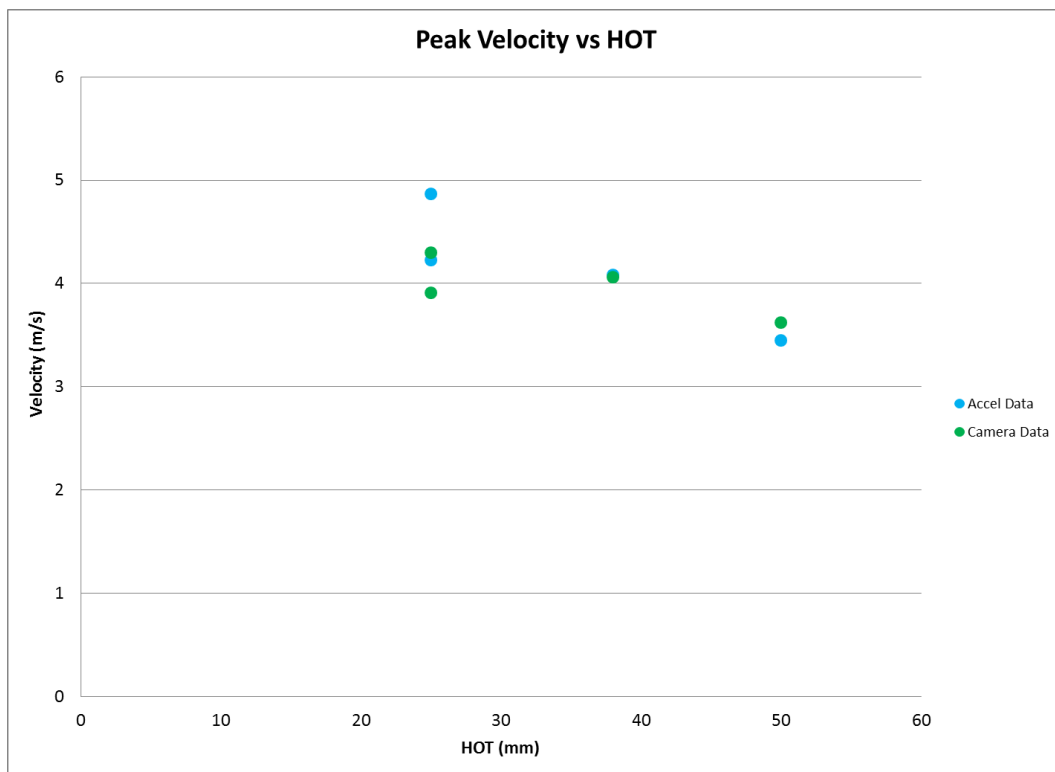
Figure 4.13: Comparison of peak velocity for accelerometer and camera data

The data for Figure 4.13 was taken for test numbers four through seven as seen in Table 4-1. The peak velocities match up very well. As such the impulse and kinetic energy will be reported using the values calculated from the peak velocity obtained from the accelerometer. The impulse and kinetic energy as a function of height of target are displayed in Figure 4.14 and Figure 4.15.

63
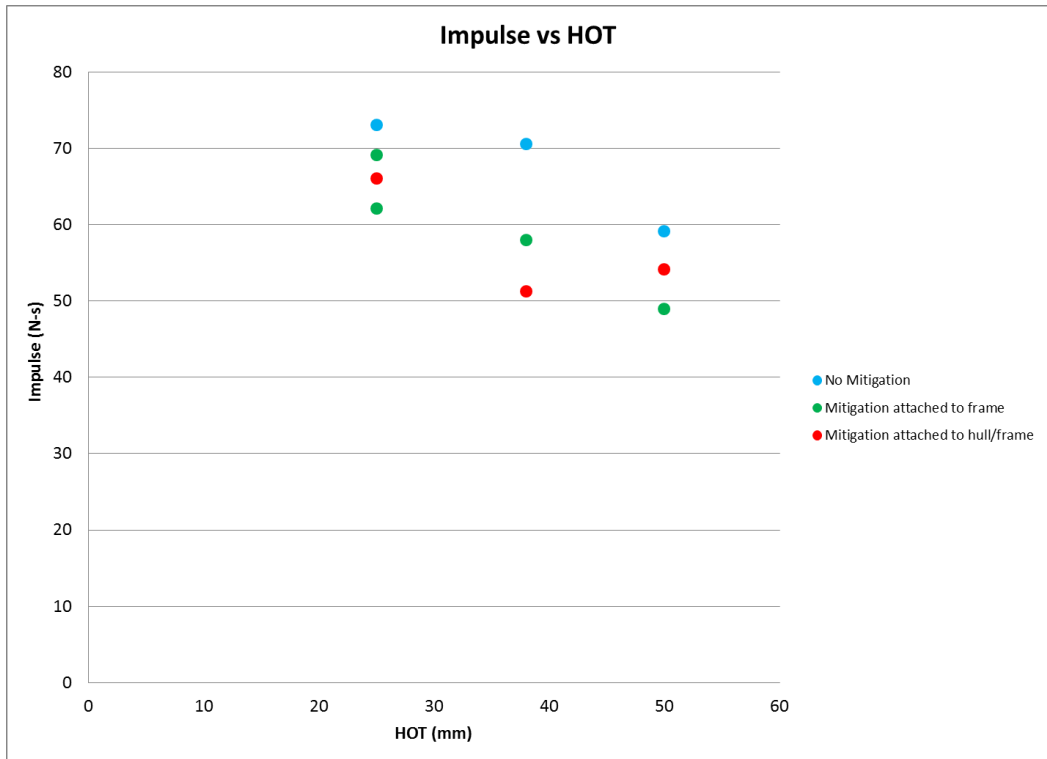
Figure 4.14: Impulse versus height of target
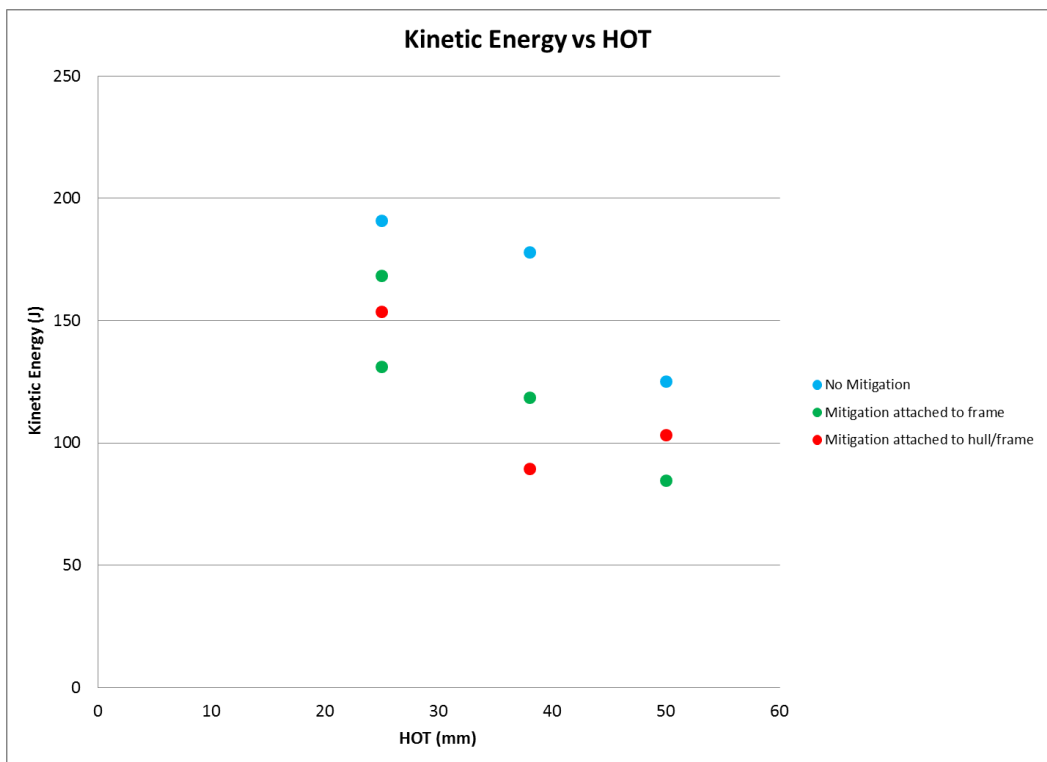
Figure 4.15: Kinetic energy versus height of target

The first and primary take-away from the graphs in this section is that the crushing of thin-walled cylinders as a source of mitigation of acceleration can have a tremendous effect. At a height of target of 25 millimeters, the peak frame acceleration is decreased from close to 1500g's to around 190g's. Going a step further, if the cylinder height is increased by a factor of two, and the accordion stretching of the cans is added to the initial crushing by attaching the can to the frame, the acceleration level can be decreased to around 90 g's.

To put this into perspective, using the cube-root scaling law and scaling this result up to full-scale, for this series of testing, in the worst case scenario (no mitigation, 25 centimeter HOT full-scale) a passenger would experience an acceleration of 150g's – a fatal level. Using the hull/frame attached cans at a HOT of 50 centimeters full-scale, a passenger in the vehicle would experience around 9g's. This is around the same level of acceleration experienced by a fighter pilot in an ejection seat.

The next take-away from this series of tests comes as the realization that the impulse and kinetic energy levels also benefit from the addition of thin-walled cylinders as mitigation. It appears that a 10-20 percent drop in impulse can be expected at each HOT. The same trend hold true for kinetic energy with the drop being on the neighborhood of 20-35 percent.

4.4 Number of Thin-Walled Cylinders Study

The next series of tests is aimed at determining how the addition of more thin-walled cylinders separating the hull and the frame affects the acceleration levels of the frame. During this series of tests the number of cylinders is incrementally

increased to determine this effect. In addition, impulse and kinetic energy are studied as a function of cylinder number.

4.4.1 Number of Thin-Walled Cylinders Study Test Outline

In order to determine the effect of adding more cylinders between the hull and the frame, a test series was run for four different scenarios. Initially a control test containing no cylinders was run. After which the number of cylinders was increased to four, then six, then eight. A summary of the important test parameters is listed in Table 4-2. Each test will be run with the cylinder attached only to the hull.

Table 4-2: Test matrix for the number of thin-walled cylinder study

Test Number	Charge Mass (g)	DOB (mm)	SOD (mm)	# of Cylinders	Cylinder Material	Cylinder OD (mm)	Cylinder ID (mm)	Height of Target (mm)
Control	4.4	10	40	0	-	-	-	25
1	4.4	10	40	4	Aluminum	66	65.8	25
2	4.4	10	40	6	Aluminum	66	65.8	25
3	4.4	10	40	8	Aluminum	66	65.8	25

As can be seen in Table 4-2, the thin-walled cylinders used for this study are of the same outer diameter and wall thickness of the cylinders used for the HOT study. Namely, a typical aluminum beverage can is used. It was decided to test the worst-case HOT in every instance for this study. This decision was made for two reasons. The primary reason for determining that a 25 millimeter height of target should be used comes as the fact that vehicles in the field face situations where vehicle roll-over is a very real concern. To combat this, it is often desired that the vehicle center of gravity be as low as possible. By testing the 25 millimeter high cylinders, a determination of the effectiveness of the mitigation techniques for a low center of gravity vehicle can be made.

Another reason for testing the 25 millimeter cylinders comes as the fact that the acceleration levels of the 50 millimeter HOT tests are simply too low to be easily measured. Upon examining the acceleration signals from the 50 millimeter HOT tests (Figure 4.16) it is not too difficult to imagine that the peak acceleration comes from the low frequency vibrations of the frame as opposed to a sharp acceleration peak resulting from hull to frame contact. Because of the extremely low acceleration levels of the 50 millimeter HOT, a more effective study of the effect of increasing the number of cylinders can be made at the 25 millimeter HOT. A comparison of the two different HOT test accelerations can be seen in Figure 4.16.
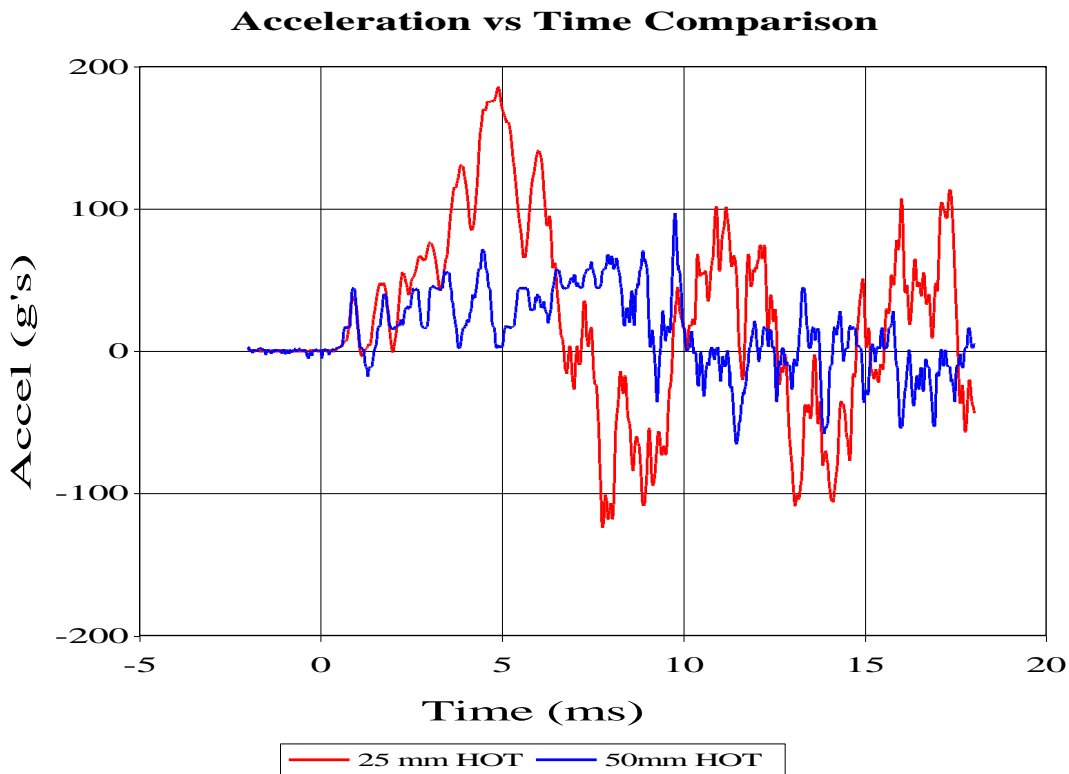
Figure 4.16: Comparison of acceleration signals for 25mm HOT and 50mm HOT

Before launching into the results of the number of cylinder study, the placement of cylinders should be expanded upon. For the four cylinder test, the

cylinders were place at equal intervals along the longer portion of the frame. When the number of cylinders increased to six, two cylinders were added to the mid-way point along the shorter sides of the frame. At eight, two additional cylinders were added in between the two cylinders along the long portion of the frame. A picture detailing the placement can be seen in Figure 4.17.
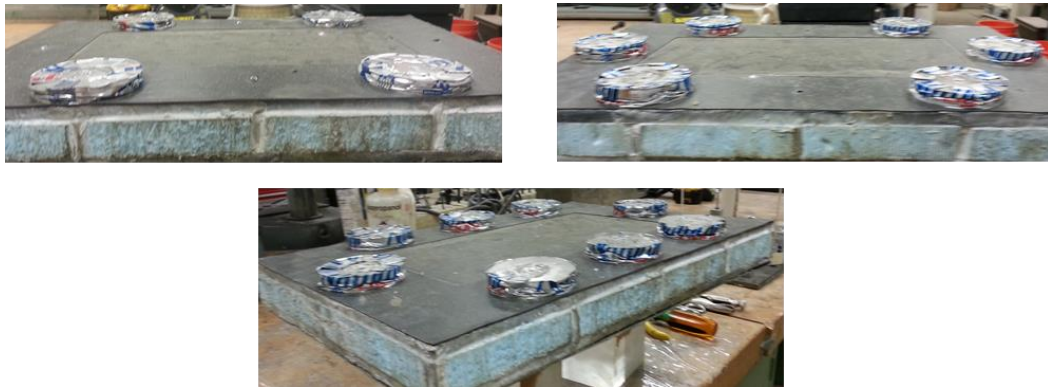
Figure 4.17: Cylinder placement for four, six, and eight cylinder tests

4.4.2 Number of Thin-Walled Cylinders Study Test Results

One of the initial interesting results coming from increasing the number of cans happens to be the general shape of the acceleration pulse. From looking at the test with four cylinders separating the hull and the frame, it appears as if there is a strong element of low frequency frame vibration that adds an element to the acceleration signal. When the cylinder number increases, that low frequency vibration seems to be eliminated. An illustration of this is seen in Figure 4.18. The red signal represents the four can test, with the blue and green signals representing six and eight cans respectively. After the initial peak acceleration, the four can test has a substantial vibration signal at a defined frequency. This vibratory characteristic does not appear in either of the other tests.

Accel vs Time (# of Can Comparison)
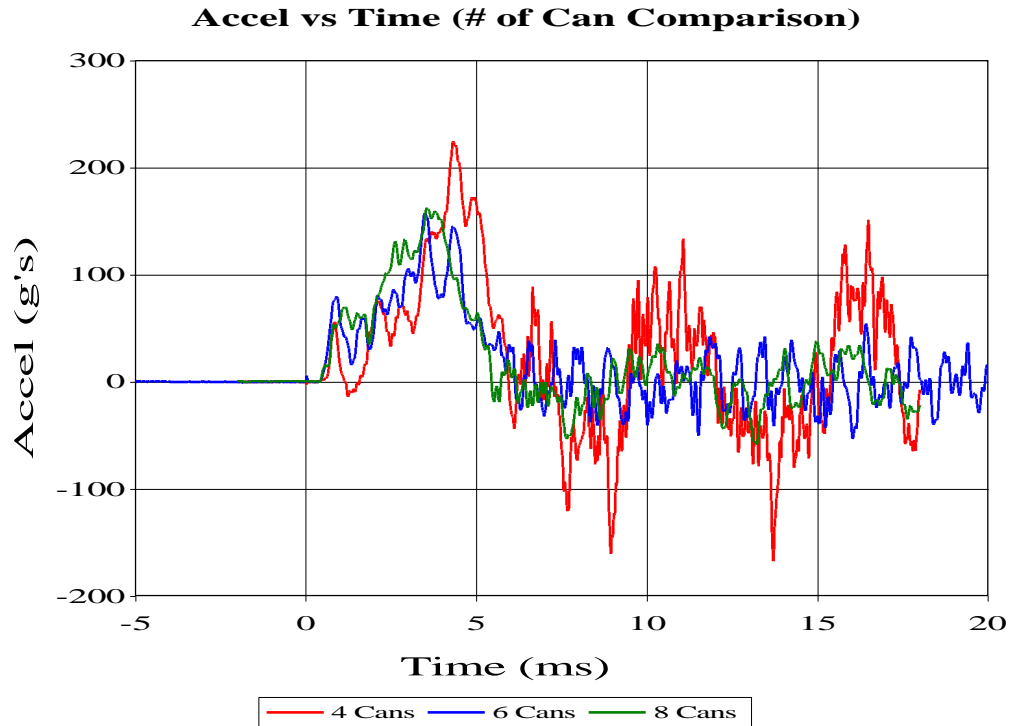
Figure 4.18: Comparison of acceleration signals for four, six, and eight cans

   The overall effect of increasing the number of cylinders is also presented here. As in other tests, the average peak acceleration for each test is determined and plotted versus number of cans. In addition to the acceleration, the effect on impulse and kinetic energy is also reported. As in the HOT study, the velocities used to determine impulse and kinetic energy are determined by the first integration of the acceleration signal. A summary of this study can be seen in Figure 4.19, Figure 4.20, and Figure 4.21.
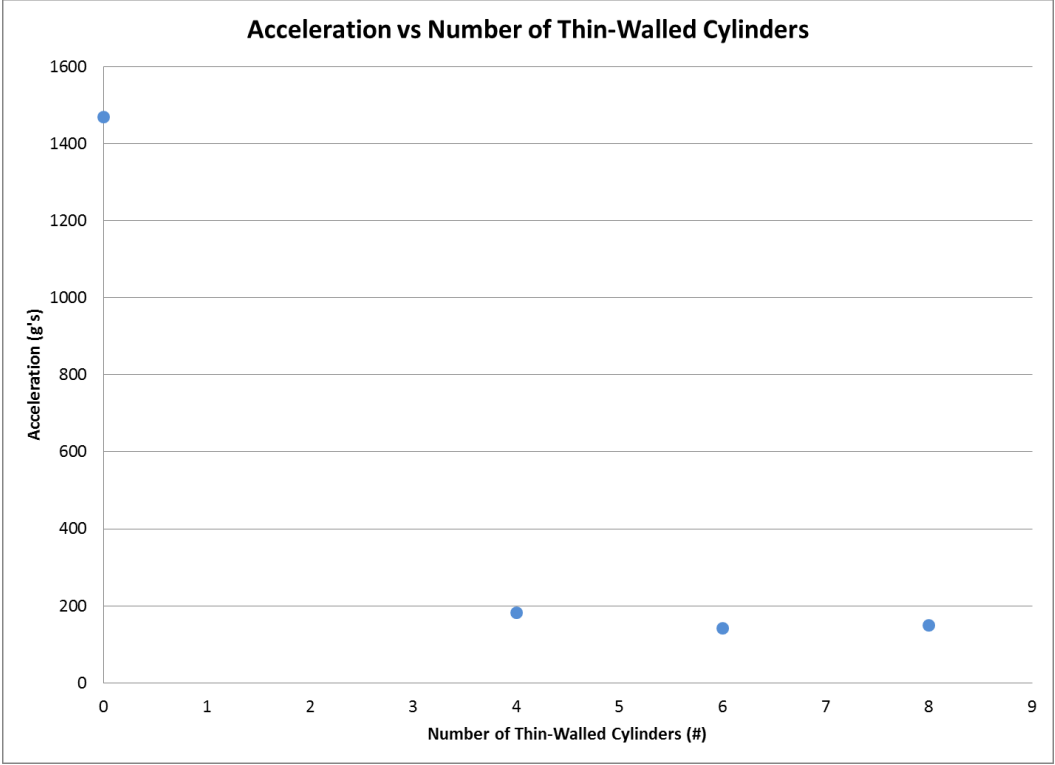
Figure 4.19: Acceleration versus number of thin-walled cylinders
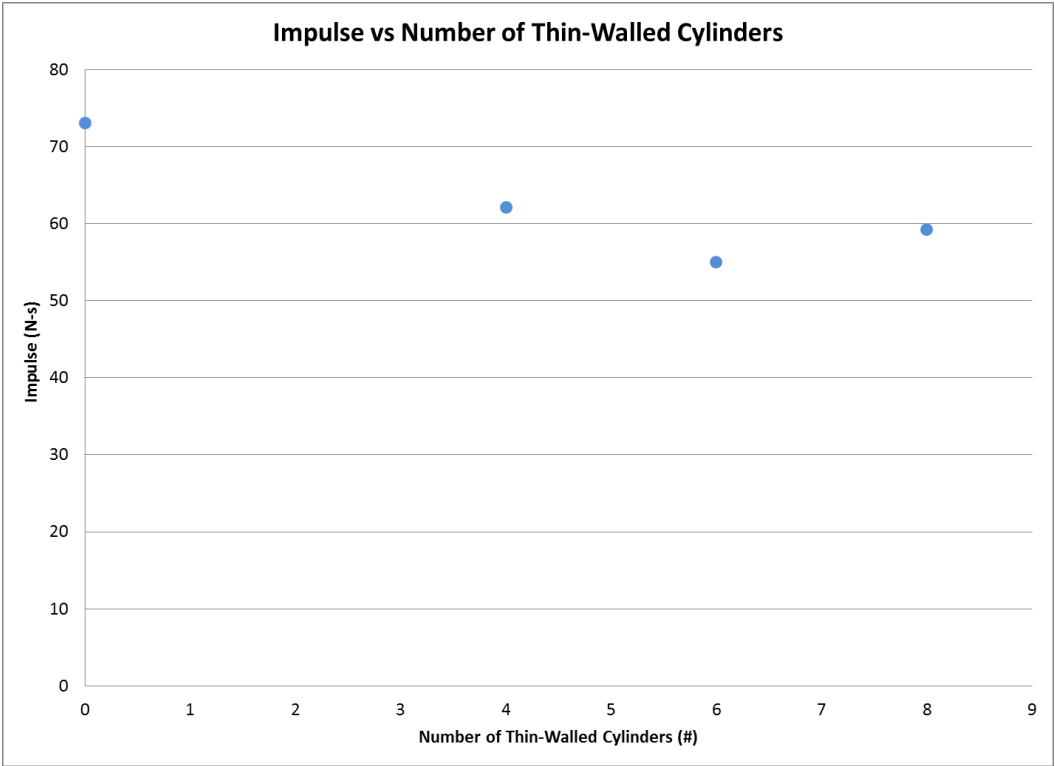
Figure 4.20: Impulse versus number of thin-walled cylinders
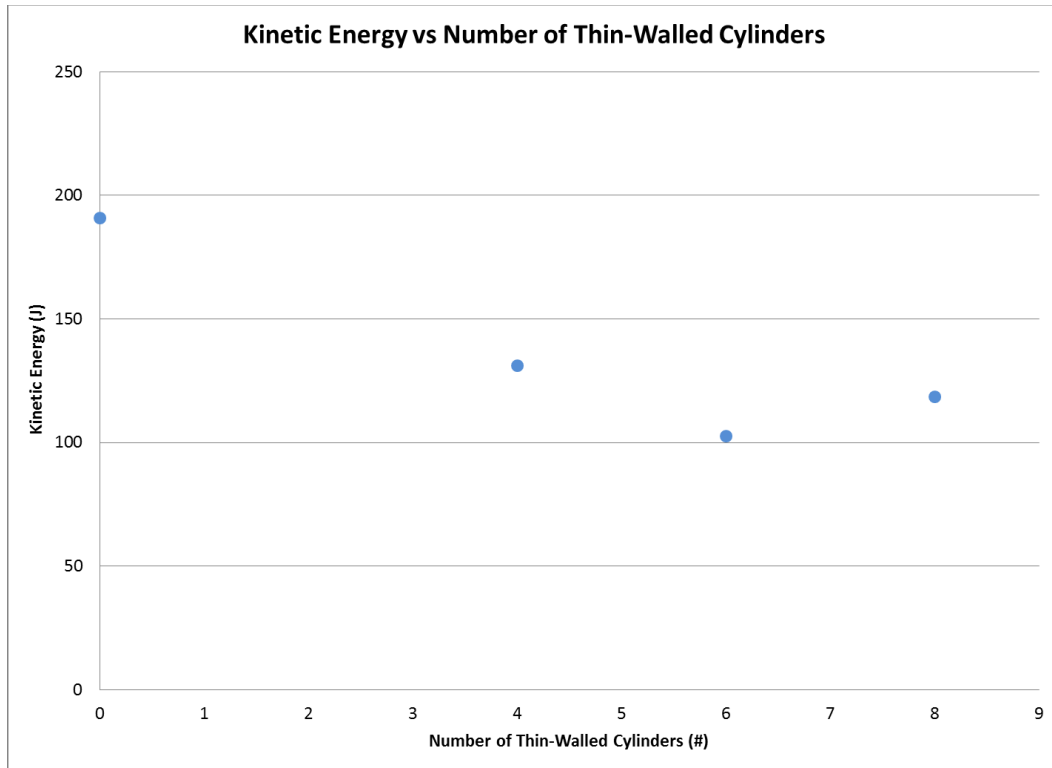
Figure 4.21: Kinetic energy versus number of thin-walled cylinders

From looking at Figure 4.19, Figure 4.20, and Figure 4.21 some general remarks should be made. It appears as if there is a slight benefit to be realized in peak acceleration by increasing the number of cylinders to six and eight. Full-scale acceleration levels decrease from around 18 g's to somewhere in the neighborhood of 14 to 15 g's. While not a drastic drop the benefit is definitely there. Additionally, as mentioned previously, it looks like increasing the number of cans may damp out low frequency frame vibration; significantly reducing the duration of time a passenger might experience high levels of acceleration.

As an added benefit of introducing more thin-walled cylinders to a vehicle as acceleration mitigation, impulse levels and kinetic energy also dip. A maximum decrease in impulse of approximately 25 percent occurs during the six cylinder test.

A similar drop in kinetic energy is seen, though the magnitude of the decline is closer to 45 percent.

4.5 Outer Diameter Study

The next series of tests is aimed at determining how changing the outer diameter of the thin-walled cylinder affects the acceleration levels of the frame. During this series of tests the outer diameter of the cylinders was increased and decreased from the previously tested cylinder size to determine this effect. In addition, impulse and kinetic energy were also studied as a function of cylinder outer diameter.

4.5.1 Outer Diameter Study Test Outline

To study the effect of an increased and decreased outer diameter of the mitigating cylinders, a series of four tests was run. In this series, in addition to the control test where no mitigation was present, tests were run with the outer diameter varying from 53 to 73 millimeters. The cylinders used for this test are beverage containers having the same wall thickness made from the same material, but of different outer diameters. The test matrix can be viewed in Table 4-3.

Table 4-3: Test matrix for outer diameter study

Test Number	Charge Mass (g)	DOB (mm)	SOD (mm)	# of Cylinders	Cylinder Material	Cylinder OD (mm)	Cylinder ID (mm)	Height of Target (mm)
Control	4.4	10	40	0	-	0	0	25
1	4.4	10	40	4	Aluminum	66	65.8	25
2	4.4	10	40	4	Aluminum	73	72.8	25
3	4.4	10	40	4	Aluminum	53	52.8	25

As in the number of thin-walled cylinder study, a height of target of 25 millimeters is used for this series of tests; for the same reasons as listed in that

section. From examining Table 4-3, it should also be noted that only four cylinders were used in each of these tests. For each cylinder, an aluminum disc was cut matching the inner diameter of each cylinder. These discs serve as the top and bottom caps for the cylinders, creating an identical mounting technique for each test. This is shown back in Figure 4.9. The discs also help maintain the thin-walled cylinders' circular shape, as the cylinders tend to deform when the crenellations are cut into the sides and folded over. The final note before discussing test results is that the cylinders were only mounted to the hull.

4.5.2 Outer Diameter Study Test Results

As in the previous series of tests, the first comparison between the separate tests of this series will be of the actual acceleration signals. When comparing the three tests with cylinders it is seen that each acceleration signal has the same low frequency vibrations present. This backs up the previous hypothesis that, when excited from the four points of contact of the thin-walled cylinders, the frame vibrates at a low frequency resulting in a relatively high acceleration level. The acceleration signals are seen in Figure 4.22. The red line represents the smallest outer diameter, the blue line represents the middle outer diameter size, and the green line portrays the acceleration envelope of the simulated vehicle frame that utilized the cans with the largest outer diameter.

Accel vs Time (Outer Diameter Comparison)
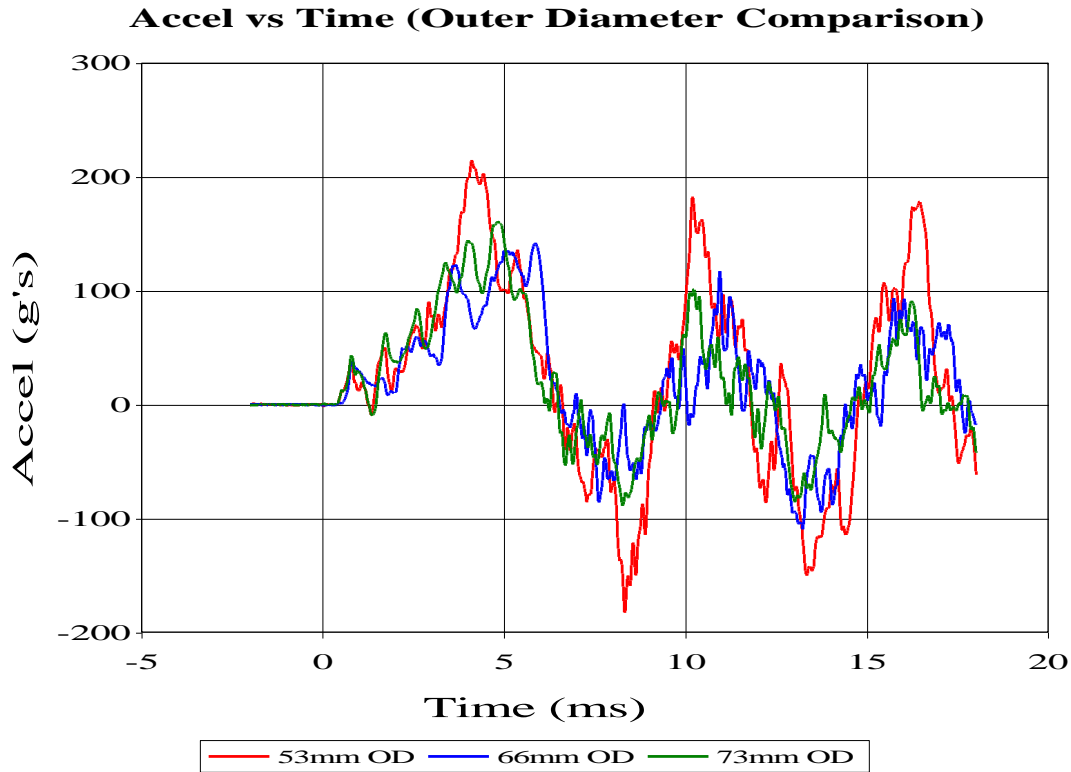
Figure 4.22: Acceleration signal comparison for outer diameter study

It is now necessary to look at the overall trend in average peak acceleration

obtained from each test. The peak impulse and kinetic energy will also be reported

for completeness. The velocity used to calculate impulse and kinetic energy was

determined from the first integration of each accelerometer signal. The results are

displayed in Figure 4.23, Figure 4.24, and Figure 4.25.
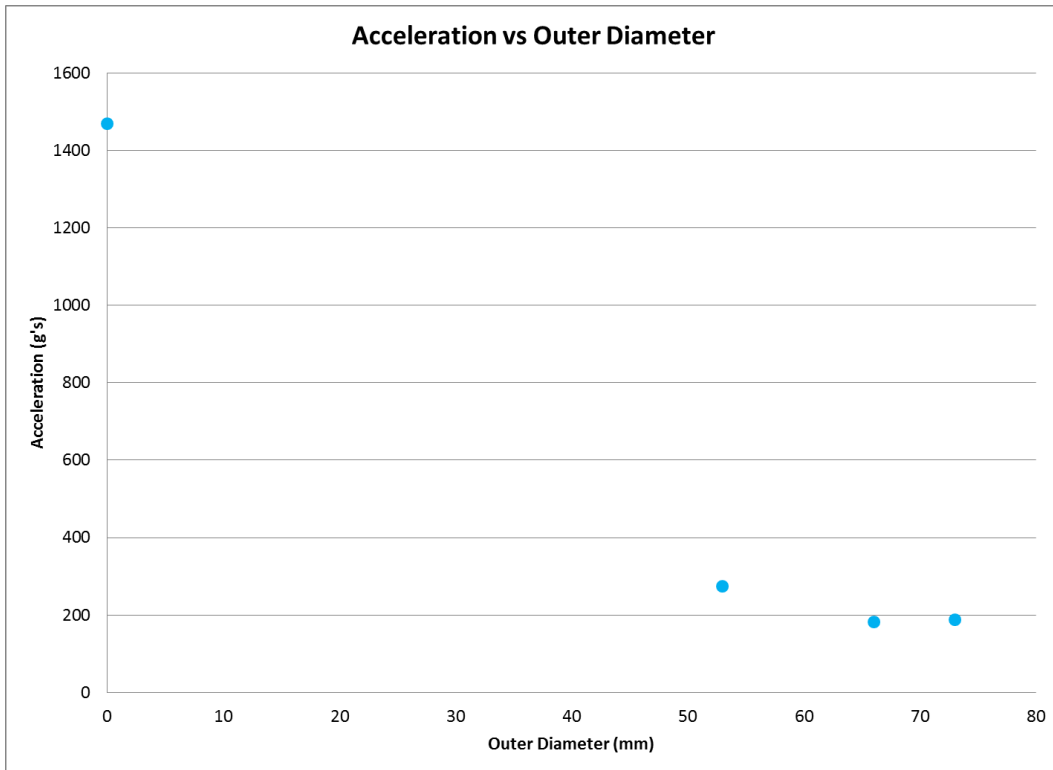
Figure 4.23: Acceleration versus outer diameter of mitigation cylinders
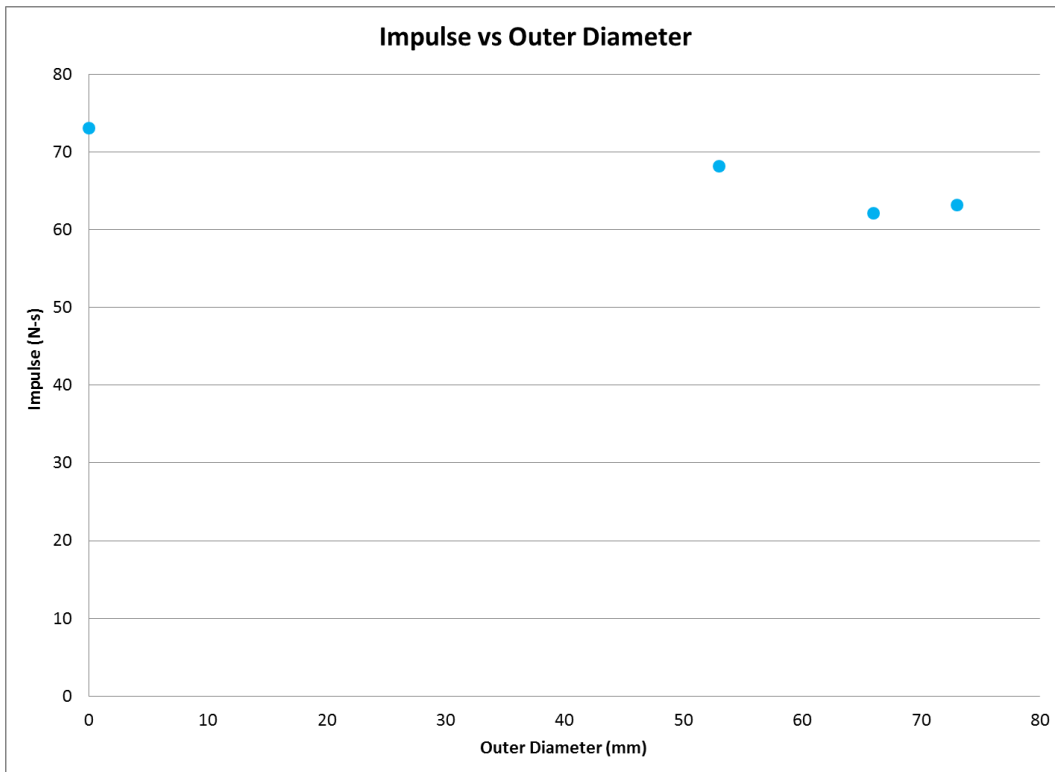
Figure 4.24: Impulse versus outer diameter of mitigation cylinders
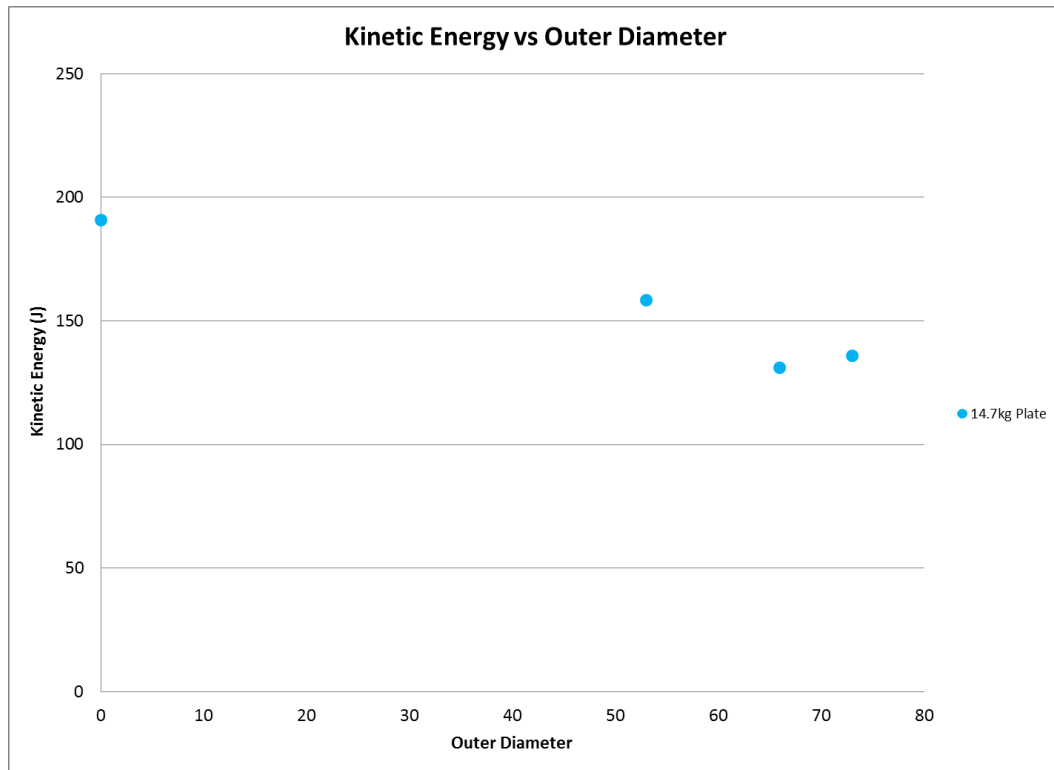
Figure 4.25: Kinetic energy versus outer diameter of mitigation cylinders

After examination of Figure 4.23, Figure 4.24, and Figure 4.25 a few

observations are in order. Starting with the graph displaying acceleration, it is seen

that at the 53 millimeter outer diameter, the acceleration of the frame decreases from

the baseline value of 1470 g's to around 275 g's. The sharp decline of acceleration

continues at 66 millimeter outer diameter where the acceleration drops to around 180

g's. After which it appears as if the acceleration value levels off somewhat, and a

drastic change is not noted when moving from a 66 millimeter outer diameter to a 73

millimeter outer diameter. The same trend is noted with the impulse and kinetic

energy. The values of each actually increase slightly from the 66 millimeter case to

the 73 millimeter case.

4.6 Wall Thickness Study

76

The final complete series of mitigation tests is aimed at determining how changing the wall thickness of the thin-walled cylinder affects the acceleration levels of the frame. During this series of tests the wall thickness of the cylinders is increased from the previously tested cylinder size to determine this effect. In addition, impulse and kinetic energy is also studied as a function of cylinder wall thickness.

4.6.1 Wall Thickness Study Test Outline

To test the effect of wall thickness on acceleration, impulse, and kinetic energy levels, the test preparation is a bit more involved. In previous tests, beverage cans with the necessary geometric characteristics were used as the mitigation material. This provided a cylinder, uniform in wall thickness, with a seamless construction. Beverage cans of varying wall thicknesses could not be found, so thin-walled cylinders of varying wall thicknesses had to be constructed.

The thin-walled cylinders created for this series of tests consisted of aluminum alloy 1100/1145 shim stock ordered from McMaster Carr, and the VHB tape from 3M. The shim stock was cut using a razor blade to the required dimensions, and a 13 millimeter wide strip of VHB tape placed at the end of the length of metal. The other end of the metal strip was then pressed onto the VHB tape creating a cylinder of uniform thickness, disregarding the thicker area at the 13 millimeter wide overlap of the shim stock. The shim stock in contact with the VHB tape was superficially prepared using sandpaper and rubbing alcohol to ensure a strong bond so that when crushed, the can would not split at the seam. A series of pictures portraying the method of can construction is shown in Figure 4.26.

77

Figure 4.26: Process of creating thin-walled cylinder from shim stock

The initial test of this series involved replicating a previously performed test, but this time performing the test with a shim stock cylinder as opposed to a commercially made cylinder. In addition to this comparison, two additional tests were completed with different wall thicknesses from the original test. The test matrix for the wall thickness study can be seen in Table 4-4.

Table 4-4: Test matrix for wall thickness study

Test Number	Charge Mass (g)	DOB (mm)	SOD (mm)	# of Cylinders	Cylinder Material	Cylinder OD (mm)	Cylinder Wall Thickness (mm)	Height of Target (mm)
Control	4.4	10	40	0	-	0	0	25
1	4.4	10	40	4	Aluminum (commercial)	66	0.1	25
2	4.4	10	40	4	Aluminum (shim)	66	0.1	25
3	4.4	10	40	4	Aluminum (shim)	66	0.15	25
4	4.4	10	40	4	Aluminum (shim)	66	0.2	25

From the test matrix note that these test were performed at a height of target of 25 millimeters; done for previously stated reasons. Also, for each of the tests only four thin-walled cylinders were used for mitigation. The cylinders were only attached to the hull and not the frame.

4.6.2 Wall Thickness Study Test Results

Before delving into the effects of wall thickness on acceleration, impulse, and kinetic energy, the results from the two tests run comparing commercially produced aluminum cans to the shim stock cans will be analyzed. It was observed that the VHB tape held together perfectly during the tests and no splitting of the shim stock cans at the seam occurred. The cans crumpled as effectively as a commercially produced can as well. The test results for acceleration and velocity from the first integration of the acceleration are shown in Table 4-5.

Table 4-5: Test results for commercial versus shim stock cylinders

Test Number	# of Cylinders	Cylinder Material	Cylinder OD (mm)	Cylinder Wall Thickness (mm)	Height of Target (mm)	Avg Peak Accel (g's)	Avg Peak Velocity (m/s)
1	4	Aluminum (Commercial)	66	0.1	25	183	4.225
2	4	Aluminum (Shim)	66	0.1	25	182.75	4.235

From looking at Table 4-5 it is very clear that the thin-walled cylinders produced from shim stock and VHB tape perform the same as the commercially produced, seamless cans. As such the test series studying the effects of wall thickness can be directly compared to the tests studying the effects of height of target, number of cans, and outer diameter. It is also beneficial in that, as will be seen later, cylinders from other materials might be made in a similar method and compared to the earlier mitigation studies.

The next graph will highlight the differences in the acceleration signal. Similar to the instance when the number of cylinders was increased, as the wall thickness increases, the low frequency frame vibration seems to diminish. Though not as drastic of a damping effect as increasing the number of cans, it is still

recognizable. The easiest way to highlight this low frequency frame vibration damping effect is to study the Fourier Spectra for each of the three wall thicknesses. Refer to Figure 4.27 to witness the weakening of the low frequency frame vibrations as the walls of the cylinder become thicker.

FFT Comparison ~ Wall Thickness Study
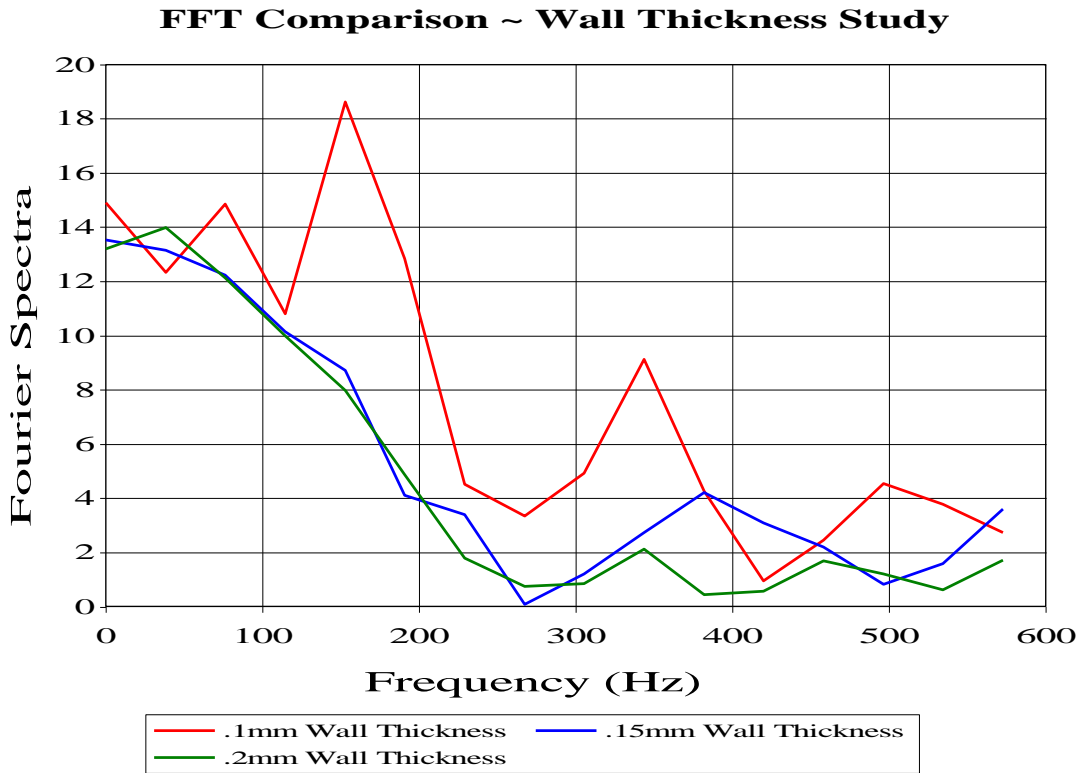
Figure 4.27: Fourier Spectra comparison for tests in the wall thickness study

In addition to the dampening of the low frequency frame vibrations, it appears as if increasing the wall thickness of the mitigation cylinders hold other benefits as well. To illustrate, the plots showing the acceleration, impulse, and kinetic energy of the frame for all of the tests performed are reported here. As in the previous test series, the velocity is taken from the first integral of the accelerometer output. Figure 4.28, Figure 4.29, and Figure 4.30 display the three test outputs as a function of increasing wall thickness of each mitigation cylinder.
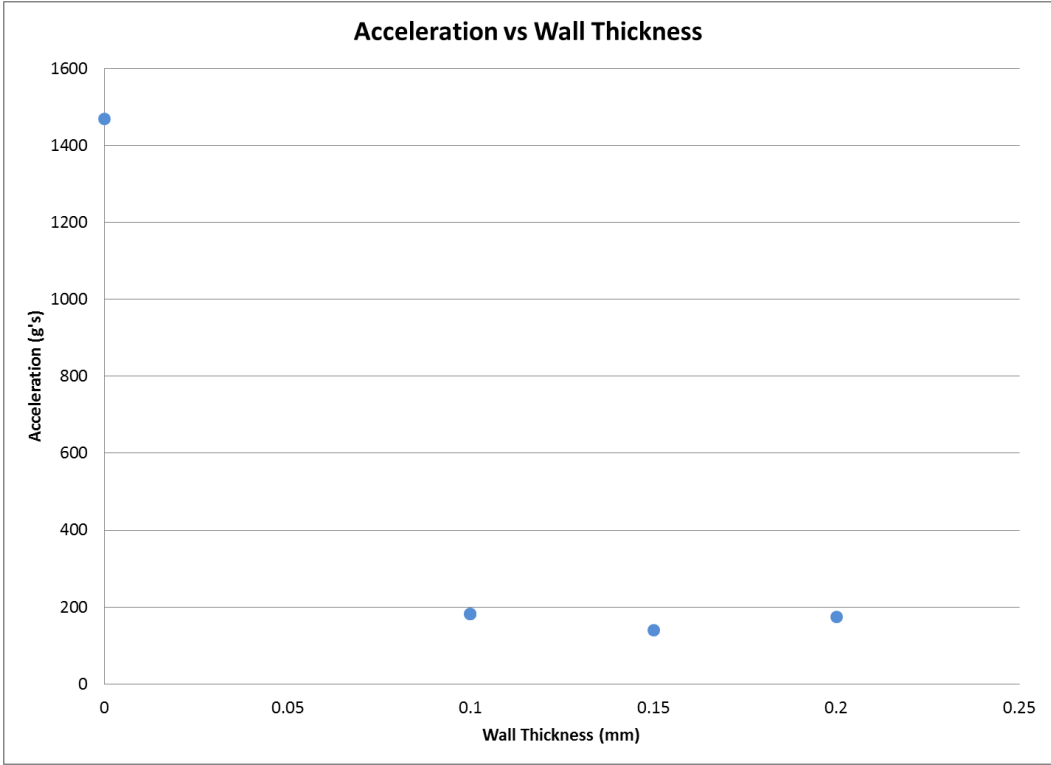
Figure 4.28: Acceleration versus wall thickness of mitigation cylinders
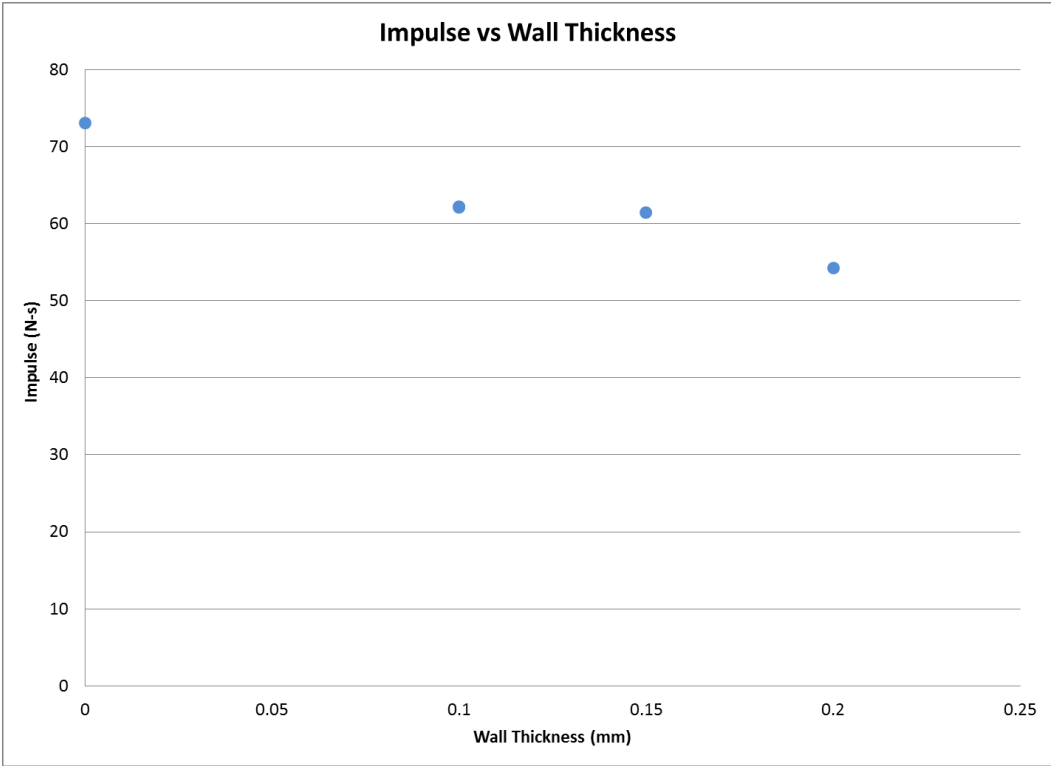
Figure 4.29: Impulse versus wall thickness of mitigation cylinders

81
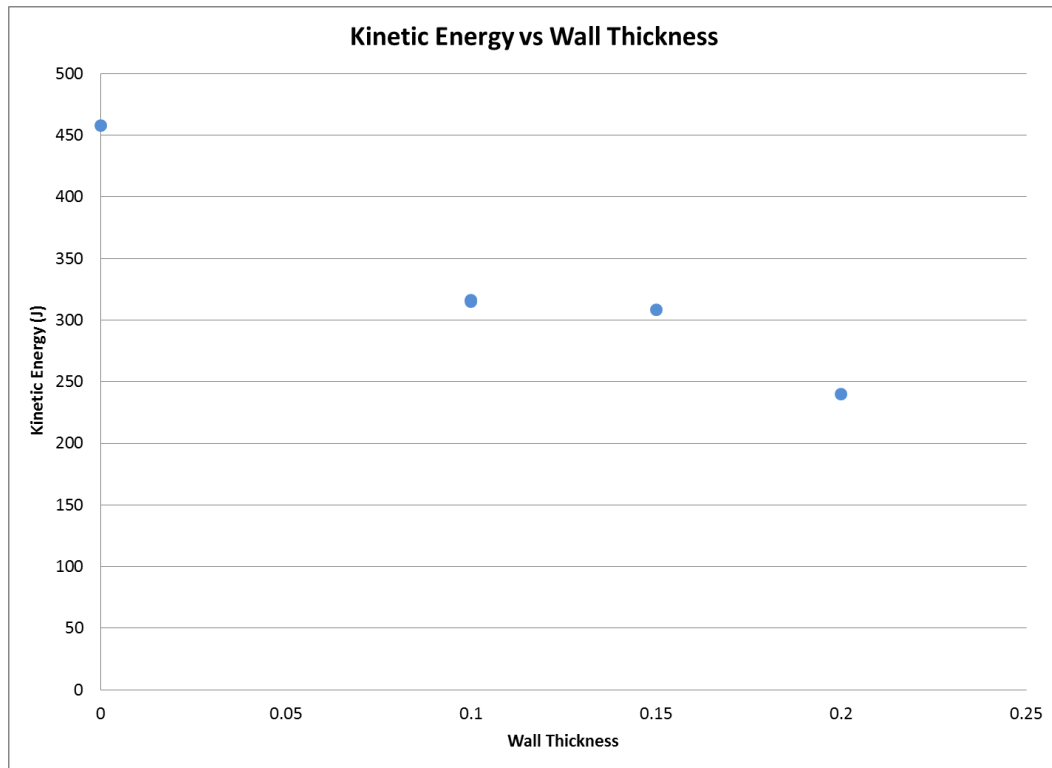
Figure 4.30: Kinetic energy versus wall thickness of mitigation cylinders

The initial indication from viewing Figure 4.28 is that the cylinder wall thickness has little notable effect. A minor decrease in acceleration accompanying the increase in wall thickness from .1 to .15 millimeters is directly followed by an increase of the same magnitude with an increase in wall thickness from .15 to .2 millimeters. Going further however, one finds a benefit in increasing the wall thickness. For the impulse and kinetic energy, each value decreases steadily with each increase in the thickness.

The final result stemming from the wall thickness study comes as a visual observation. After each test the cylinders are inspected to make sure no tearing of the can occurred. At this point it was noted that the cans crushed in significantly different ways as the wall thickness increased. Pictures of each platform of cylinders (post-test) are shown in Figure 4.31. From these photos it is noted that the .1

millimeter thick cylinders crushed completely with many folds in the material. The .15 millimeter can underwent semi-complete crushing with nice folds in the material as well. At the point when the wall thickness reached .2 millimeters, it is noted that the cylinder does not undergo complete crushing and that there are a few larger areas on the surface of the can that show little or no plastic deformation.
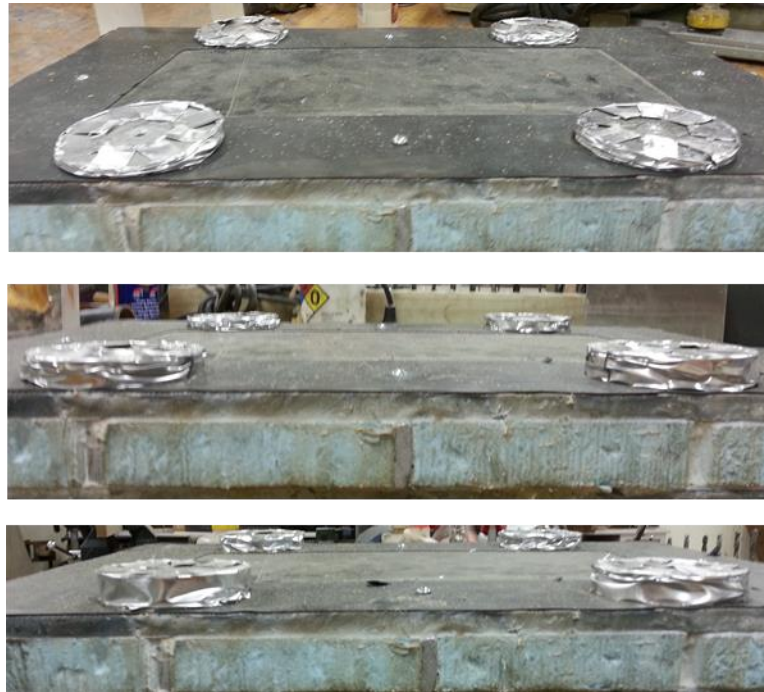
Figure 4.31: Crushing characteristics of .1mm (top) .15mm (middle) and .2mm (bottom) wall thickness cylinders

4.7 Cylinder Material Study

The next series of tests conducted was very brief. The series aimed at viewing the effects of changing the metal material of the thin-walled cylinders. To achieve this, a steel cylinder with the same wall thickness and outer diameter as the aluminum cylinders was created using the shim stock method described above. The test results are shown below in Table 4-6.

Table 4-6: Test results for cylinder material study

Test Number	# of Cylinders	Cylinder Material	Cylinder OD (mm)	Cylinder Wall Thickness (mm)	Height of Target (mm)	Avg Peak Accel (g's)	Avg Peak Velocity (m/s)
1	4	Aluminum (shim)	66	0.1	25	183.0	4.2
2	4	Steel (Shim)	66	0.1	25	203.3	3.8

From viewing the results in Table 4-6, it is seen that the difference between the two types of cylinders is minor. Due to the fact that the steel cylinders did not make a remarkable difference, for better or for worse, it was decided to spend effort studying other areas as opposed to creating cylinders out of various other materials. This concludes the portion of the research involving using thin-walled cylinders for mitigation of acceleration, impulse, and kinetic energy on small-scale vehicles.

4.8 Mitigation Study on Small-Scale Vehicle Tests Summary

This chapter mainly focused on the effects of changing the geometrical properties of thin-walled cylinders to study each effect on the mitigation of acceleration. Before this was done, it was shown that the hull flexibility can play a great role in the resulting frame vibration. Each of these tests was conducted on a small-scale vehicle shape utilizing a semi-rigid hull. Geometrical realism was kept in mind when determining the shape and size of the vehicle and the mitigation components.

The first series of tests in this chapter determined the effect of changing the HOT, from 25 millimeters to 50 millimeter by increments of 12.5 millimeters, on acceleration, impulse, and kinetic energy of the simulated vehicle. Three series of tests were run at each HOT: one with air in between the hull and the frame, one with thin-walled cylinders attached the hull as mitigation, and one with thin-walled

cylinders attached to the hull and the frame (resulting in a stretching of the cylinder after the initial crushing) as mitigation.

For this study it was found that by adding a thin-walled cylinder in between the hull and the frame, the acceleration decreased to an average of ten percent of the acceleration experienced by the frame with air separation. If the cylinder was attached to the hull and the frame, the acceleration values dropped to an average of 80 percent of the acceleration experienced by the frame with the cylinder attached only to the hull. A near-linear decline in acceleration values was noted for the mitigation tests where the acceleration values decreased by 50 percent when the HOT changed from 25 millimeters to 50 millimeters.

When the HOT changed with air separating the hull and the frame, the impulse of the maximum HOT was 80 percent of the minimum HOT. With cylinders in place, the impulse at the highest HOT was around 75 percent of the impulse at the lowest HOT. The average impulse values when mitigation was present were 85 percent of the impulse values when air separated the hull and the frame. Attaching the cylinders to the hull and the frame as opposed to just the hull does not seem to have an appreciable effect.

The kinetic energy changed in a similar way as the HOT increased. As HOT increased with air, the largest HOT was 65 percent of the kinetic energy of the smallest HOT. With cylinders in between the hull and the frame, the maximum HOT was 56 percent of the minimum HOT. When adding cylinders to the vehicle, the kinetic energy values were, on average, 70 percent of the value of the kinetic energy when only air was present. As with the impulse values, attaching the cylinders to the

hull and the frame (as opposed to only the hull) does not seem to affect kinetic energy. It was also seen in this section that the velocity as obtained by the integration of the accelerometer signal correlates very well with the velocity calculated from the slope of the displacement/time curve when tracking the visual targets on the frame using high speed video.

The next section focused on the changes in acceleration, impulse, and kinetic energy of the simulated vehicle when the number of thin-walled cylinders increased from four to eight in increments of two. It was initially noted that as the number of cylinders increased, the low frequency frame vibrations shown in the accelerometer signal became less pronounced. In addition to this result, with six cylinders attached to the hull, the best case acceleration value resulted and was ten percent of the acceleration value with no mitigation present. With six cylinders used as mitigation, the impulse decreased to 75 percent of the value of impulse resulting from a test with no mitigation. A larger decrease in kinetic energy of approximately 50 percent occurred when using six cylinders as opposed to no mitigation.

When studying the effect of changing the outer diameter of the cylinder, the acceleration values seem to depend much more on this variable. It seems as if smaller diameter cylinders do not perform as well as larger diameter cylinders. The acceleration of the two larger diameter cases studied were around 12 percent of the acceleration value for no mitigation. The impulse on the other hand did not see as drastic of a change as it did in the series where the number of cylinders was increased; the largest outer diameter cylinder had an impulse of 85 percent of the impulse value obtained with no mitigation. The kinetic energy of the simulated

vehicle with the largest outer diameter cylinders was only 70 percent of the kinetic energy from the test with no mitigation.

The final series of tests studied the effect of changing the wall thickness of the cylinders. Wall thicknesses of .1, .15, and .2 millimeters were each tested. Similar to the case where the number of cylinders was increased, the low frequency frame vibration becomes less pronounced as the wall thickness of the cylinder increases. The acceleration value is smallest when the wall thickness of the cylinder is .15 millimeters thick, and is only ten percent of the acceleration value with no mitigation present. The minimum impulse occurs at a wall thickness of .2 millimeters and is 73 percent of the maximum value of impulse when no mitigation is present. Similarly, the kinetic energy is lowest for a cylinder wall thickness of .2 millimeters and is 52 percent of the maximum kinetic energy value reported when no mitigation is present. Steel cylinders were also tested and were found to have no major effect on acceleration, impulse, and kinetic energy values.

Chapter 5 – Polyurea Study

5.1 Introduction/General Information

This section of this research aims at developing a better understanding of the effects of polyurea coatings structures subjected to dynamic loading. Initially, cantilevered beams coated in polyurea were tested using a high-pressure gas gun. These tests were followed by tests of polyurea coated thin-walled cylinders used as a mitigating technique under blast loads.

5.1.1 Polyurea Information

The polyurea used for this portion of the research is manufactured by Specialty-Products, Inc. and is designated HM-VK. It is an ultra-high strength hand-mixable polyurea elastomer. This specific polyurea was chosen for its high gel-time of 18 minutes and lower viscosity. These two properties allow the polyurea to be used in a mold to accurately create test specimens for this study. A description of the dry properties of the polyurea (as obtained from the HM-VK technical data sheet) is shown in Table 5-1.

Table 5-1: Polyurea dry properties for HM-VK [27]

DRY PROPERTIES @ 125 mils (1.67 mm)*	
Tensile Strength ASTM D412	6671 PSI (46.36 mpa) Average
Elongation ASTM D412	506% Average
Hardness (Shore A) ASTM D2240-81	95 (0s)
Hardness (Shore D) ASTM D2240-81	48 (0s)
Modulus 300% ASTM D412	1395 psi (9.7 mpa)
Service Temperature	-30°F - +250°F (-34°C - +121°C)

5.1.2 Polyurea-Beam Molding Process

The molding process mentioned previously should be described in more detail before moving on to the specific polyurea studies. Throughout the cantilever beam testing regime, it was required to apply different thicknesses of polyurea to steel beams. In order to control the thickness of each polyurea coating, a molding process was used. The mold used to control the thickness of the polyurea consists of two portions. The first portion contains four, 2.54 centimeter square cross sectioned, steel bars connected such that the cavity in the middle of the bars creates a space where a beam may be set without any gaps between the beam and the walls of the mold. On the bottom of the four steel bars, a 6.35 millimeter steel sheet is attached via machine screws to create a level platform on which the steel bar may be laid. The second portion of the mold is dubbed the press. The press is simply a piece of aluminum machined so that a pre-determined height of the aluminum bar can be inserted into the mold forcing excess polyurea to exit and controlling the height of the polyurea that will be left to coat the beam. A visualization of the mold is shown in Figure 5.1.
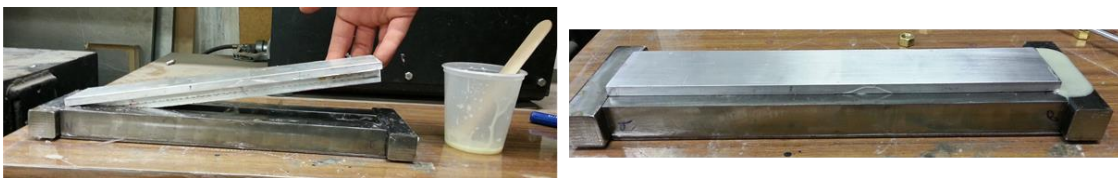
Figure 5.1: The open (left) and final pressed (right) configuration of the polyurea mold

Each cantilever beam is prepared the same way for each test. Initially the beam of specific dimensions is superficially prepared by grinding the surface on which the polyurea is to be poured. The surface is then cleaned with isopropyl alcohol to remove any residual oils and heated with a heat gun. These steps are taken to ensure a strong and proper bond between the polyurea and the metal. All surfaces

of the mold are treated with a water/ethane homopolymer mold release agent to prevent the polyurea from bonding to the mold. The beam is then placed in the treated mold. The proper portion of each component of the polyurea mixture (1:4 – A:B by weight) is measured out in a plastic cup using an electronic scale. Once thoroughly mixed, the polyurea is poured onto the hot surface of the beam. The press portion of the mold is then placed into the mold component housing the beam/polyurea and pressed down until the lip of the aluminum bar contacts the upper surface of the steel portion of the mold. The mold is left alone for at least 12 hours before being taken apart and releasing the newly coated metal beam.

5.1.3 Accelerometer Mounting for Cantilever Beam Testing

In addition to being viewed by high speed camera, each beam test was conducted with an accelerometer mounted to the end of the beam for data collection purposes. As with the other portions of this research, the accelerometer mounting technique proved to be challenging. Initially, the metal foam mounting pad set-up shown in Figure 3.5 was used to mount the accelerometer to each beam. This test set-up, however, proved to be ineffective. When double integrated, the displacement curve from the accelerometer signal did not match up with the displacement signal developed by tracking a target placed on the tip of the beam. Instead, the signal had very odd characteristics as seen in Figure 5.2.
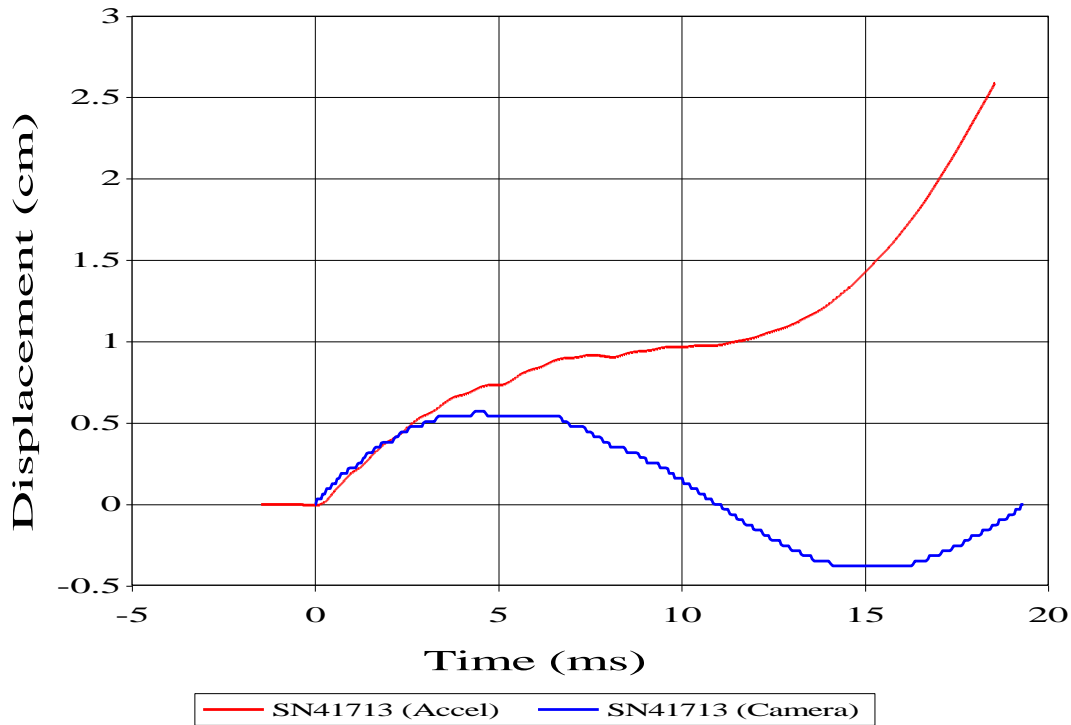
Figure 5.2: Displacement versus time comparison for accelerometer (red) and camera (blue) data

The blue curve in this graph represents the camera data and the red curve

shows the double integrated accelerometer signal. After watching the high speed

video data it was determined that the mounting of the accelerometer on the metal

foam pad caused the accelerometer to sit too far off of the longitudinal axis of the

beam. This in turn caused the accelerometer to move in an odd jerky fashion,

creating a lot of transverse motion of the instrumentation.

To overcome this difficulty in measuring the acceleration of the tip of the

cantilever beam, a hole was drilled at the tip of each beam, just under where the gas

gun projectile makes contact. A firm rubber tube was created for each bar and

forcefully pressed into the drilled hole. Into this rubber tube, the accelerometer was

pressed. The force required to press the accelerometer into the rubber sleeve was

large, thus ensuring that the accelerometer would not slip in the rubber sleeve throughout the testing process. A photograph of the accelerometer mounting technique is seen in Figure 5.3.
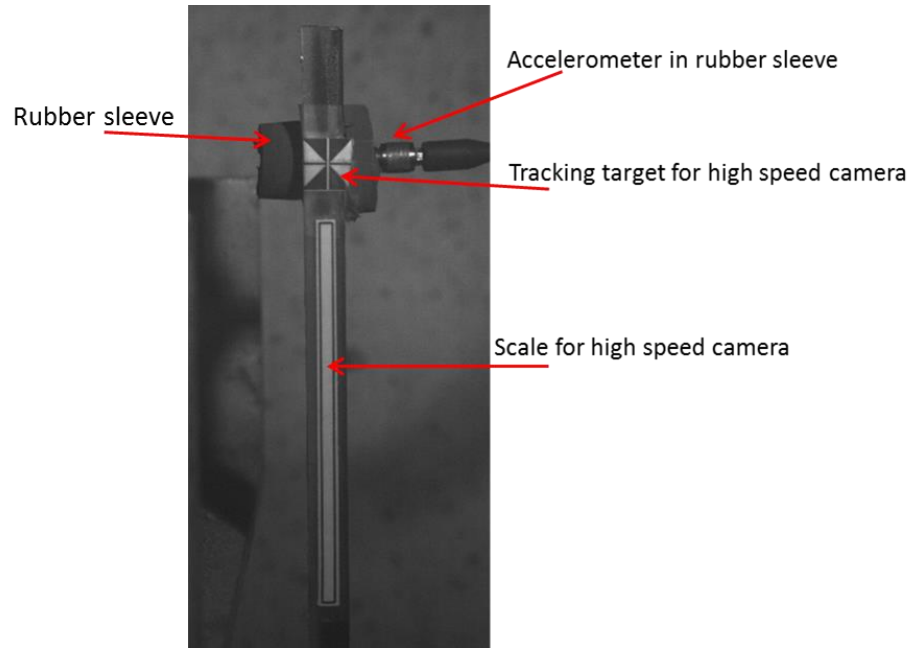
Figure 5.3: Beam set-up for cantilever beam tests

By mounting the accelerometer in the rubber sleeve as shown in Figure 5.3, the accelerometer moves with the neutral axis of the beam and does not incur any transverse motion during the test. As a result, it was discovered that the displacement curves determined from the accelerometer and high speed camera match much better. An example of this is shown in Figure 5.4. In order for the data to be reported in this section, the displacement versus time for the accelerometer and high speed video must match up.
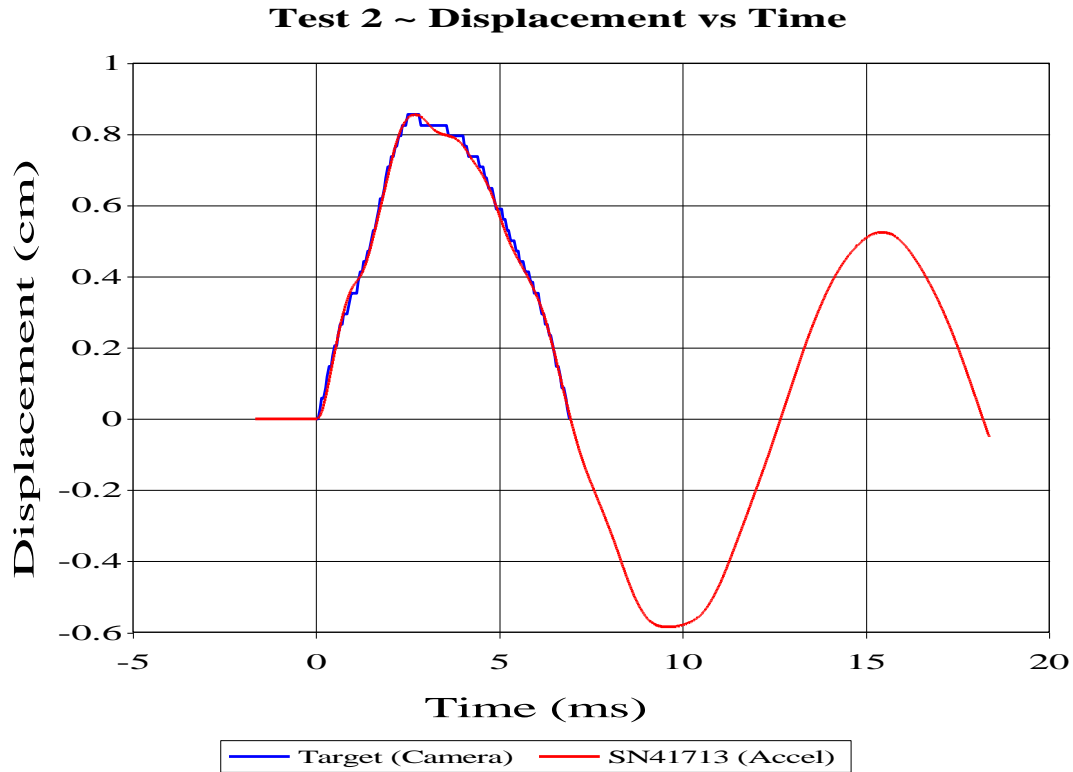
Figure 5.4: Example of a displacement versus time comparison for rubber mounted accelerometer

5.2 Preliminary Polyurea Beam Tests

5.2.1 Cantilever Beam Set-Up

Before going into each specific series of tests for the polyurea coated beams, it is necessary to specify how each beam will be placed in the cantilever support in relation to the oncoming projectile. The first item of note is that each beam is 25.4 centimeters long with the first 2.54 centimeters being secured in the cantilever support. The axis of the accelerometer is placed 2.54 centimeters below the tip of the beam. Each beam is placed such that the projectile fired from the gas gun hits the tip of the beam in the center of the beam width so that the beam does not twist upon impact.

93

A number of beam set-ups were tested to determine which face of the bar (the metal side or the polyurea side) should be contacted with the projectile. Three different scenarios were tested: projectile contacting the steel (polyurea in compression), projectile contacting the polyurea (polyurea in tension), and the polyurea at the area of contact ground off so that the projectile contacted the steel but still put the polyurea in tension. The situation of these preliminary tests is shown in Figure 5.5.

Steel side contact   Polyurea side contact   Steel contact on polyurea side
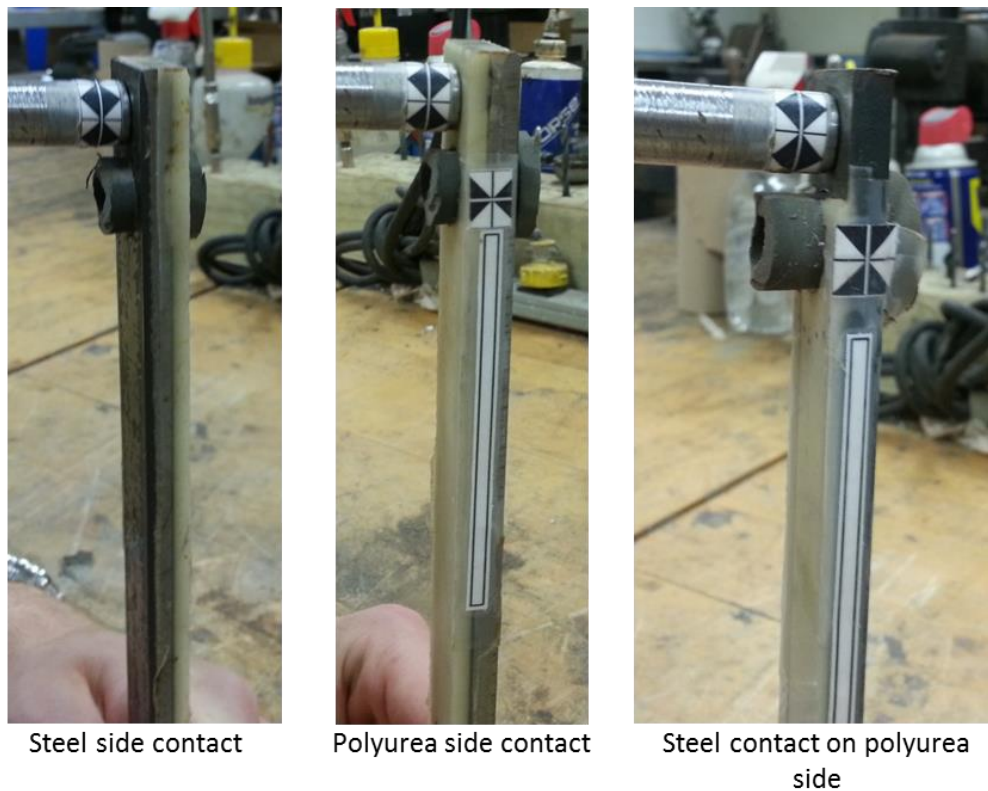
Figure 5.5: Contact configuration for preliminary polyurea tests

5.2.2 Preliminary Test Results

Four test outputs were examined for each test. The peak acceleration, peak velocity (obtained from the accelerometer), peak displacement, and half wavelength time (time for the bar to pass through its initial resting point after having travelled

through the maximum displacement a single time) will all be reported for each test. The results of situating the beam in the cantilever for the three scenarios portrayed in Figure 5.5 are displayed in Figure 5.6, Figure 5.7, Figure 5.8, and Figure 5.9. Each configuration was tested twice to determine test scatter. The blue bars show the values for the initial tests and the red bars give the value for the repeat test for each scenario.

Bar Peak Acceleration

	Steel Side ~ Steel Contact	Polyurea Side ~ Polyurea Contact	Polyurea Side ~ Steel Contact
Initial Test	5078	4217	3873
Repeat Test	4755	4028	4102
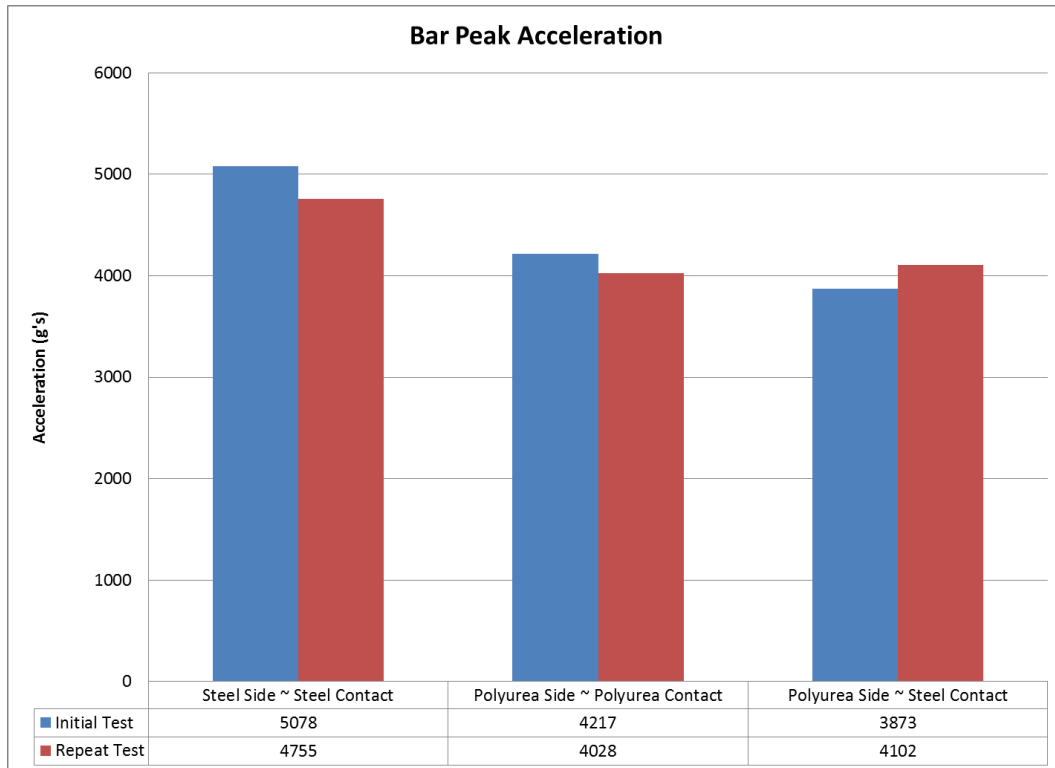
Figure 5.6: Peak acceleration for preliminary polyurea beam tests
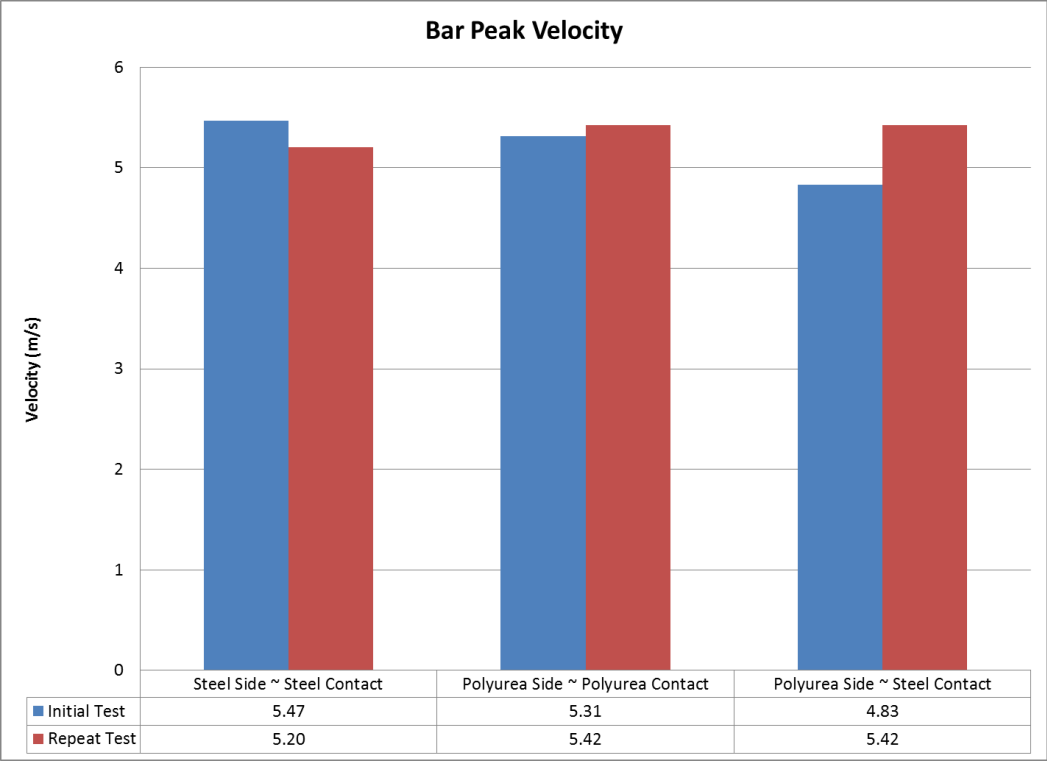
Figure 5.7: Peak velocity for preliminary polyurea beam tests
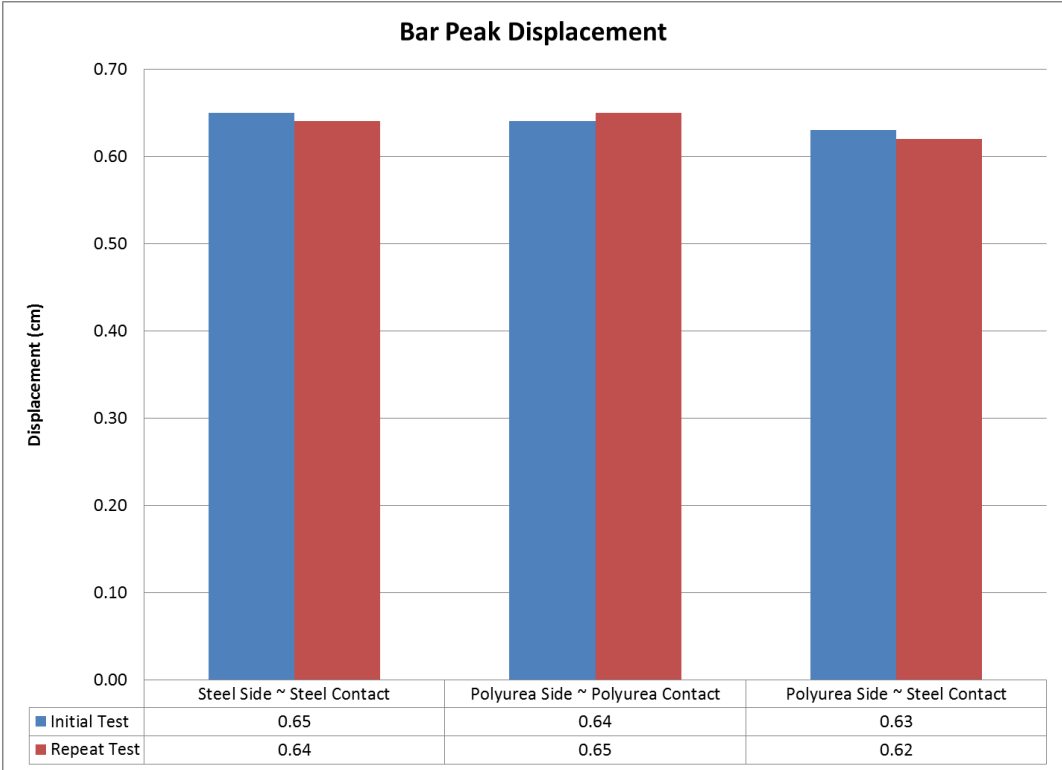
Figure 5.8: Peak displacement for preliminary polyurea beam tests
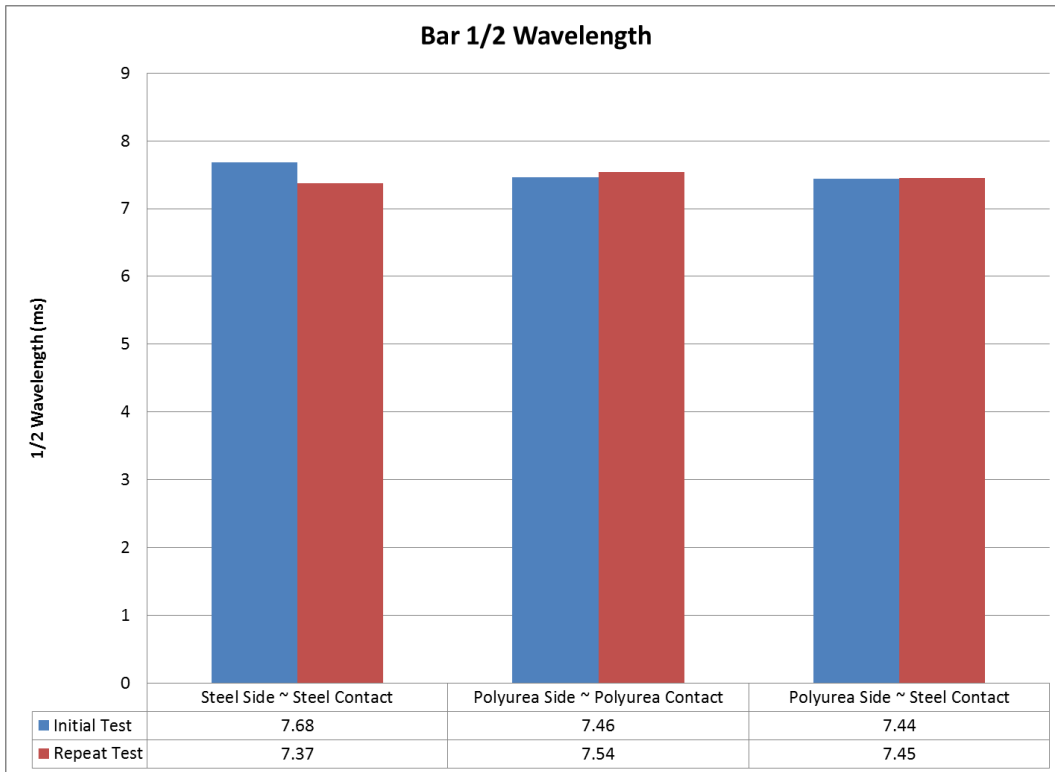
Figure 5.9: Half wave time for preliminary polyurea beam tests

From looking at the four figures it is noted that situation of the polyurea side
to the oncoming projectile only has a slight effect on acceleration and negligible if
any effect on velocity, displacement, and half wavelength time. The slight benefit in
acceleration values results from the bar being placed so that upon initial deflection of
the beam, the polyurea is put into tension. There does not appear to be any effect on
any test output when the polyurea at the tip of the beam is removed, resulting in a
projectile to steel interaction. As such, each of the cantilevered beam tests in what
follows were conducted with the polyurea side facing the projectile, without
removing the polyurea from the tip of the beam.

5.3 Cantilevered Beam General Study

97

5.3.1 General Study Test Outline

The first series of tests run for polyurea coated bars studied the effects of increasing polyurea thicknesses on steel beams of the same outer dimensions. Baseline tests were run with two different bare steel beams to determine the variance in behavior for two different beams of steel cut from the same bar. After these initial tests, three different thicknesses of polyurea were applied to steel beams and tested.

As a quick note, looking at Figure 5.5, it is seen that there is a target taped to the end of the projectile. For each test the projectile is tracked for an inch of travel using high speed video. The slope of the displacement versus time curve for the projectile is determined to be the velocity of the projectile for each test, and must be in the range of 8.4-8.6 meters per second in order for the test to be accepted. The outline of the tests for the general study is seen in Table 5-2. Each test is performed twice to display data scatter and repeatability.

Table 5-2: Test matrix for general polyurea thickness study

Test Number	Bar Number	Steel Mass (g)	Polyurea Mass (g)	Total Mass (w/ accel) (g)	Bar Thickness (mm)	Polyurea Thickness (mm)	Total Thickness (mm)
4	3	302.6	0	314.1	6.22	0.00	6.22
6	3	302.6	0	314.1	6.22	0.00	6.22
8	1	300.3	0	312.5	6.20	0.00	6.20
9	1	300.3	0	312.5	6.20	0.00	6.20
17	2	301.5	12.6	326.8	6.23	1.58	7.81
18	2	301.5	12.6	326.8	6.23	1.58	7.81
24	1	300.3	18.3	329.7	6.20	3.11	9.30
25	1	300.3	18.3	329.7	6.20	3.11	9.30
27	3	302.6	21.4	334.6	6.22	4.76	10.97
28	3	302.6	21.4	334.6	6.22	4.76	10.97

5.3.2 General Study Test Results

At the conclusion of the general study series of tests, as in the preliminary tests, four variables are analyzed and plotted. The peak acceleration and the peak velocity obtained from the accelerometer are plotted as a function of polyurea thickness. The displacement and half wave time are also taken from the accelerometer and plotted as a function of polyurea thickness. The graphs are shown in Figure 5.10, Figure 5.11, Figure 5.12, and Figure 5.13.
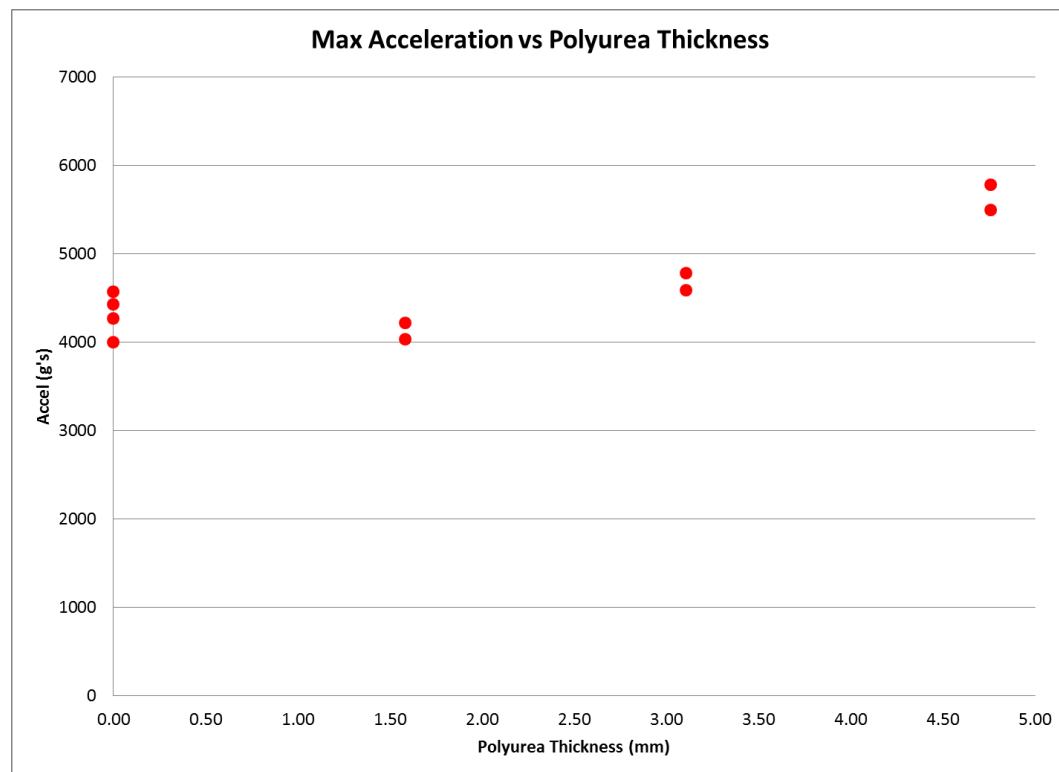
Figure 5.10: Peak acceleration versus polyurea thickness
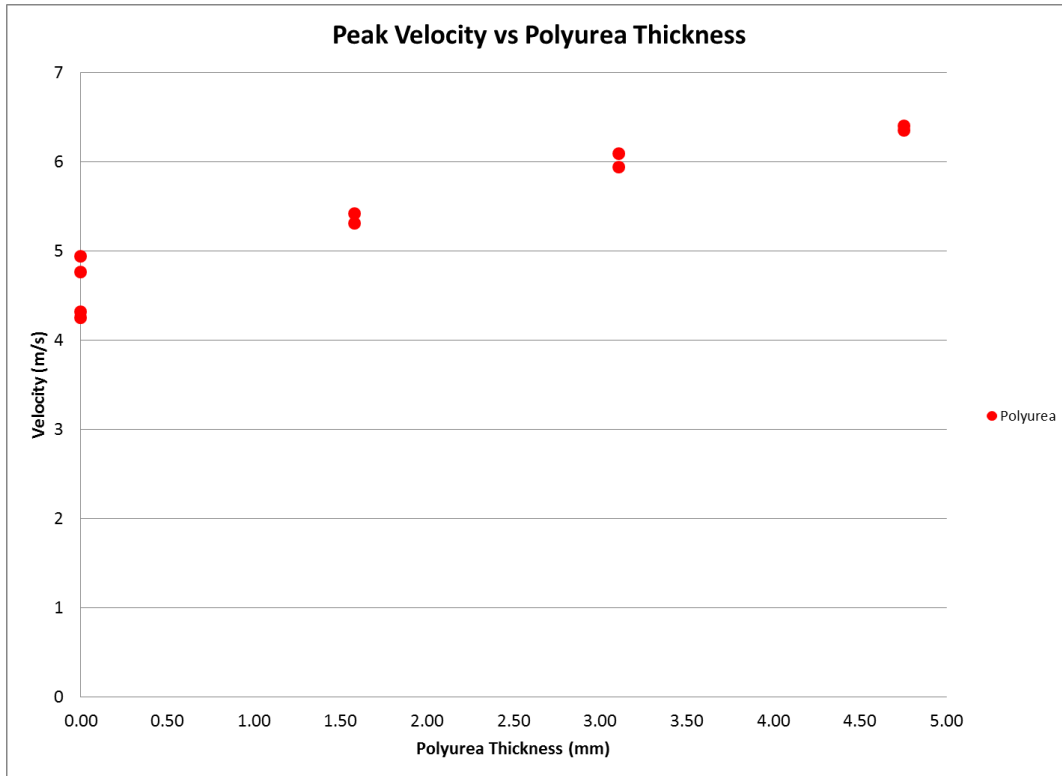
Figure 5.11: Peak velocity versus polyurea thickness
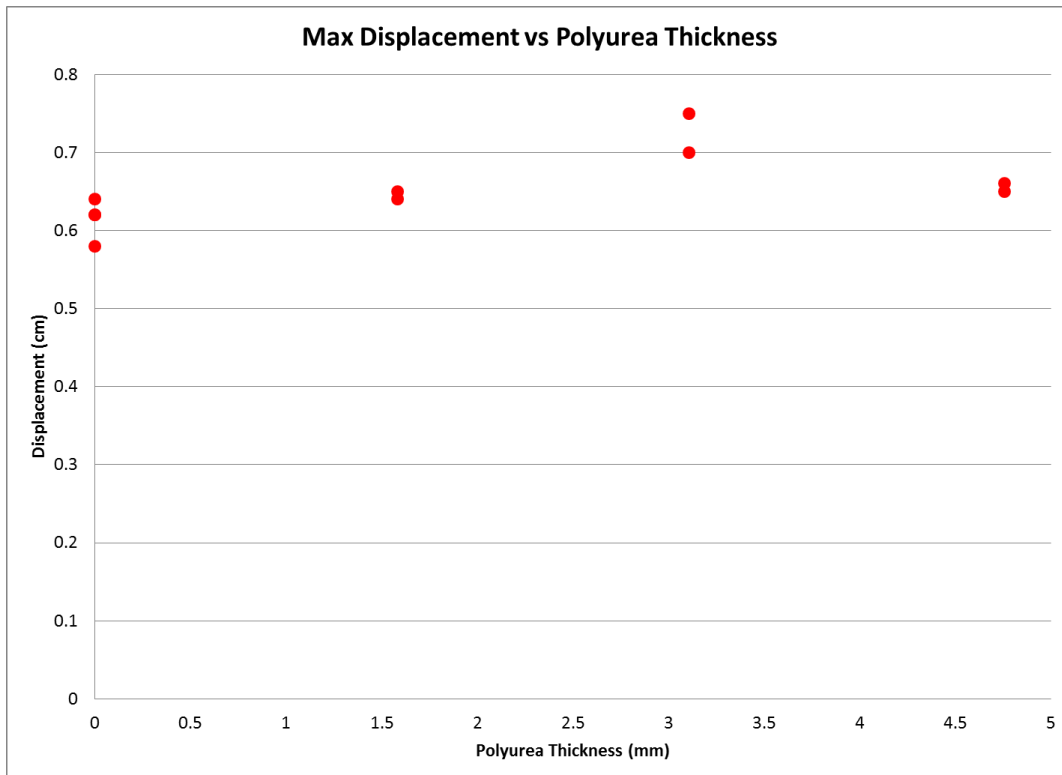
Figure 5.12: Maximum displacement versus polyurea thickness

100
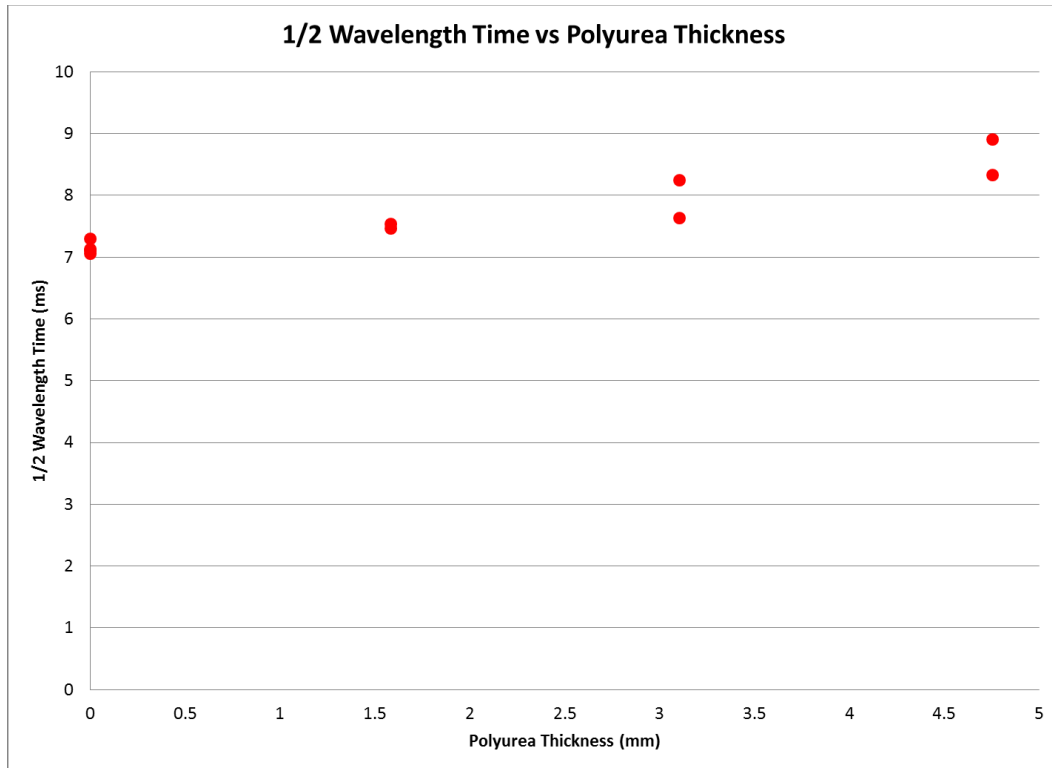
Figure 5.13: Half wavelength time versus polyurea thickness

The above figures show a very interesting and unexpected result. The tip acceleration of bars coated in polyurea increases with polyurea thickness, and at the final thickness (with the polyurea about two millimeters thinner than the steel) the acceleration level is around 1000g's higher than the baseline steel bar. The tip velocity increases across the board as well as the half wavelength time. The only variable that does not show a trend of increasing is the peak displacement. Peak displacement increases until the polyurea thickness reaches approximately three millimeters at which point it drops. Despite the peak and decline of the displacement curve, the lowest displacement of the tip of the beam occurs for a beam without a polyurea coating.

101

5.4 Cantilevered Beam Mass Study

5.4.1 Mass Study Test Outline

After having seen the unexpected trend in polyurea coated beams, it was determined that a series of tests should be run to further explore this behavior. To this end a set of tests was conducted where the mass of each bar was kept constant as the polyurea mass increased. This was performed by using a mill to shave specific thicknesses of metal off of steel beams. A polyurea coat having the same mass as the removed steel was then applied to each beam. The mass of the each beam was kept at the mass of the baseline beam from the first series of tests. The tests were run in the same configuration as the previous series of tests. The matrix of tests is seen in Table 5-3.

Table 5-3: Test matrix for polyurea beam mass study

Test Number	Bar Number	Steel Mass (g)	Polyurea Mass (g)	Total Mass (w/ accel) (g)	Mass Ratio (Polyurea/Steel)	Bar Thickness (mm)	Polyurea Thickness (mm)	Total Thickness (mm)
a	3	302.6	0	314.1	0.000	6.22	0	6.22
b	3	302.6	0	314.1	0.000	6.22	0	6.22
c	1	300.3	0	312.5	0.000	6.20	0	6.20
d	1	300.3	0	312.5	0.000	6.20	0	6.20
12	6	281.8	23.4	316	0.083	5.88	3.49	9.37
15	6	281.8	23.4	316	0.083	5.88	3.49	9.37
17	4	273.9	25.8	310.2	0.094	5.68	4.33	10.01
18	4	273.9	25.8	310.2	0.094	5.68	4.33	10.01
19	5	265.2	37.8	313.8	0.143	5.46	5.88	11.34
20	5	265.2	37.8	313.8	0.143	5.46	5.88	11.34
21	5	265.2	37.8	313.8	0.143	5.46	5.88	11.34

In addition to the test matrix listed above, the bare beams of varying masses were also tested before applying polyurea to them. This was done to get more information on how the polyurea coatings affect each bar. The tests for this series are shown in Table 5-4.

102

Table 5-4: Additional tests for baseline comparison of shaved steel bars

Test Number	Bar Number	Steel Mass (g)	Polyurea Mass (g)	Total Mass (w/ accel) (g)	Mass Ratio (Polyurea/Steel)	Bar Thickness (mm)	Polyurea Thickness (mm)	Total Thickness (mm)
3	6	281.8	0	293	0	5.88	0	5.88
4	6	281.8	0	293	0	5.88	0	5.88
6	5	265.2	0	275.6	0	5.46	0	5.46
7	5	265.2	0	275.6	0	5.46	0	5.46
8	4	273.9	0	284.9	0	5.68	0	5.68
10	4	273.9	0	284.9	0	5.68	0	5.68

5.4.2 Mass Study Test Results

As with the other two cantilever beam studies the four test outputs (acceleration, velocity, displacement, and half wave time) were all analyzed at the end of each test. These values were then plotted as a function of the polyurea to steel mass ratio. The results can be seen in Figure 5.14, Figure 5.15, and Figure 5.16.
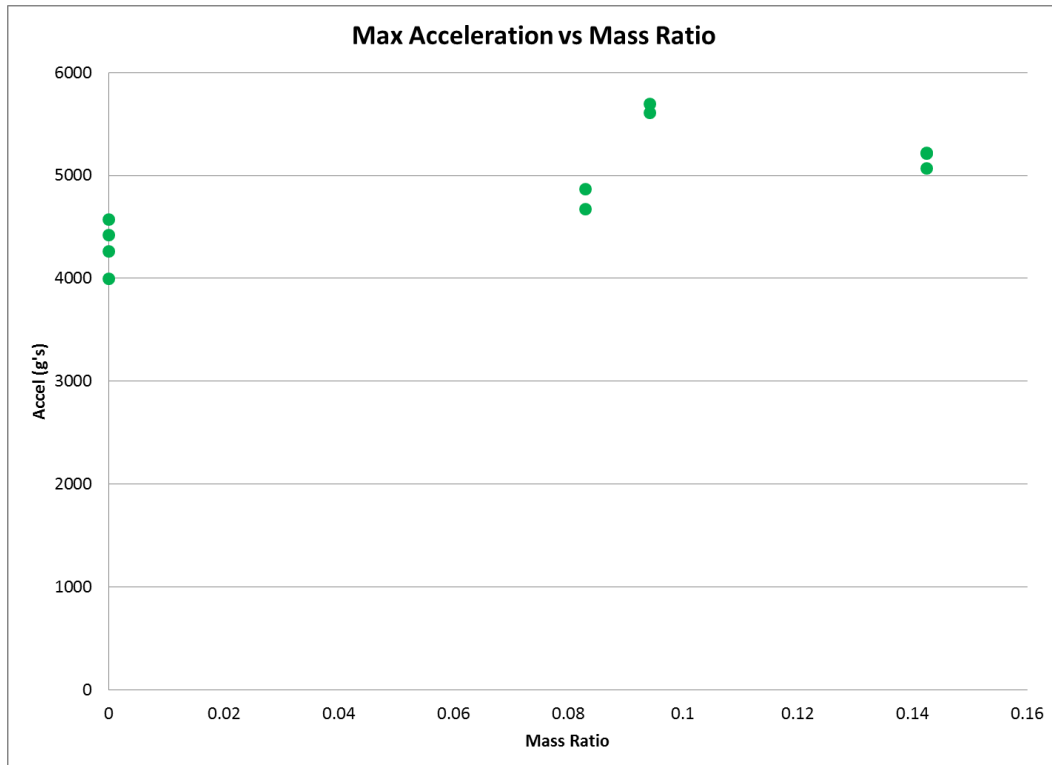
Figure 5.14: Peak acceleration versus polyurea to steel mass ratio
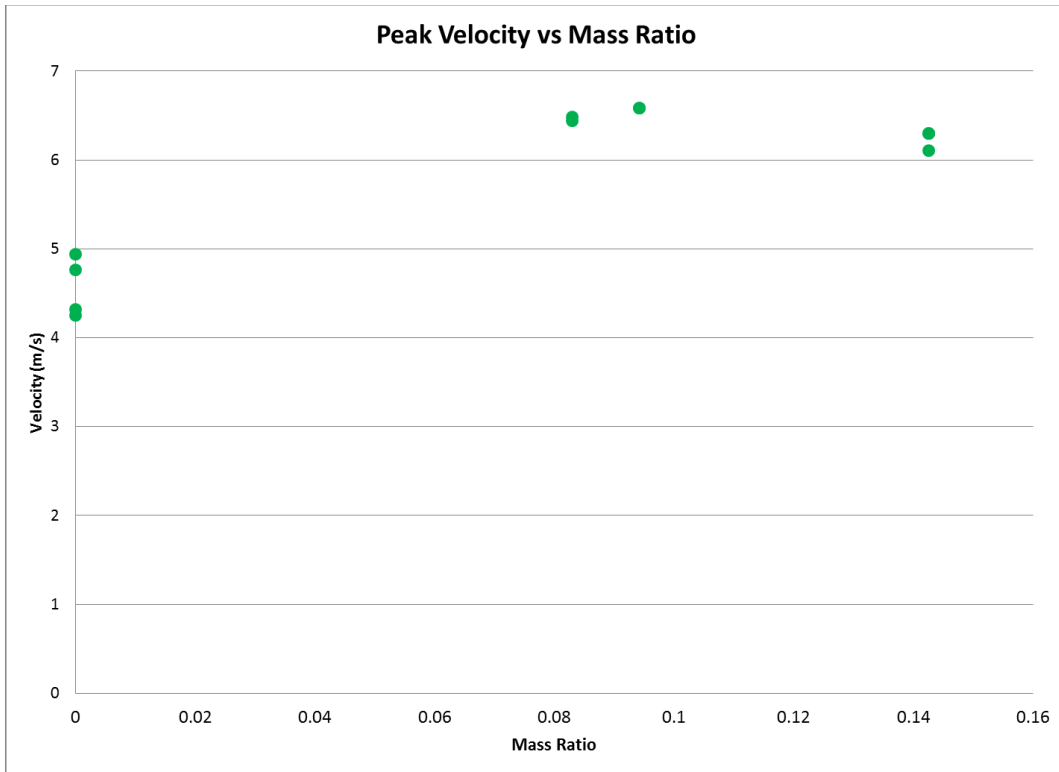
Figure 5.15: Peak velocity versus polyurea to steel mass ratio
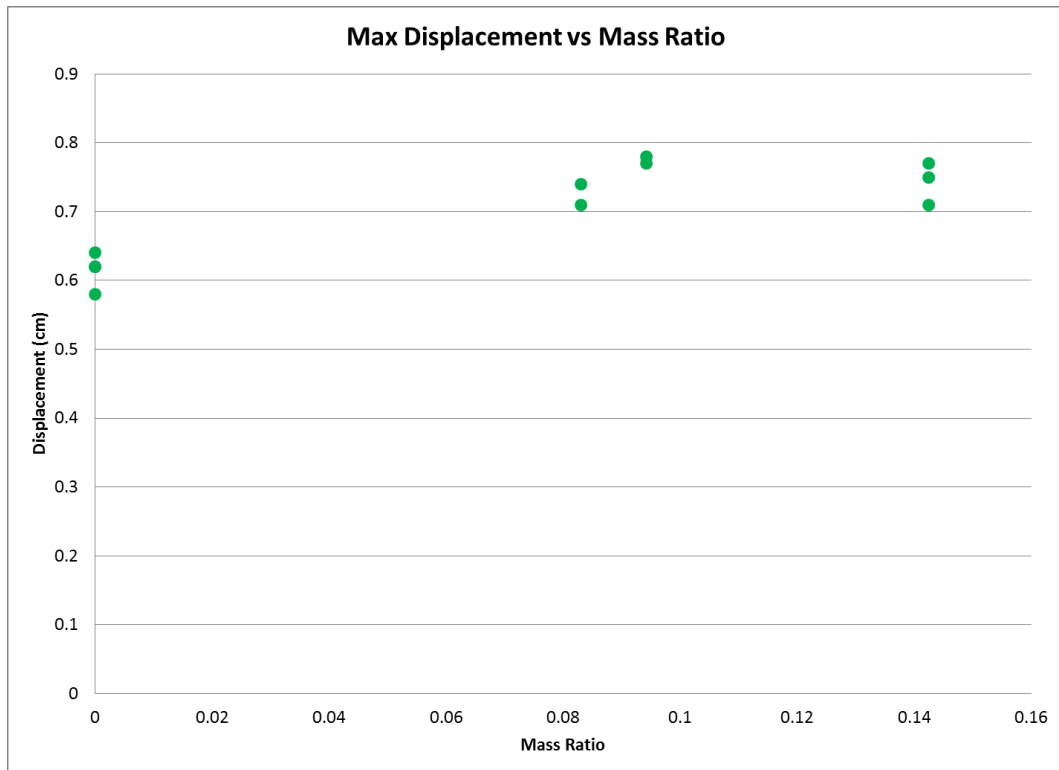
Figure 5.16: Peak displacement versus polyurea to steel mass ratio
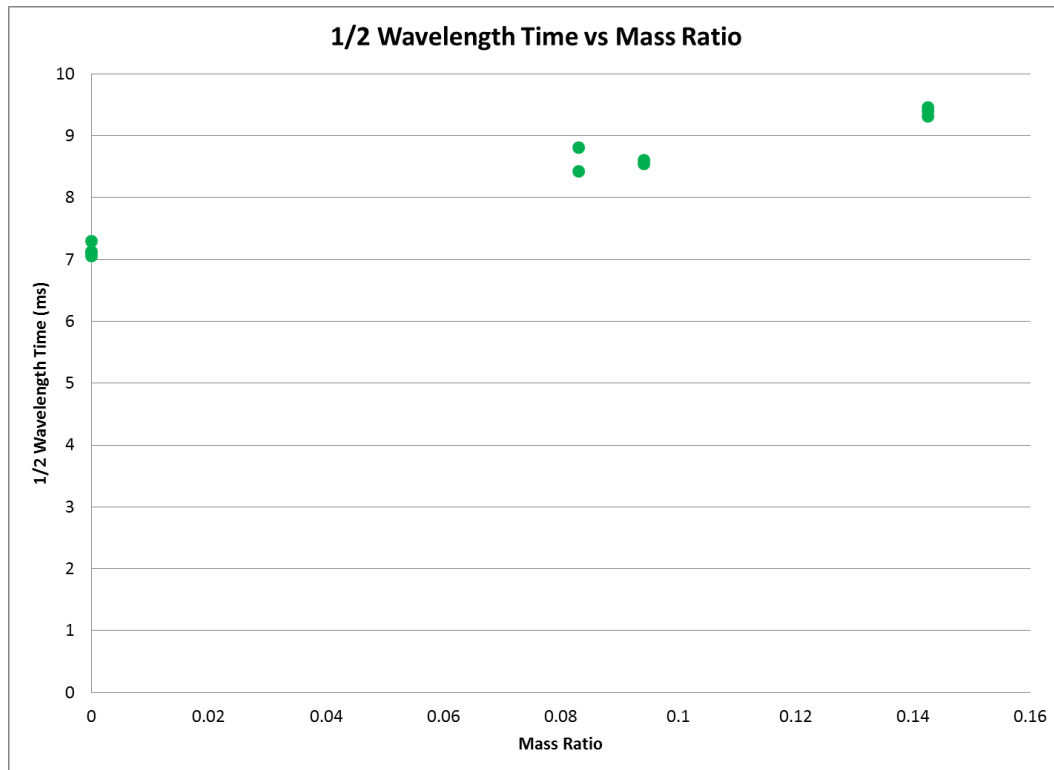
Figure 5.17: Half wavelength time versus polyurea to steel mass ratio

Similar to the general study, an increase across the board occurs for all test variables. The acceleration of the beam tip increases for increasing mass ratio, though not as cleanly as it did for the general study. The half wavelength time increases steadily with mass ratio. Peak velocity and peak displacement seem to either level off or start to decrease slightly at the upper ends of the mass ratio curves. Either way, the level of velocity and displacement are noticeably higher for the polyurea/steel bars than that of the bare steel bars.

As a further look into the effect of polyurea coatings on steel bars, the acceleration, velocity, displacement, and half wavelength times of the polyurea coated bars are compared to the levels of the same bars without polyurea coatings. Each bar, both in its coated and uncoated state, is tested twice and the values averaged. The results are shown in Figure 5.18, Figure 5.19, Figure 5.20, and Figure

105

5.21. For these figures the blue bars indicate levels of the bare steel bar and the red bars are the levels after coating.
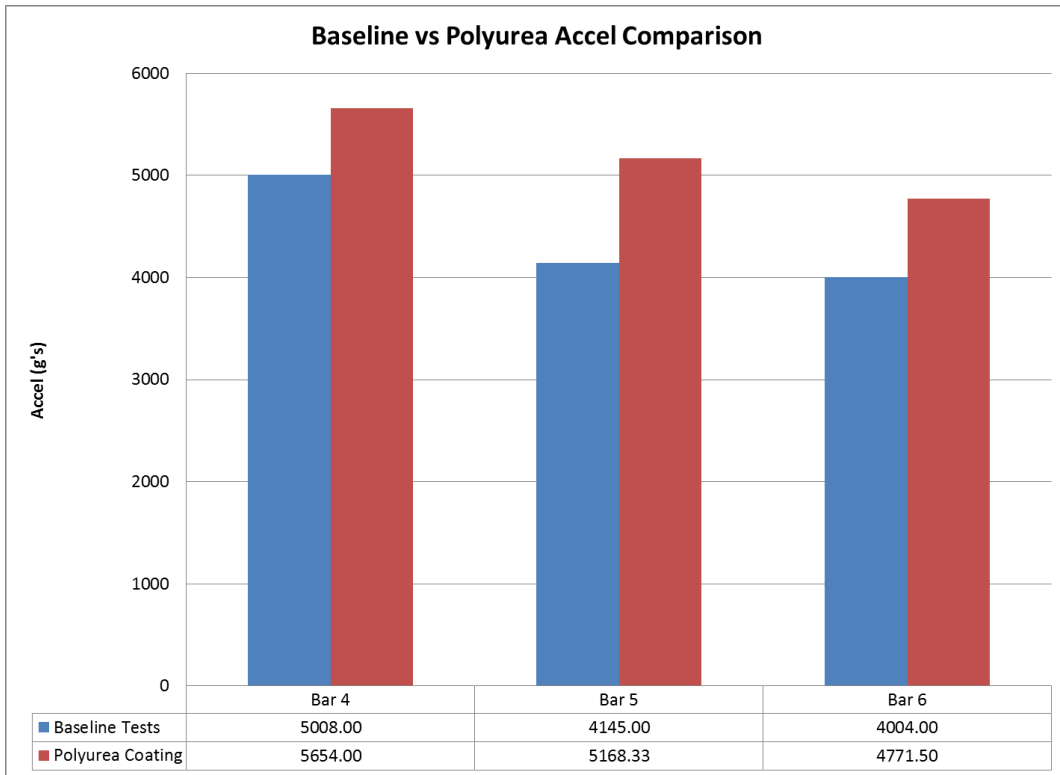
Figure 5.18: Acceleration comparison between bare and coated beams
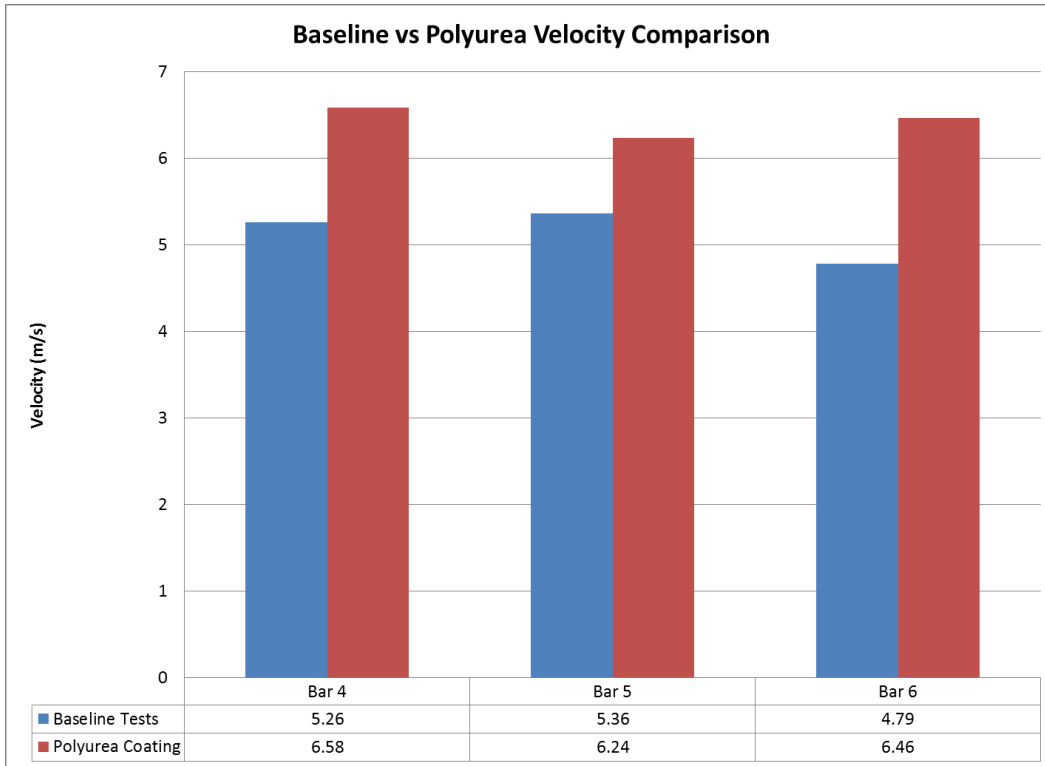
Figure 5.19: **Velocity comparison between bare and coated beams**

	Bar 4	Bar 5	Bar 6
Baseline Tests	5.26	5.36	4.79
Polyurea Coating	6.58	6.24	6.46
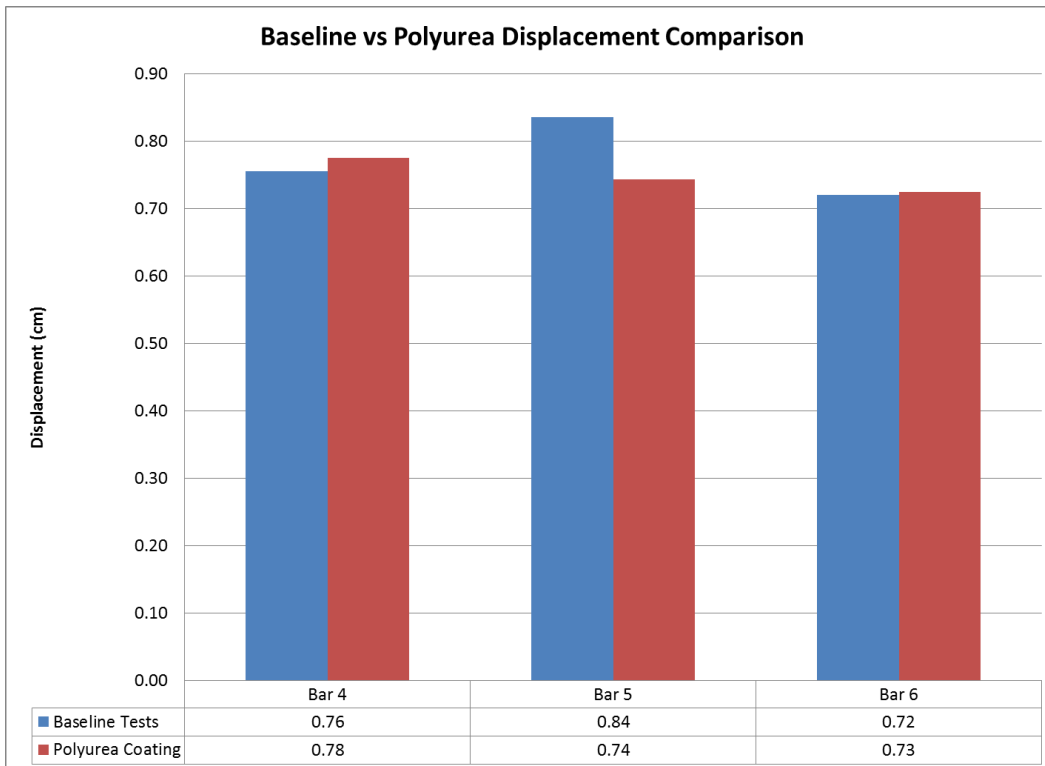
Figure 5.20: **Peak displacement comparison between bare and polyurea coated beams**

	Bar 4	Bar 5	Bar 6
Baseline Tests	0.76	0.84	0.72
Polyurea Coating	0.78	0.74	0.73
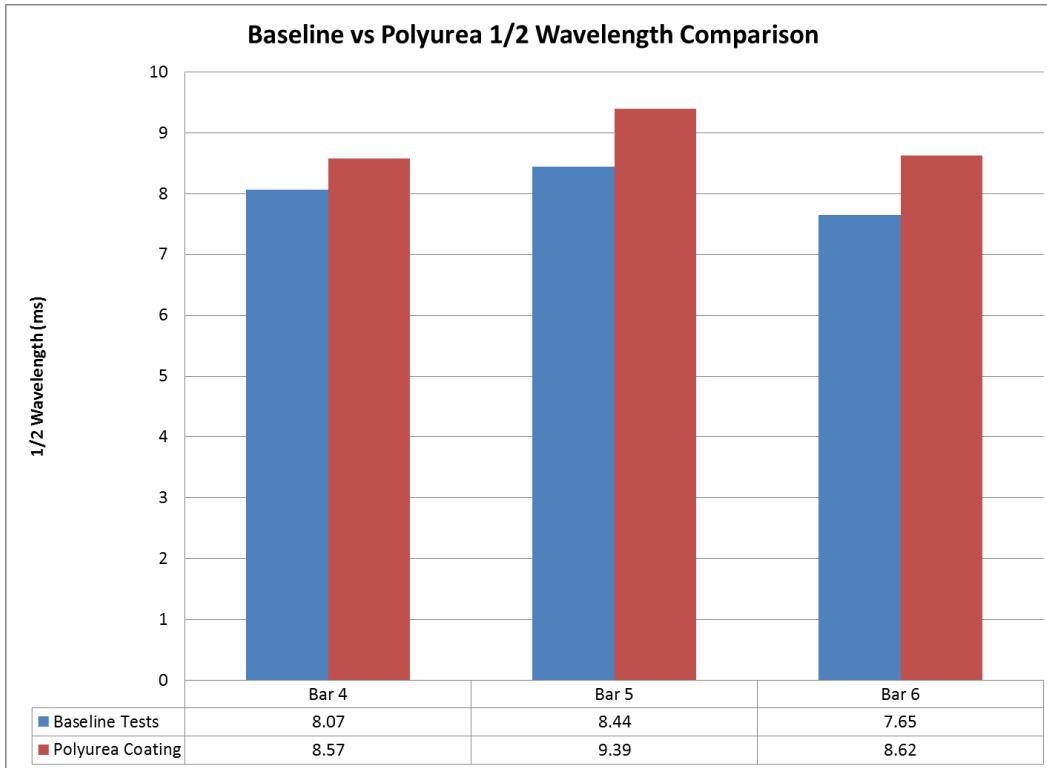
Figure 5.21: Half wavelength time comparison between bare and coated beams

Referring to Figure 5.18, Figure 5.19, Figure 5.20, and Figure 5.21 the apparent trend of polyurea coated beams behaving more extremely seems to continue. The acceleration, velocity, and half wavelength time all increase for each bar when a polyurea coat is applied to it. The only category in which the outcome is less certain is the peak displacement. For two of the three bars the displacement is practically the same. For "Bar 5" (the lightest of the bunch) once the polyurea coat is applied, the peak displacement decreases.

5.5 Cantilevered Beam Segmented Constraint Study

5.5.1 Segmented Constraint Study Test Outline

The next series of tests used the same polyurea coated beams that the general study used. In this study the effect of putting the polyurea in shear as a dampening

mechanism is examined. To place the polyurea coating in shear, a series of shear tabs were bonded onto the surface of the polyurea. Plunkett and Lee have shown that by constraining a viscoelastic layer to place it in shear, positive effects on damping can be made [28]. Following suit, the equation developed by Plunkett and Lee is used to determine the optimum length for the segmented constraints for each bar. The following equation is used:

$$L_{optimum} = 3.28 * \sqrt{\left(\frac{h_1 * h_2 * E}{G} \right)}$$

In this equation, h_1 is the thickness of the constraining layer, h_2 is the thickness of the polyurea, E is the modulus of elasticity of the constraining layer, and G is the shear modulus of the polyurea. Using this equation an optimum length using .1 millimeter thick aluminum shim stock was found. The aluminum shim was then bonded to the surface of the polyurea using the same polyurea material. The polyurea in between the tabs was cut thus creating segmented constraints for each bar, and allowing the polyurea layer to undergo shear deformation during testing. A picture of the segmented constraints can be seen in Figure 5.22.

Figure 5.22: Segmented constraint bars

5.5.2 Segmented Constraint Study Test Results

Each bar with its shear constraining layer was tested twice and each of these

tests compared with the tests from the general study. Acceleration, velocity,

displacement, and half wavelength time are all reported. The graphs are seen in

Figure 5.23, Figure 5.24, Figure 5.25, and Figure 5.26. In each of the graphs the red

points indicate the bars with the shear tabs bonded on the surface and the green points

are the same points from Figure 5.10, Figure 5.11, Figure 5.12, and Figure 5.13 from

the general study.
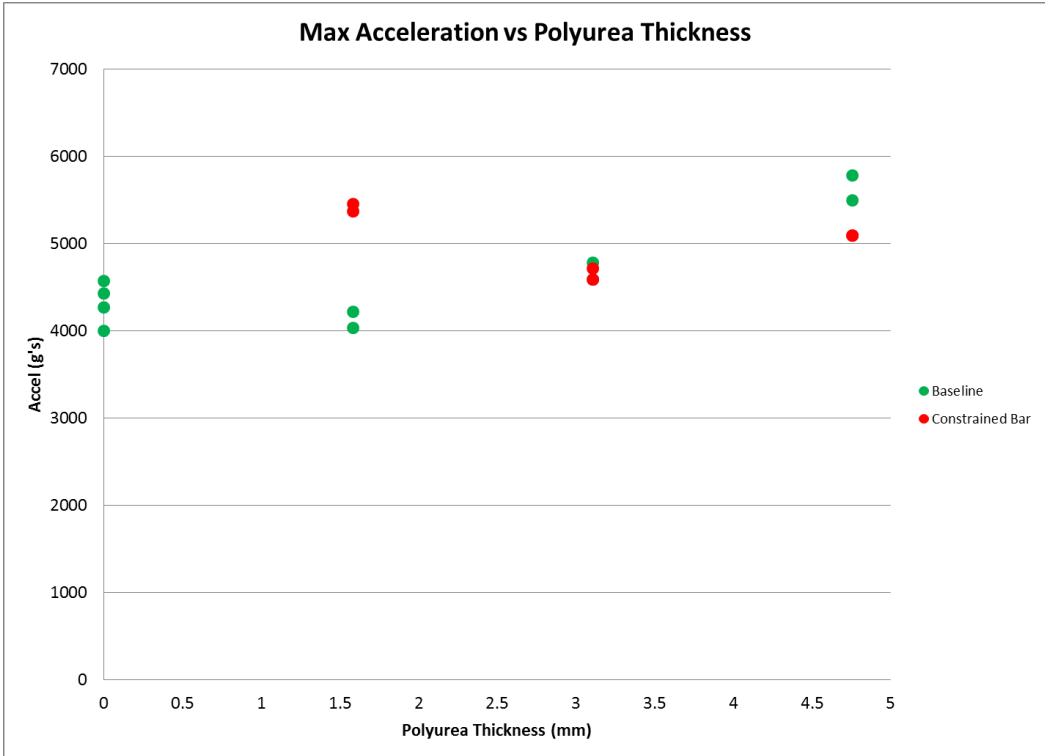
Figure 5.23: Acceleration comparison for shear constrained bars
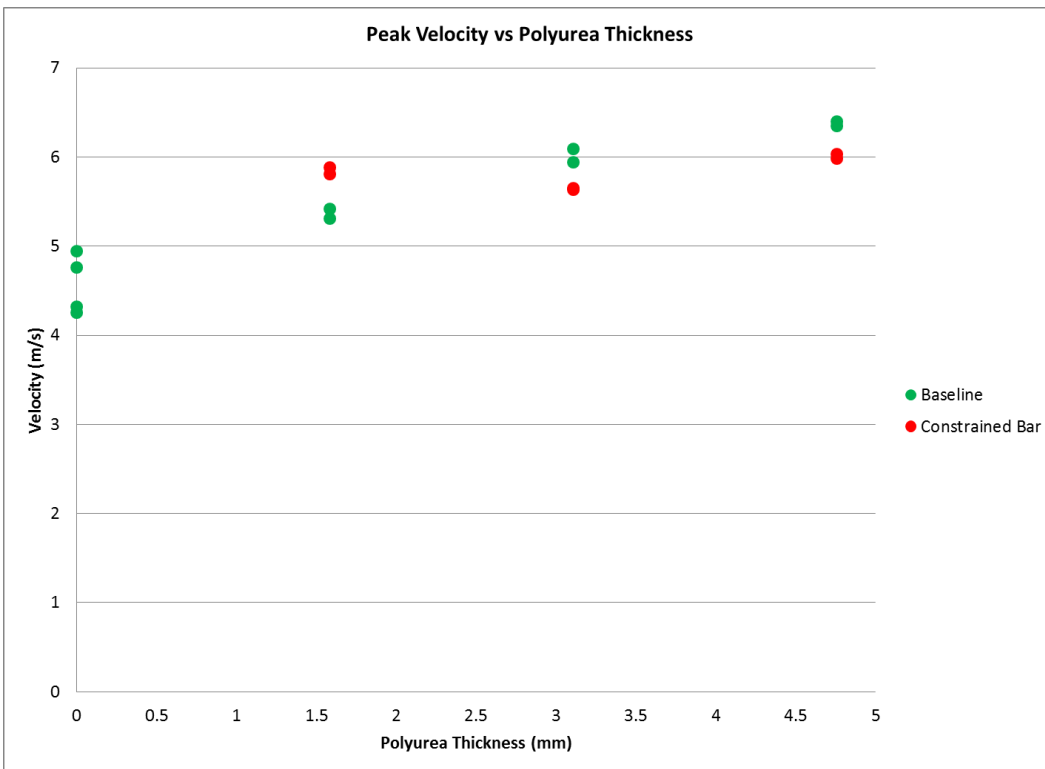
Figure 5.24: Velocity comparison for shear constrained bars

111
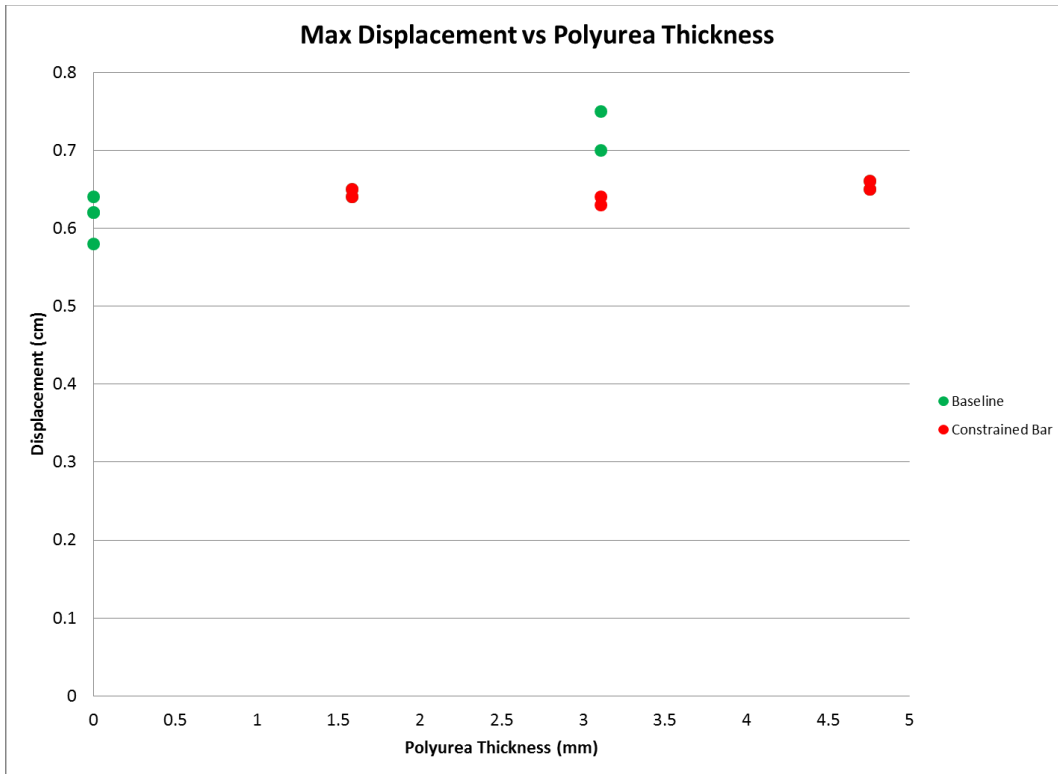
Figure 5.25: Displacement comparison for shear constrained bar
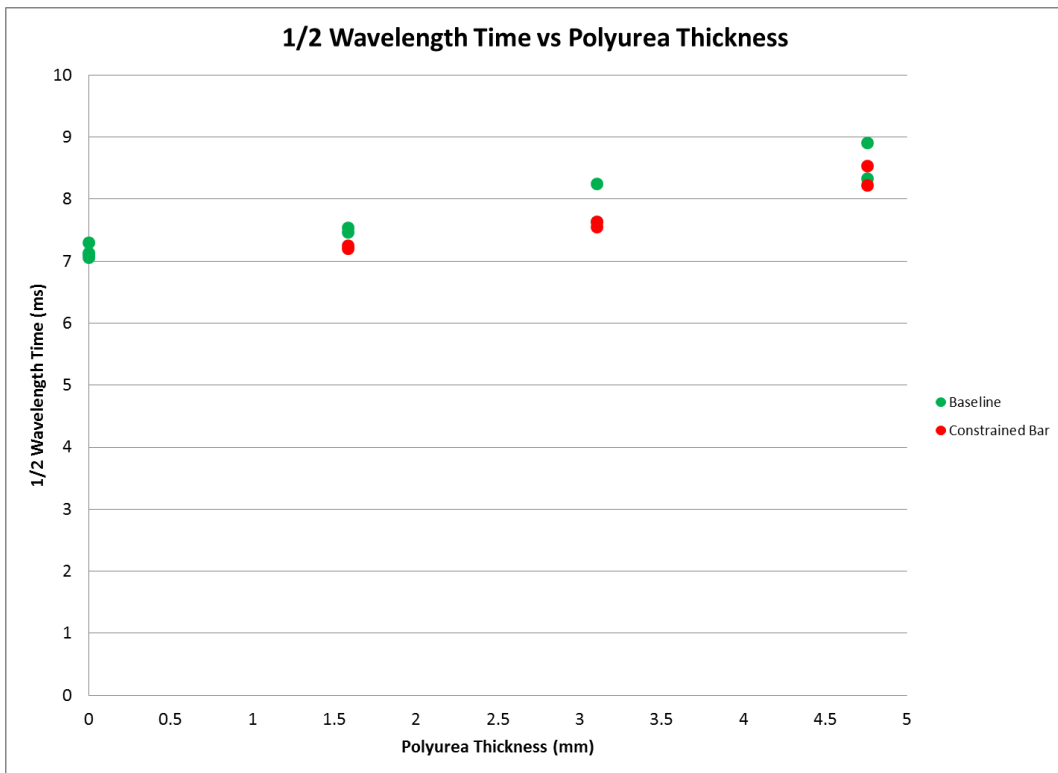
Figure 5.26: Half wavelength comparison for shear constrained bar

From looking at the previous four graphs, it is tough to draw a strong conclusion. The acceleration level at the lowest polyurea thickness is significantly higher with the shear constraint and slightly lower at the highest thickness with the points overlaying one another at the intermediate polyurea thickness. The velocity is higher for the shear bar at the lowest polyurea thickness and slightly better for the latter two test cases. Outside of the middle thickness, for which the shear beam displacement is significantly lower, the displacement of the bars with and without shear tabs is identical. As for half wavelength time, it appears as if there is not a significant change to be noted from adding shear constraints to the polyurea.

5.6 Coated Cylinder Blast Test Study

5.6.1 General Information

To better understand the dynamic effects of coating structures with polyurea, a number of thin-walled cylinder crushing tests were run. Since crushing of thin-walled cylinders has already been proven to be an effective means of mitigation using small-scale vehicle shapes, a more practical means of comparison between non-coated and coated cylinders was developed. This series of tests utilized a single thin-walled cylinder in between two circular aluminum plates. The aluminum plates are termed the hull (bottom) and the frame (top); the same as the scaled vehicle testing. The plate characteristics are listed in Table 5-5.

Table 5-5: Polyurea coated cylinder test plate characteristics

Frame Material	Frame Diameter (cm)	Frame Thickness (cm)	Frame Mass w/ Targets and accels (kg)	Hull Material	Hull Diameter (cm)	Hull Thickness (cm)	Hull Mass (kg)	Total Plate Mass (kg)
Alum 6061	16.51	2.74	1.43	Alum 6061	16.51	2.82	1.27	2.74

The thin-walled cylinder was created from aluminum shim stock in the manner described in the wall thickness study section. The exception to that cylinder fabrication process comes as the step in which the cylinder is coated with polyurea. In order to apply the polyurea to the shim stock, the shim stock is laid flat on a level table. The area to be coated in polyurea is left uncovered and the rest of the shim stock is covered in masking tape. The uncovered aluminum is prepared through sanding of the surface and cleaning with isopropyl alcohol. A specific mass of polyurea for each test is mixed and applied to the prepared surface using a small paint brush. A sample photograph of the coating process is shown in Figure 5.27.
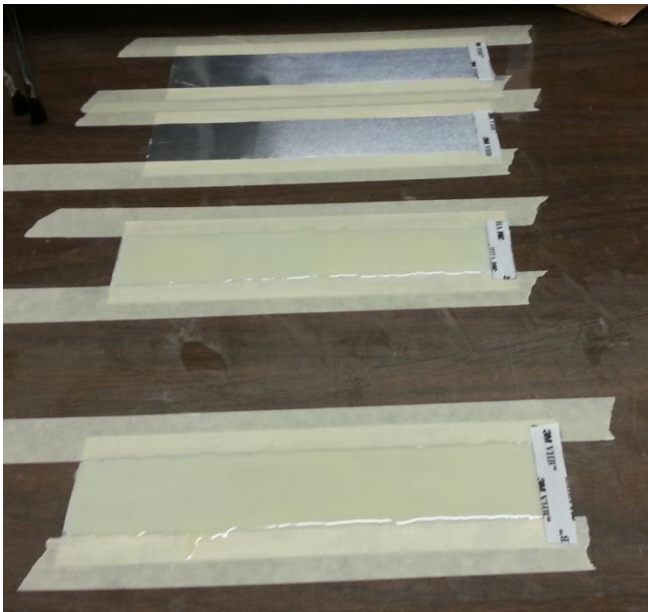
Figure 5.27: Polyurea coated shim stock (bottom) and bare shim stock prepared for coating (top)

Once coated with polyurea, the shim stock is left to sit for 12 hours before proceeding to create the cylinder shape by connecting the two ends of the shim stock with VHB tape. The same steps of cutting the crenellations in the top and bottom portion of the can and attaching thin discs of aluminum to the top and bottom of the can as end caps are then taken. At the end of the whole process, eight thin-walled

cylinders are created – two with no polyurea coat and six cans with three different coating thicknesses.

Tests for this study are conducted using stand-off blocks set to 40 millimeters in height. A 2.2 gram charge is buried at ten millimeters in a saturated sand bed prepared as previously described. The thin-walled cylinders are connected to the hull only, and the frame is equipped with four targets for high speed video tracking and two accelerometers on opposite sides of the plate.

The accelerometers are placed at the node of the frame (determined through nodal testing with a high-pressure gas gun) using a new type of mechanical filter. The rubber sleeve accelerometer holder from the cantilever beam tests inspired the idea for the accelerometer situation in this test series. The same firm rubber used in the polyurea coated bar study was machined to create an accelerometer sleeve to be placed in holes drilled through the plate at the node location. The accelerometer is then forced into the rubber. A picture of the frame set-up and the total plate set-up can be viewed in Figure 5.28.
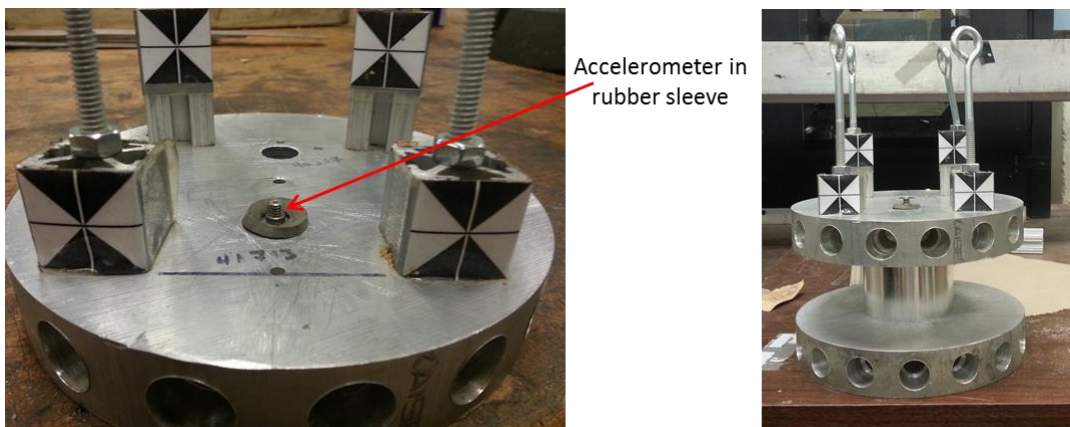
Figure 5.28: Accelerometer placement (left) and plate set-up (right) for coated can tests

Before describing the tests conducted for this study it should be noted that this series of tests aims only at describing the differences in acceleration, impulse, and

kinetic energy of the frame that arise from coating thin-walled cylinders with polyurea. The charge mass has been decreased to result in manageable acceleration signals but the other test characteristics have remained the same. As such the test results are not meant to be indicative of full-scale levels experienced by a passenger in a vehicle that experiences blast loading.

5.6.2 Coated Cylinder Study Test Outline

As mentioned previously, to study the effects of coating thin-walled cylinders with polyurea, eight different tests were run. Two baseline tests with bare cans were tested initially followed by six tests with coated cans. The variable that changed and is reported here is the mass ratio of polyurea applied to the thin-walled cylinder. The test matrix for this study is seen below in Table 5-6.

Table 5-6: Test matrix for polyurea coated can study

Test Number	Charge Mass (g)	DOB (mm)	SOD (mm)	# of Cylinders	Cylinder Material	Cylinder OD (mm)*	Cylinder ID (mm)*	Cylinder Height (mm)*	Cylinder Mass (g)*	Polyurea Mass (g)	Mass Ratio (Poly/Alum)
2	2.2	10	40	1	Aluminum	66	65.8	38.1	3.07	0	0.00
3	2.2	10	40	1	Aluminum	66	65.8	38.1	2.89	0	0.00
4	2.2	10	40	1	Aluminum	66	65.8	38.1	6.95	3.88	1.27
5	2.2	10	40	1	Aluminum	66	65.8	38.1	7.1	4.03	1.32
6	2.2	10	40	1	Aluminum	66	65.8	38.1	10.65	7.58	2.48
7	2.2	10	40	1	Aluminum	66	65.8	38.1	11.28	8.21	2.68
10	2.2	10	40	1	Aluminum	66	65.8	38.1	18.12	15.05	4.92
11	2.2	10	40	1	Aluminum	66	65.8	38.1	18.75	15.68	5.12
*Note: Values reported with an * denote those takes of the shim stock cylinder before the coated in polyurea											

5.6.3 Coated Cylinder Study Test Results

Similar to the mitigation studies conducted with the thin-walled cylinders, the initial test for test validity is the comparison of the displacement curve developed

116

from the tracking of the targets using high speed video with that of the double integrated acceleration signal. It should be mentioned that due to the small size and weight of the test plate, slight offsets in charge location or plate placement resulted in significant rotation of the frame. As such the accelerometer displacement was plotted alongside all four target displacement curves to make sure it fell in among them. Samples of the acceleration signal along with the displacement curve comparison are shown in Figure 5.29 and Figure 5.30.
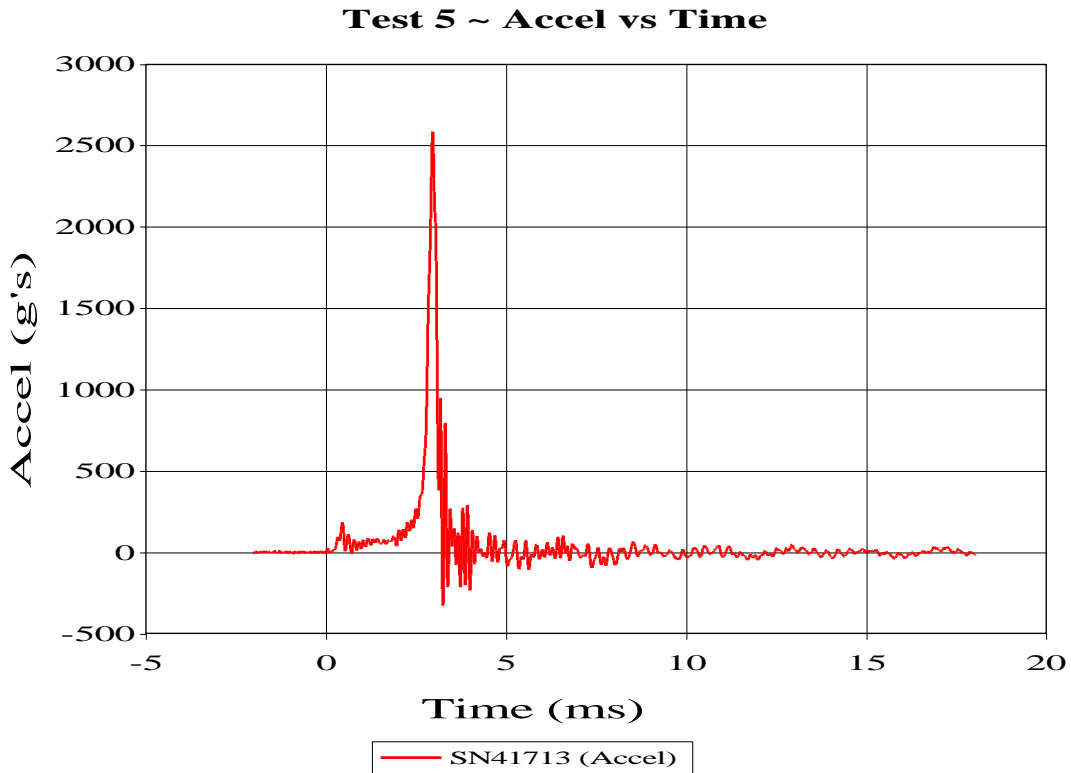
Figure 5.29: Acceleration signal from a polyurea coated cylinder test
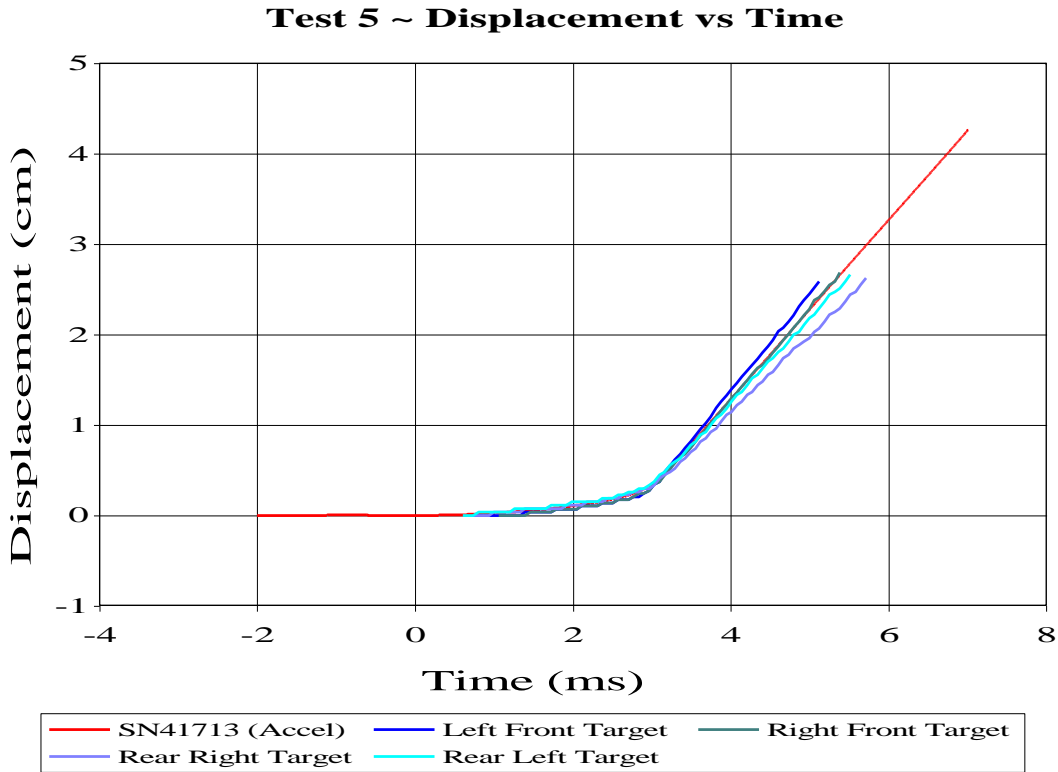
Figure 5.30: Accompanying displacement versus time curve comparison for accelerometer and camera data

From viewing the sample graphs it should be noted how clean the acceleration signal looks. This is believed to be a direct result of encasing the accelerometer in rubber; thus practically eliminating all vibrational frequencies with the exception of the acceleration pulse delivered by the blast. The displacement signals from the high speed camera and the accelerometer also match very nicely. This is the case for all tests reported.

Another area of interest is viewing how the acceleration signal changes with the increasing mass of polyurea applied to the thin-walled cylinder. To this end a sample signal from one accelerometer for four testing scenarios is plotted on the same graph. The result is shown in Figure 5.31.
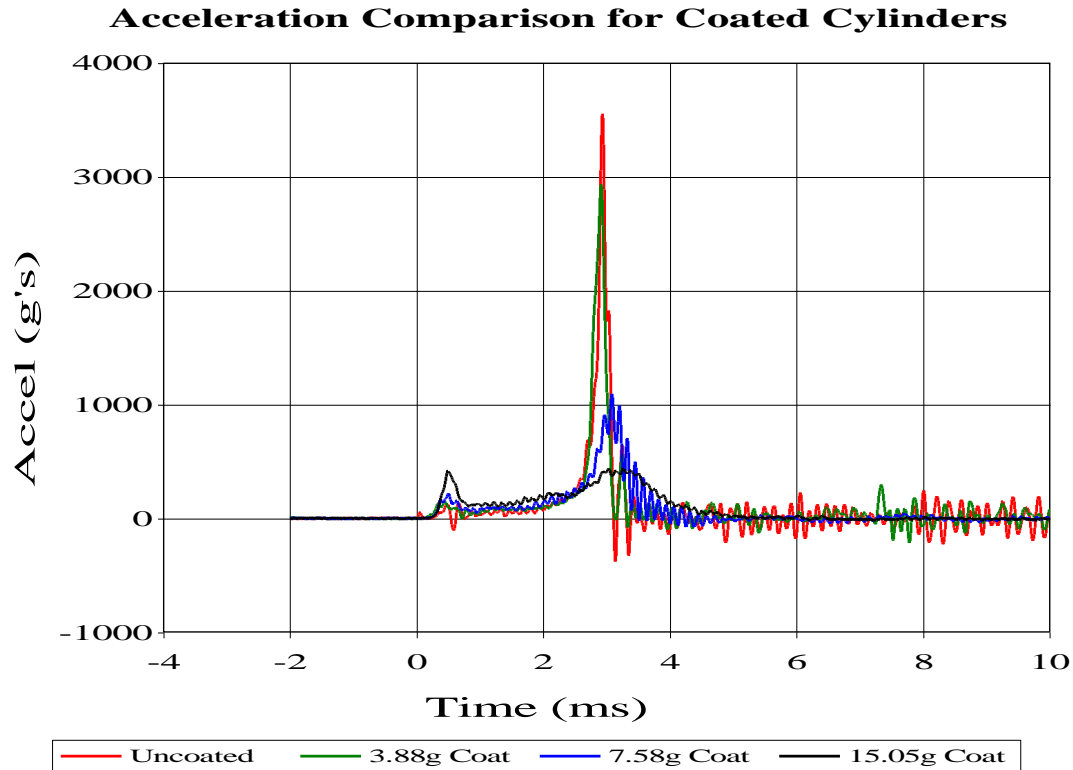
Figure 5.31: Acceleration signal comparison for various coatings

From studying Figure 5.31 a couple of observations can be made. The first and most obvious is how the peak acceleration decreases as the mass of polyurea applied to the cylinder increases. The second is that the time over which the acceleration pulse is delivered stretches out as the mass of the coat increases. So though the acceleration signal is lower it is delivered over a significantly larger period of time.

It might be helpful to view the final deformed state of each of the testing scenarios. At the end of each test, the cylinder was detached from the hull and compared with the other test cylinders. It was noted that as the mass of the polyurea coating increased, the recovered height of the cylinder also increased. A visual of the final cylinder deformations (post-test) is presented in Figure 5.32.

Figure 5.32: Front view of crushed cylinders increasing in polyurea mass from left to right

From Figure 5.32 it is clearly seen that as the mass of polyurea applied to the aluminum base increases, the final deformation of the can decreases. It should be noted that each cylinder underwent severe crushing in every test. After the initial crushing, the cylinders with the polyurea coating rebounded and recovered a portion of their initial height. There was no delamination of polyurea from the metal substrate noted in the thinner coats, and only minor delamination of the polyurea from the aluminum as the mass of the polyurea increased. A measurement of the height of the crushed cylinder was made in each scenario and averaged to determine how much height each cylinder recovered after the blast event. These results are shown in Table 5-7.

Table 5-7: Recovered height of blast-tested polyurea-coated cylinders

Test Number	Approximate Mass Ratio (Polyurea/Aluminum)	Initial Cylinder Height (mm)	Post-Test Cylinder Height (mm)
2 & 3	0	38	6.7
4 & 5	1.3	38	16
6 & 7	2.5	38	31
10 & 11	5	38	35

Finally a comparison between the acceleration, impulse, and kinetic energy is made. Each variable is plotted against the mass ratio of polyurea to aluminum of each cylinder. The velocity used to calculate the impulse and kinetic energy is

developed from the first integration of the accelerometer signal. These plots are

shown in Figure 5.33, Figure 5.34, and Figure 5.35.
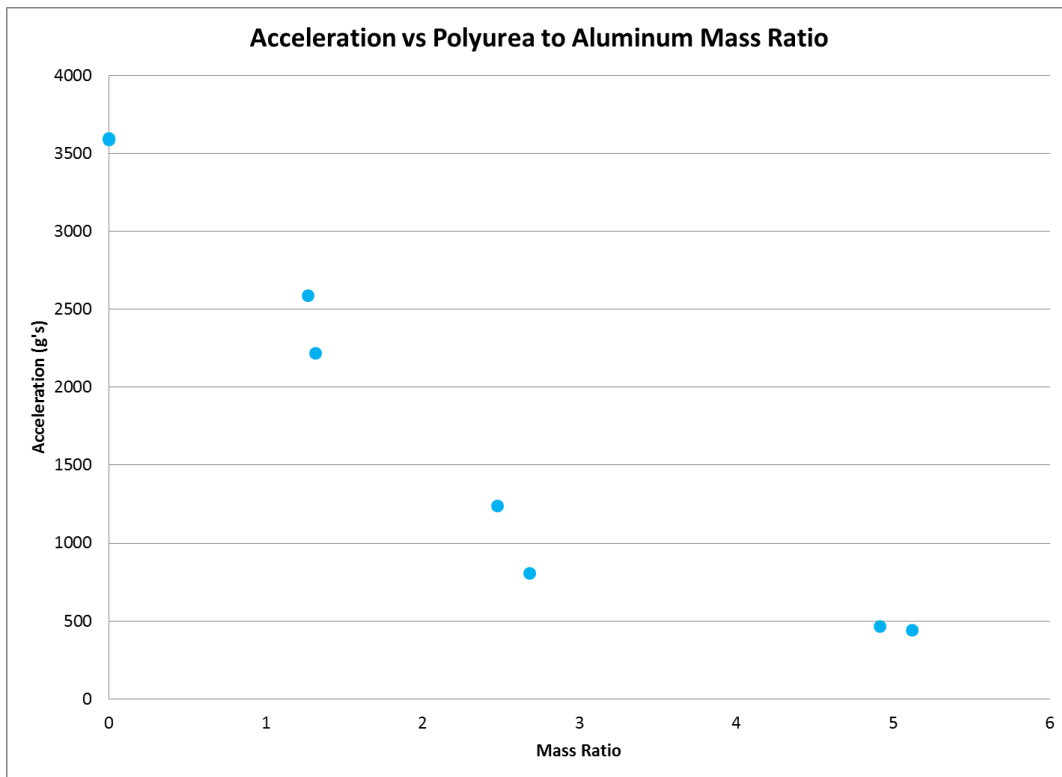
Figure 5.33: Acceleration versus mass ratio for coated cylinders
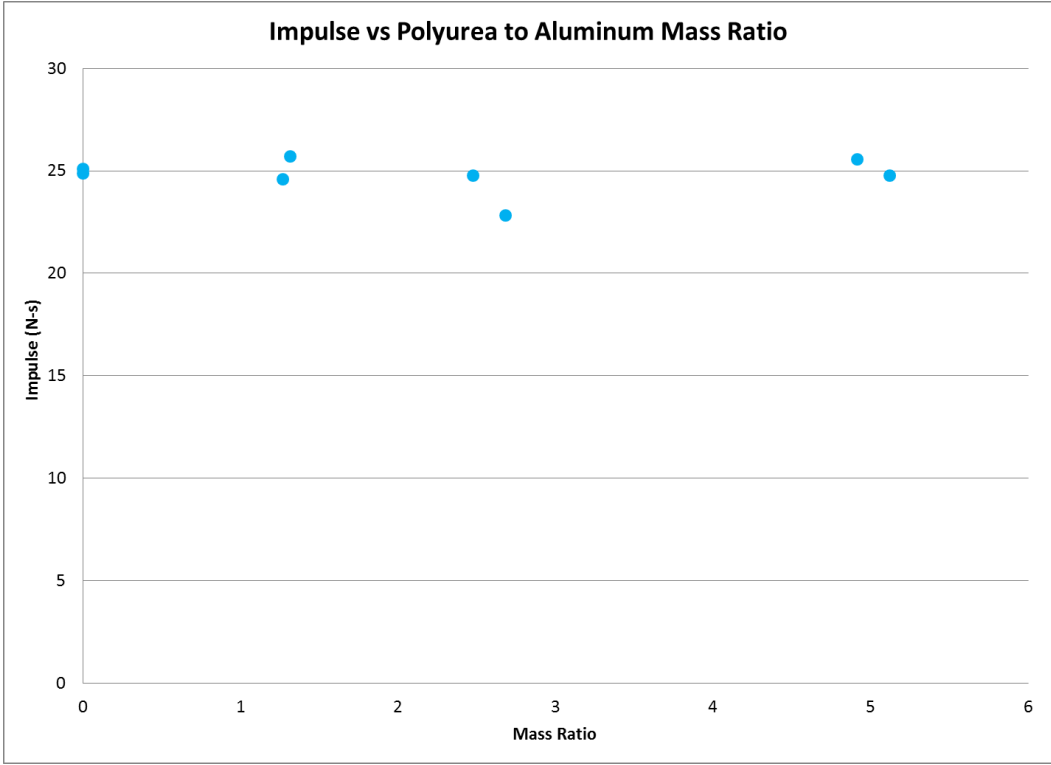
Figure 5.34: Impulse versus mass ratio for coated cylinders
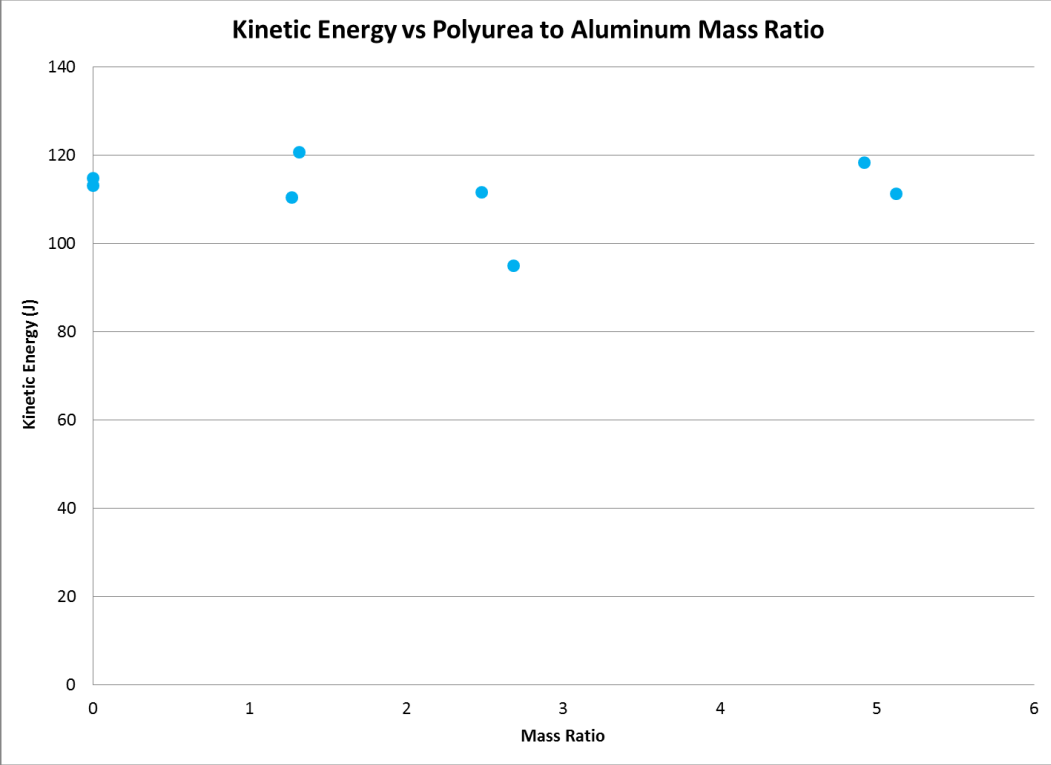
Figure 5.35: Kinetic energy versus mass ratio for coated cylinders

From viewing the graphs a few observation can be made. The first and most important is how much of a decline in acceleration is obtained through coating thin-walled cylinders with polyurea. Studying Figure 5.33 it is noted that by adding the mass of the metal substrate in the form of a polyurea coating, the acceleration levels of the frame can be reduced to 30 percent of the value experienced by the frame that utilized only an uncoated cylinder. In the wall thickness study it was noted that only marginal gains were made by doubling the wall thickness, and thus the cylinder mass. Also it should be noted that the mass of the cylinders is negligible compared to the mass of the hull/frame combination. From Figure 5.34 and Figure 5.35 it should be noted that the effect on impulse and kinetic energy is negligible.

5.7 Polyurea Study Tests Summary

The initial two series of tests in this chapter studied the effect of coating steel beams in polyurea and dynamically testing each beam using a high-pressure gas gun. It was found that the bare steel beam performed better than a coated steel beam when comparing the acceleration, velocity, peak displacement, and half wavelength time of the tip of the beam. With small polyurea to steel mass ratios, it was found that the acceleration and tip displacement values of a coated beam could be as much as 25 percent greater than that of an uncoated beam. The velocity of coated beams could be as much as 40 percent greater than the uncoated beam and the wave time can increase to the neighborhood of 20-35 percent greater when coated with polyurea.

When blast testing a target plate utilizing a hull/frame design (with a single cylinder as mitigation), a different trend in frame acceleration is noted. The peak

123

acceleration of the frame decreases dramatically when the mass ratio of the polyurea to aluminum is around one or higher. The largest benefit is obtained using a five to one polyurea to aluminum mass ratio coated cylinder as mitigation. In this scenario the acceleration value decreases to 12 percent of the acceleration value obtained with an uncoated cylinder. There seems to be negligible effects on the frame velocity when comparing the uncoated and the coated cylinder tests.

Chapter 6 – Concluding Tests

6.1 Similar Mass Ratio Cantilever Beam Study

6.1.1 Similar Mass Ratio Cantilever Beam Study Test Outline

After the completion of the polyurea-coated cylinder tests in which two plates were explosively loaded, it was seen that by coating an aluminum thin-walled cylinder with polyurea, significant benefits in the peak acceleration are realized. Referring to the results of the polyurea to steel mass ratio study performed with cantilevered beams, this positive impact of the polyurea coating on the cylinders may come as a surprise. It is seen in Figure 5.14 that a general increase in acceleration is expected as the polyurea to steel mass ratio of a coated beam increases.

In hopes of clarifying this result, a final series of cantilever beam tests were carried out. It was noted that the mass ratios of the beam tests and the cylinder tests were not equivalent with the beams having a polyurea to steel mass ratio in the neighborhood of .08-.15 while the cylinders had a mass ratio anywhere from one to five. To create a more equivalent series of tests, it was necessary to process cantilever beams with a mass ratio in the same neighborhood as that of the cylinders.

These beams were created by cutting the mass of the metal base of the beam by switching the metal from steel to aluminum, and also by decreasing the thickness of the metal from 6.2 millimeters to 3.18 millimeters. An uncoated beam was tested in addition to two beams with mass ratios in the desired range. The test matrix can be seen in Table 6-1. Each beam was tested twice to show data scatter and repeatability.

Table 6-1: Test matrix for similar mass ratio cantilever beam study

Test Number	Beam Number	Beam Thickness (mm)	Beam Mass (g)	Polyurea Thickness (mm)	Polyurea Mass (g)	Beam Length (cm)	Beam Total Mass w/ accel (g)	Polyurea/Steel Mass Ratio
1	1	3.18	54.81	0	0	25.4	65.93	0
2	1	3.18	54.81	0	0	25.4	65.93	0
3	2	3.18	54.81	7.77	48.1	25.4	65.93	0.88
4	2	3.18	54.81	7.77	48.1	25.4	65.93	0.88
5	3	3.18	53	14.01	95.5	25.4	159.3	1.80
6	3	3.18	53	14.01	95.5	25.4	159.3	1.80

6.1.2 Similar Mass Ratio Cantilever Beam Study Test Results

At the conclusion of the tests mentioned in Table 6-1, the same variables plotted in the previous cantilevered beam tests are studied. Namely, peak acceleration, bar velocity, maximum displacement, and half wavelength time are all plotted versus the mass ratio of the cantilevered beam. Two tests are conducted for each beam, and these results are shown in Figure 6.1, Figure 6.2, Figure 6.3, and Figure 6.4.

126
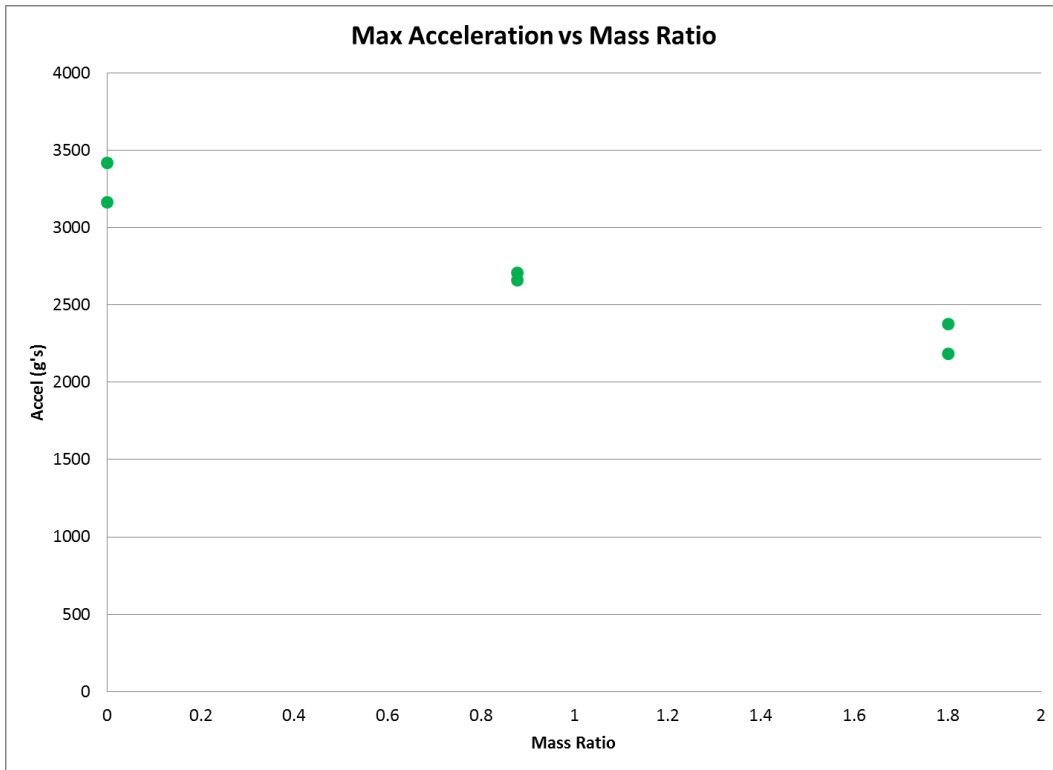
Figure 6.1: Peak acceleration versus mass ratio for aluminum cantilever beam tests
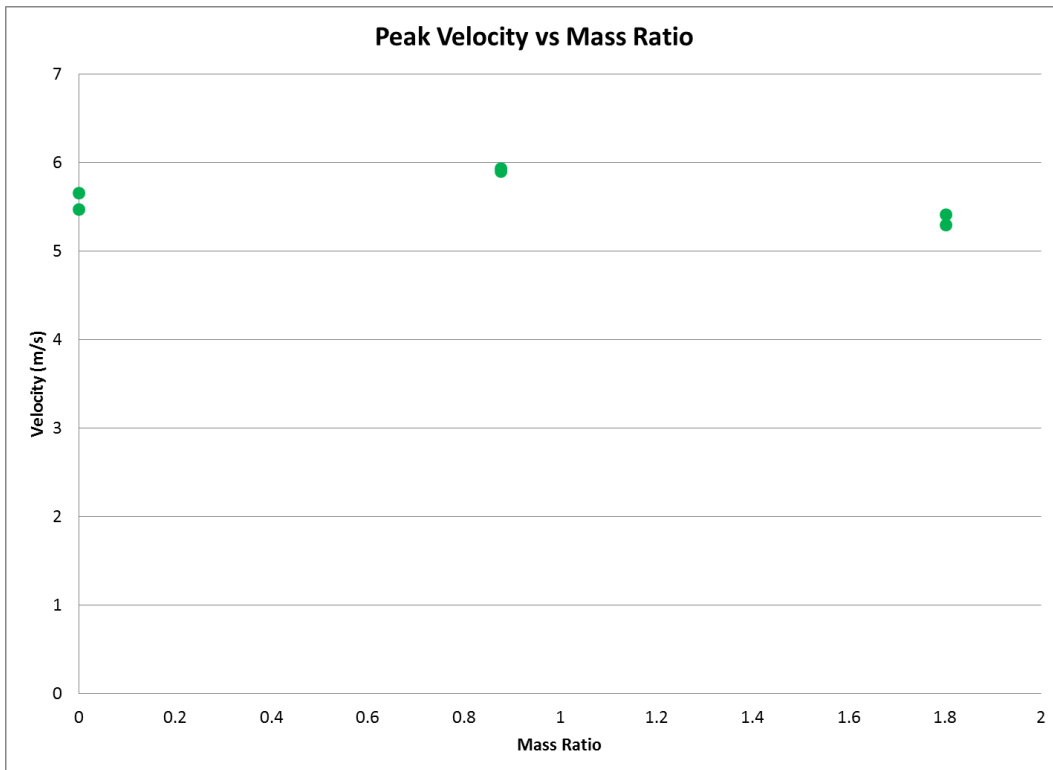
Figure 6.2: Peak velocity versus mass ratio for aluminum cantilever beam tests
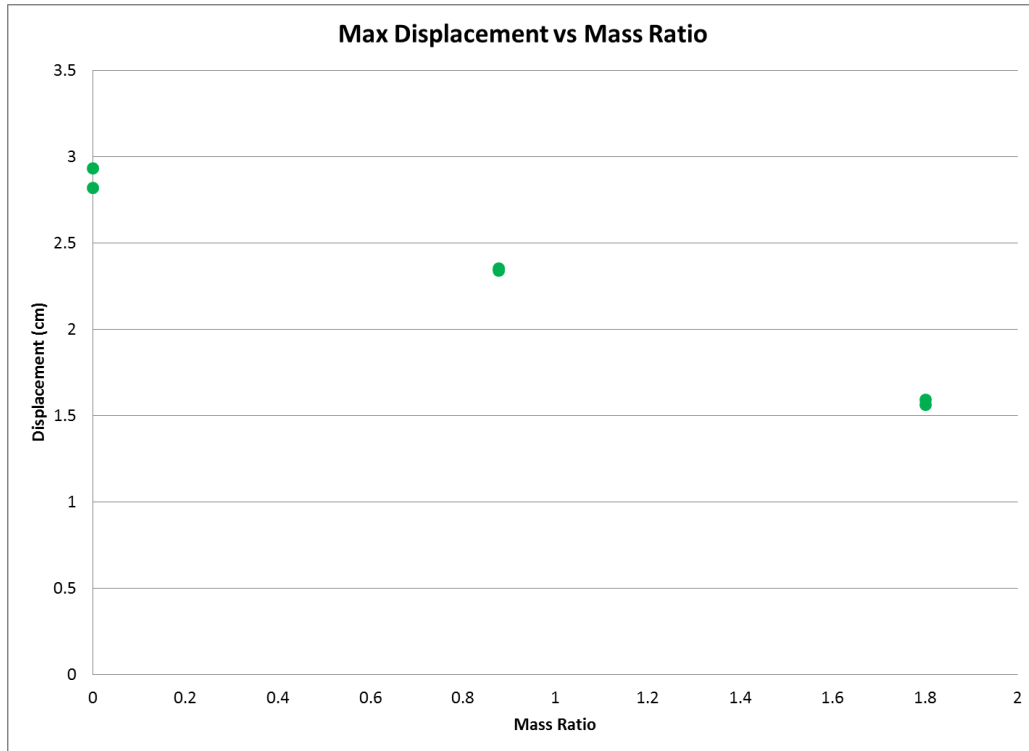
Figure 6.3: Maximum displacement of cantilevered beam versus mass ratio
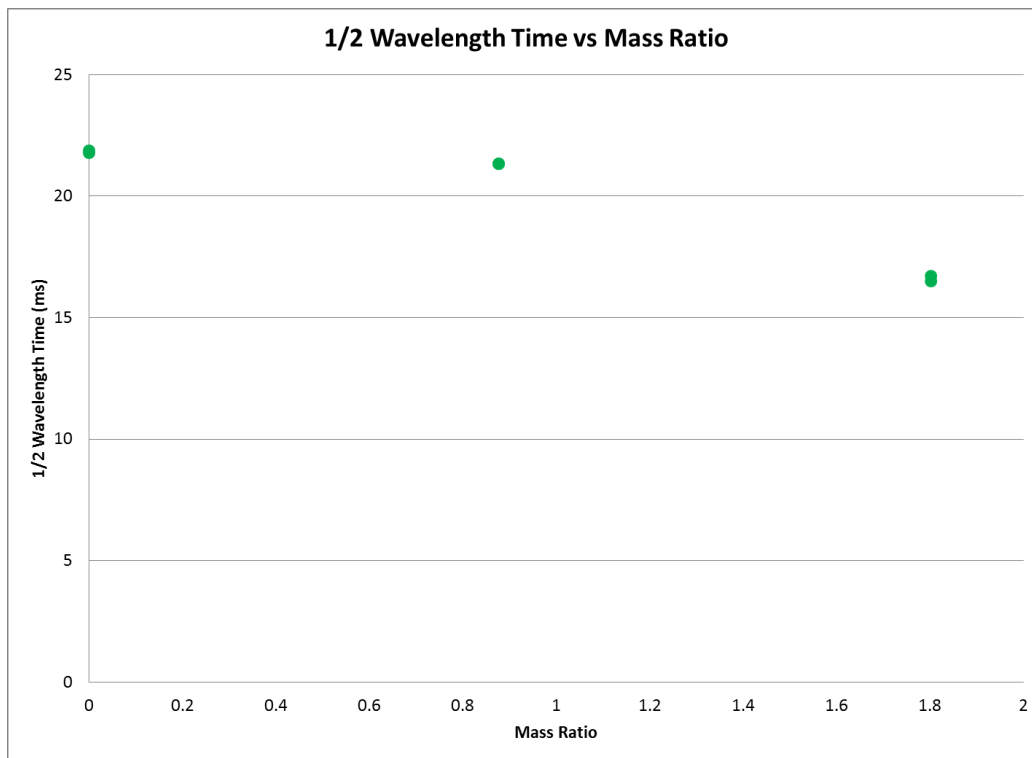
Figure 6.4: Half wavelength time versus mass ratio for aluminum cantilever beam tests

From viewing the previous four figures and comparing them with the trends developed in the steel cantilevered beam tests, it is apparent that a completely different trend has emerged. Whereas the beams with a mass ratio much less than one see increases in the peak acceleration, velocity, displacement, and half wavelength time, the beams with mass ratios greater than one see decreases in the same parameters. The one parameter that does not see dramatic changes is the peak velocity which remains relatively the same. The fact that the velocity remains relatively unchanged is encouraging as the point was made for the thin-walled cylinder tests that though the acceleration of the blast-loaded plate decreased significantly, the impulse and kinetic energy of the frame (both dependent on velocity) remained relatively steady.

It was previously noted that polymeric coatings typically act best as a dampening mechanism when placed under shear. It is also known that the shear stress in a bending beam is minimum at the free surfaces and maximum at the center of mass or neutral axis. By adding significant mass to the aluminum cantilevered beam in the form of polyurea it is suspected that the center of mass may shift closer to, or even inside of, the polymeric layer. By performing some simple geometrical calculations, the re-located center of mass is determined for each of the cantilevered beams tested in all of the studies. The distance to the center of mass (defined from the bottom of the metallic beam) is listed in Table 6-2 along with the distance that the axis has moved off of the original center of mass of the uncoated metal beam.

Table 6-2: Centroid location for all three cantilever beam series of tests

Beam Material	Test Series	Beam Thickness (mm)	Polyurea Thickness (mm)	Polyurea/Metal Mass Ratio	Center of Mass (mm)	Distance from Base Metal Center of Mass (mm)
Steel	General Study	6.22	0.00	0.00	3.11	0.00
Steel	General Study	6.20	0.00	0.00	3.10	0.00
Steel	General Study	6.23	1.58	0.04	3.19	0.07
Steel	General Study	6.20	3.11	0.06	3.24	0.14
Steel	General Study	6.22	4.76	0.07	3.33	0.22
Steel	Mass Ratio Study	5.88	3.49	0.08	3.10	0.16
Steel	Mass Ratio Study	5.68	4.33	0.09	3.04	0.20
Steel	Mass Ratio Study	5.46	5.88	0.14	3.00	0.27
Aluminum	Similar Mass Ratio Study	3.18	0.00	0.00	1.59	0.00
Aluminum	Similar Mass Ratio Study	3.18	7.77	0.88	2.62	1.03
Aluminum	Similar Mass Ratio Study	3.18	14.01	1.80	4.18	2.59

From examining the values in Table 6-2, it is seen that the center of mass does not move appreciably in each of the cases where a steel beam is coated with polyurea. The maximum distance that the center of mass moves on the steel beam is .27 millimeters, which is less than five percent of the total height of the metallic structure. However, when aluminum is used as the metal base and the mass ratio increases to .88, the center of mass shifts to a location of just over .5 millimeters from the aluminum to polyurea transition point. When additional polyurea is applied to the aluminum beam, creating a 1.8 polyurea to metal mass ratio, the center of mass actually moves one millimeter into the polyurea layer. By moving the center of mass significantly closer to the polyurea layer, the polyurea is placed under greater amounts of shear stress and is presumed to provide a more effective means of damping.

To develop a better understanding of how all of the polyurea coating results line up, the acceleration values for each series of tests were normalized by setting the acceleration of the uncoated bar or cylinder as the baseline value, and dividing each acceleration value in the series by the acceleration of each test series' respective

baseline value. By doing this, a plot was developed that directly compares the effect

on acceleration of coating structures in polyurea. This plot is shown in Figure 6.5.
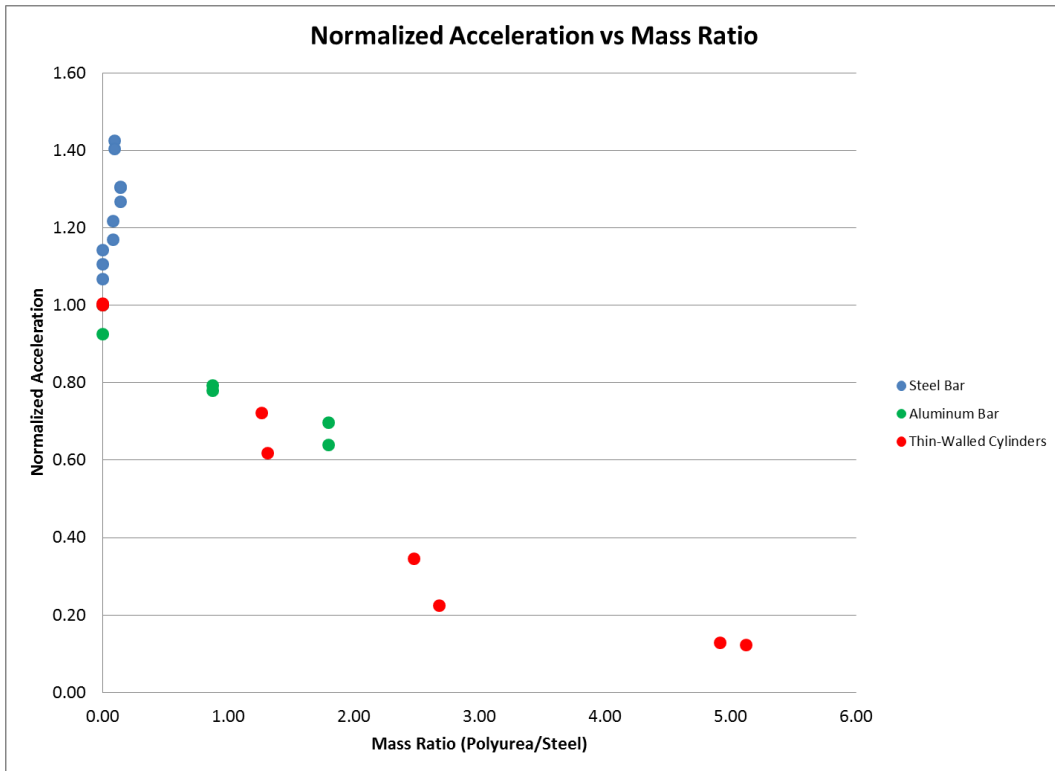
Figure 6.5: Normalized acceleration versus mass ratio for three test series

In Figure 6.5, blue is the cantilevered beam tests conducted with steel bars, the

red represents the thin-walled cylinders which were blast tested, and green shows the

acceleration value of the aluminum cantilevered beams. From this figure, the

conclusion is made that the mass ratio of a coated structure has significant importance

when considering the possibility of the coating to have an effect on peak acceleration

of a structure. Very small mass ratios may indeed have a detrimental, or no, effect on

the ability of a structure to effectively absorb a blast load, while a mass ratio greater

than one has a positive effect. This result is of significant value as steel plates are a

commonly coated material. In order for the coating to have positive effects, an

extremely thick coating would have to be applied. On the other hand, when

considering very light structures, such as the thin-walled cylinders used in this study,

a small amount of polyurea may have a very large effect.

6.2 Polyurea-Coated Thin-Walled Cylinder Tests on a Simulated Vehicle

6.2.1 Polyurea-Coated Thin-Walled Cylinder Test Outline

To conclude the research for this thesis, two tests were run using the simulated

vehicle set-up previously described. The first test involved connecting the hull of the

vehicle to the frame with six aluminum columns. This test served as a "worse-case"

scenario in which there was a rigid connection between the hull and the frame. Each

column was connected to the hull and the frame. A blast test, using a 40 millimeter

SOD and a ten millimeter DOB was performed in the saturated sand test bed

described in the mitigation chapters.

The second and final test performed for this section used six thin-walled

cylinders coated with polyurea as the connecting elements between the hull and the

frame. Each thin-walled cylinder was created with .1millimeter aluminum shim-stock

with a height of 38 millimeters and a 66 millimeter outer diameter. All six cylinders

were coated with three grams of polyurea, resulting in an approximately one to one

polyurea to aluminum mass ratio. The cylinders were connected to both the hull and

the frame so that the cylinders could crush and stretch during the test, maximizing the

amount of acceleration mitigation they have to offer.

As in each of the previous simulated vehicle tests, a 4.4 gram charge is used to

supply the blast load. Two accelerometers are embedded in rubber mechanical

filtering mounts and four targets on the frame are used for high-speed video tracking.

A new hull had to be created for these last two tests due to catastrophic failure of the composite plate used in previous simulated vehicle tests. To create the new plate, two aluminum plates (outer dimensions 9.53 millimeters thick by 30.4 centimeters wide by 45.7 centimeters long) were attached to either the top or the bottom of the same aluminum star brace that was used in the composite hull. Pictures of the two plate set-ups can be seen in Figure 6.6 and Figure 6.7.
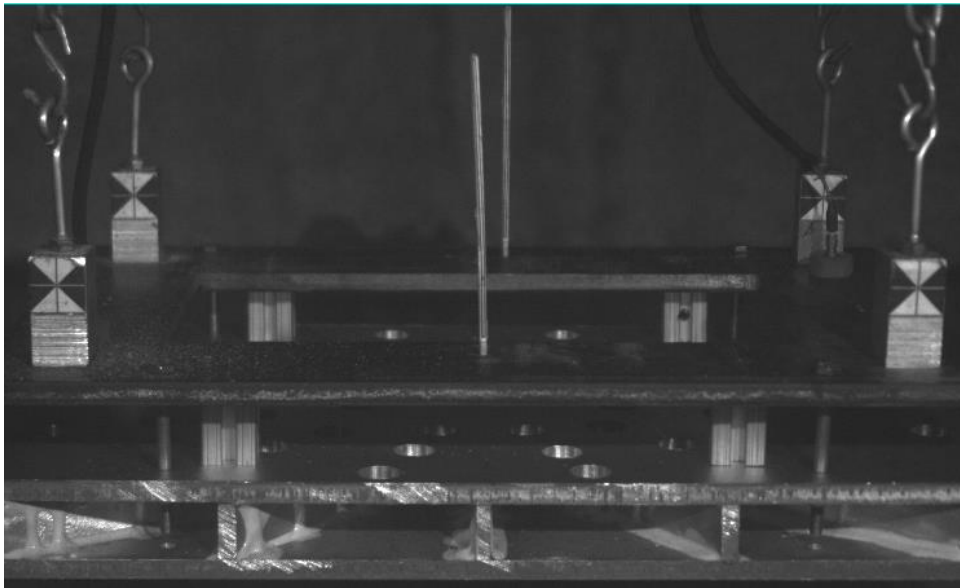
Figure 6.6: Plate set-up for solid column test
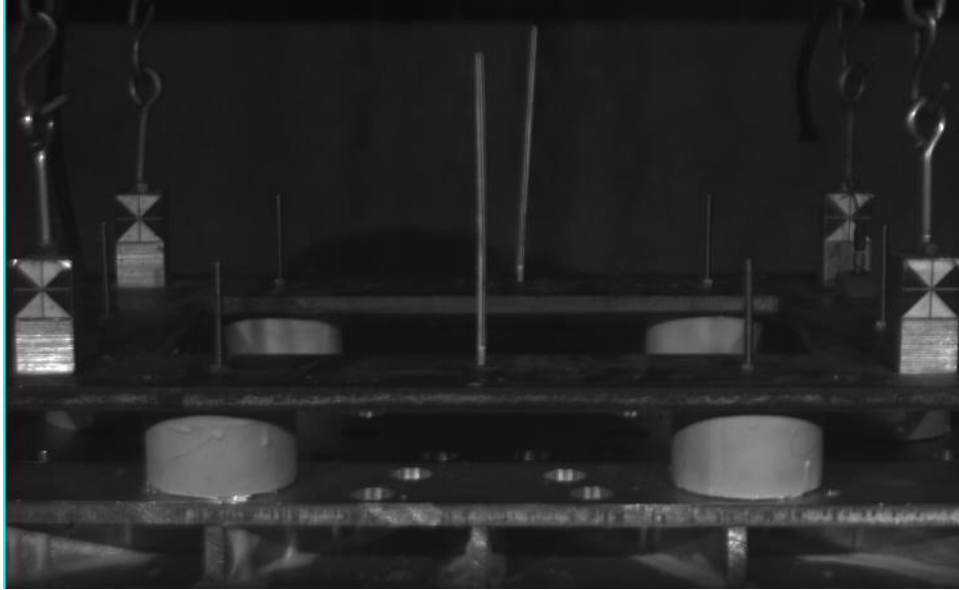
Figure 6.7: Plate set-up for polyurea-coated cylinder test

6.2.2 Polyurea-Coated Thin-Walled Cylinder Test Results

After completing each of the final two tests, the initial data verification steps were taken by comparing the displacement curve developed from the high speed video to the double integrated acceleration signal. In order for the data to have been considered worthy of reporting, the two displacement signals must show strong correlation. An example of the acceleration pulse from the solid column test and its corresponding displacement curve comparison are shown in Figure 6.8 and Figure 6.9.
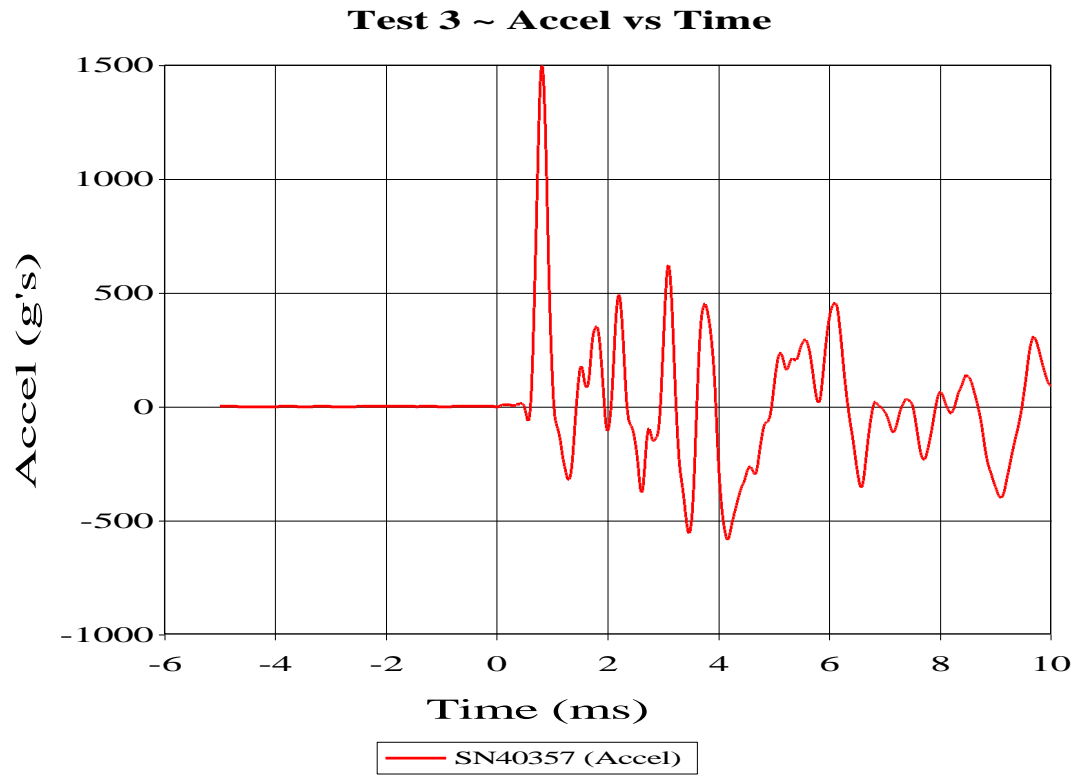
Figure 6.8: Acceleration versus time for non-deforming column attachment test
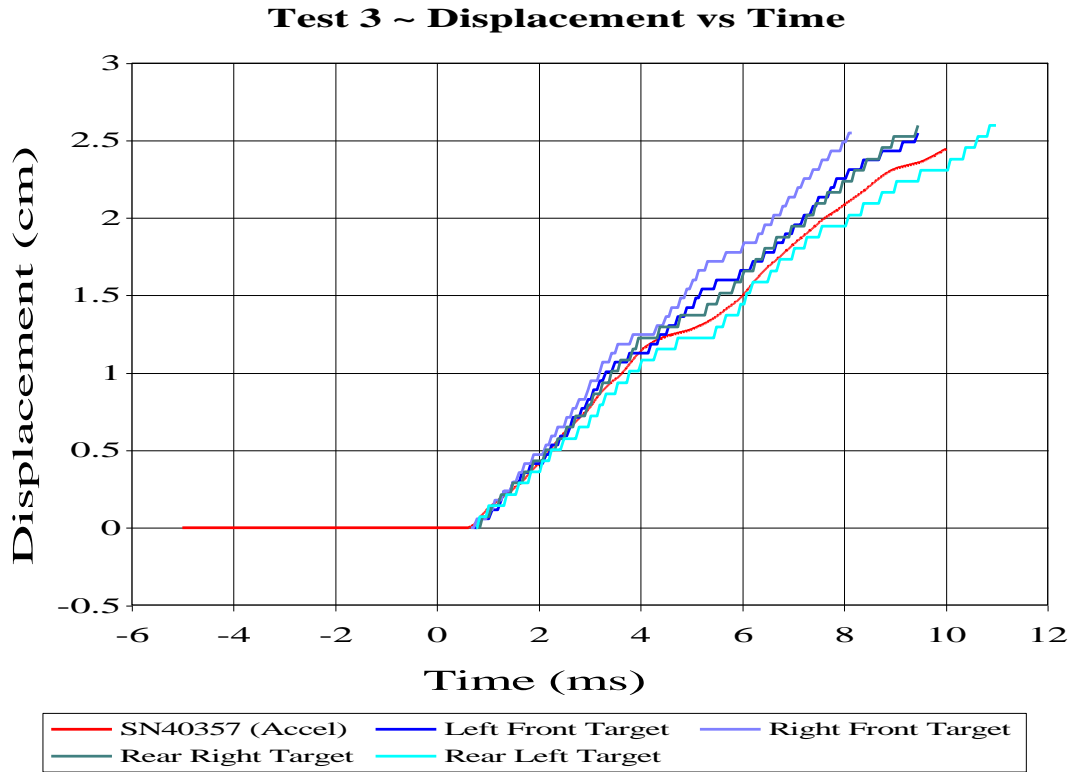
Figure 6.9: Displacement versus time comparison for accelerometer and high speed video data from non-deformable column test

Once the acceleration data has been verified, it is of interest to compare the

two acceleration profiles for each test. To this end, the acceleration profile was taken

from the same accelerometer for each of the two tests and plotted on the same graph.

The comparison between the non-deforming column test and the polyurea-coated

thin-walled cylinder test is shown in Figure 6.10.

Acceleration vs Time Comparison
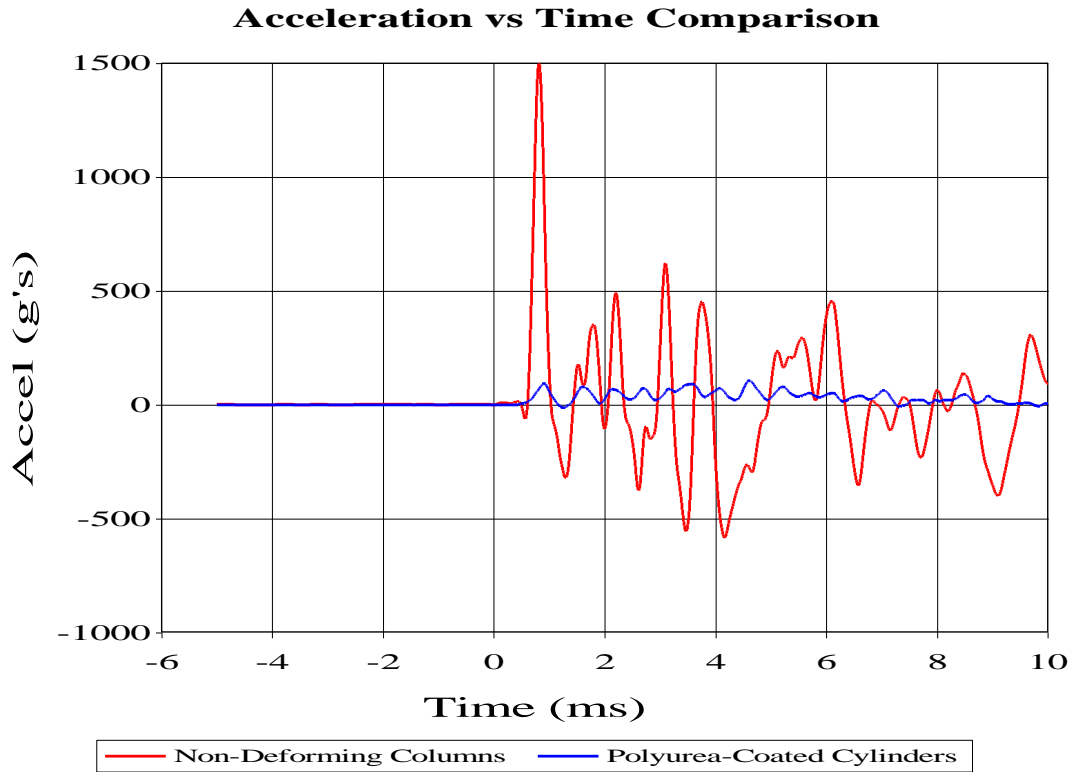
Figure 6.10: Acceleration versus time comparison for non-deforming columns and polyurea-coated cylinders

It is evident from viewing Figure 6.10 that an immense benefit comes from using thin-walled cylinders as a mitigation technique. This information however was already known from previous tests. Perhaps a more telling comparison can be made by studying how the acceleration, impulse, and kinetic energy of the simulated vehicle frame compare between the coated and uncoated cylinder tests. To perform this comparison, it is necessary to view a number of test results as a test with the cylinder number and geometry of the final test was not conducted previously in the mitigation study. As such, the information in Table 6-3 is presented so that a better understanding of the material may be obtained.

Table 6-3: Comparable test results for numerous simulated vehicle test studies

Connection Method	Number of Elements	HOT (mm)	Hull Attached	Frame Attached	Acceleration (g's)	Impulse (N-s)	Kinetic Energy (J)
Air	-	38	-	-	1458	70.56	178.00
Aluminum Cylinder	4	38	Yes	No	121.5	58.01	118.48
Aluminum Cylinder	4	38	Yes	Yes	89	51.27	89.40
Aluminum Cylinder	6	25	Yes	No	141.5	55.02	102.61
Solid Columns	6	38	Yes	Yes	1641	76.24	181.64
Coated Cylinder	6	38	Yes	Yes	108	52.96	87.65

Studying Table 6-3, a number of observations are made. Initially it is seen that by substituting non-deforming columns in the place of air as the material in between the hull and the frame, comparable values in terms of acceleration, impulse, and kinetic energy result. Moving beyond these baseline comparisons, it is noted that while the polyurea coated cylinders perform admirably with extremely low acceleration and decreased impulse and kinetic energy values, the drastic drop from the bare cylinder case is not realized. According to the tests conducted with the reduced circular plates, a 20-40 percent drop in acceleration should have occurred between the bare cylinder and the coated cylinder tests.

While slightly unexpected, the above results are not discouraging for a couple of reasons. The first reason for enthusiasm with regards to polyurea coated cylinders is due to the fact that while the bare aluminum thin-walled cylinders crushed completely during the blast tests (see Figure 4.17), the polyurea coated cylinders crushed approximately one-half of their height during the initial blast, and recovered over 90 percent of their initial height by the end of the blast event (see Figure 6.11). The relatively small initial deformation will be treated later, but at this point, the fact that the polyurea coated cylinders recover such a large percentage of their initial shape may result in a vehicle that is structurally able to drive away from a blast event.
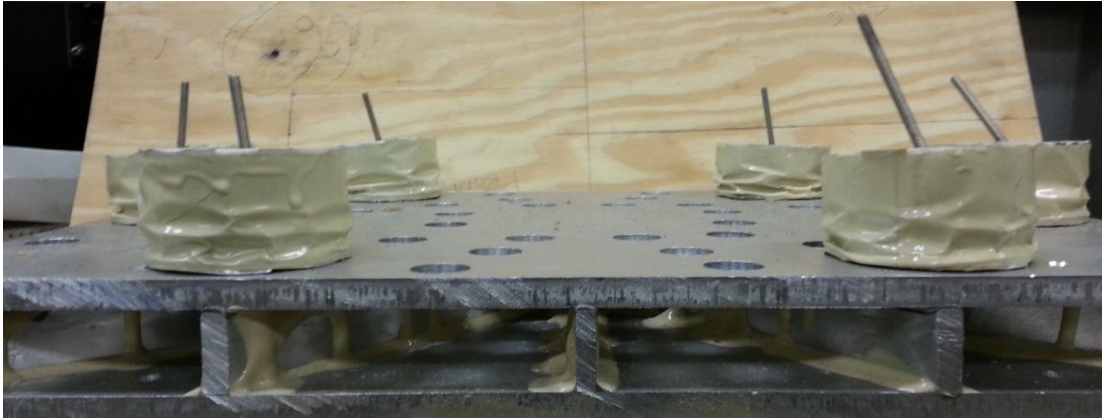
Figure 6.11: Recovered height of the polyurea-coated cylinders after blast testing

Looking at Figure 6.11, it is clearly seen that deformation of the coated cylinder occurs primarily at the lower half of the cylinder. This fact will be used in conjunction with information from the small circular plate tests to realize a further advantage of using polyurea coated cylinders as opposed to bare aluminum cylinders as a mitigation technique. The statement that needs to be made about the coated cylinder tests using the reduced-sized circular plates is that the acceleration of the baseline (uncoated cylinder) tests was dramatically greater than that of the simulated vehicle baseline (uncoated cylinder) tests. Comparing acceleration values from Figure 5.33 and Table 6-3, it is seen that the acceleration of the bare cylinder test using the circular plates and a single cylinder is in the neighborhood of 3500g's while the acceleration using bare cylinders on the simulated vehicle plates lies in the area of 100-150g's.

The increased level of loading of the smaller plates is backed up by the high speed video, in which the polyurea coated cylinders crush completely before recovering some of their height. In the case of the simulated vehicle tests, it was pointed out that the cylinders crush only partially before recovering almost all of their height. It was initially curious that a 20-40 percent acceleration drop between

uncoated and coated cans did not appear in the simulated vehicle test. However, after looking at the data in its entirety, it is not that surprising, as the acceleration levels in the simulated vehicle using bare cylinders might not be sufficient to bring out the full benefit of coating the cylinder with polyurea.

In that last statement sits a pretty powerful implication. Each of the blast tests employing a simulated vehicle was tested using a specific set of test conditions. Specifically, each test was performed in saturated sand with a 4.4 gram charge using a ten millimeter DOB and a 40 millimeter SOD. These test conditions represent a tiny fraction of the conditions experienced by a vehicle that may experience a blast event in the field. Any number of these conditions may be different in practice resulting in an explosive event more violent than those tested in this research. If a polyurea coated thin-walled cylinder may be used to mitigate acceleration to the same effect as an uncoated cylinder while undergoing a fraction of the deformation; it stands to reason that the for an explosive event in which the uncoated cylinder is over-loaded and consequently does not adequately mitigate the acceleration, a polyurea coated cylinder may act to adequately protect the inhabitants of the vehicle. Another way of viewing the above information is this – at low levels of acceleration, uncoated and coated cylinders mitigate acceleration to the same degree, it is only at high levels of acceleration that the full benefit of coating a thin-walled cylinder with polyurea may reveal itself.

6.3 Concluding Tests Summary

Hoping to shed light on why the cantilever polyurea coated steel beams behaved differently than the coated cylinders, cantilever beam tests were conducted

on polyurea coated aluminum beams with a polyurea to aluminum mass ratio in the same region as the coated cylinder tests. Upon performing these tests it was seen that the acceleration of the beam tip and the frame of the target plate using polyurea coated cylinders each decline in a similar fashion as the mass ratio increases. As in the coated cylinder case, the velocity of the tip of the coated cantilever beam does not change appreciably when the mass ratio increases. The conclusion was made that in order for the polyurea to have any positive effect in terms of acceleration mitigation, the mass ratio of polyurea to metal must be in the appropriate range.

To wrap up the research, two tests were conducted comparing a blast test using a simulated vehicle with a rigid column connection between the hull and the frame to a test where the hull and frame were connected by six polyurea coated thin-walled cylinders. While the acceleration of the mitigation test showed a drastic improvement over the rigid connection, the decline in acceleration that was expected did not occur. Examining the coated cylinder test further, it was noted that the deformation of the cylinder was much less than expected as well. Due to this fact in conjunction with viewing the acceleration levels from appropriate tests, it is hypothesized that a polyurea coated cylinder mitigates acceleration non-linearly, and that greater levels of mitigation may be realized at higher values of acceleration.

Chapter 7 – Overall Conclusions and Future Work

7.1 Conclusions

At the outset of this research program a couple of broad goals were laid out. Initially it was desired to develop an effective means of acceleration mitigation for use on explosively loaded vehicles. To achieve these goals, small-scale explosive testing was conducted in saturated sand. Simulated vehicles and more simply shaped plate combinations were utilized to study the effects of various mitigation techniques.

It was shown in this paper that acceleration levels, reported at full-scale values, can be decreased from 150 g's to levels around 10 g's by application of thin-walled cylinders alone. With the addition of a polyurea coating to the thin-walled cylinders, at very high acceleration levels, an 80-90 percent decrease in acceleration may also obtained. Furthermore, numerous geometric properties of thin-walled cylinders were experimented with showing marginal differences to the baseline acceleration mitigation. It is believed that some combination of all of the best-case scenarios for each geometric condition, in addition to a polyurea coating, applied to the cylinders would result in a mitigation technique that would allow for complete survivability of an explosive event.

It was also shown that significant improvements in impulse and kinetic energy may also be made through the use of thin-walled cylinders. Previous research has been conducted in the Dynamic Effects Lab that used shaped hulls to decrease impulse on simulated vehicles to safe levels. In addition to using shaped hulls, the thin-walled cylinders may give further aid in preventing impulse related injuries to passengers in blast-loaded vehicles.

It was also desired that a greater understanding of the effects of polyurea applied to structures be developed. Some basic research was performed through the use of polyurea coated steel and aluminum cantilever beams. The cantilever beams were tested dynamically through the use of a high-pressure gas gun, and produced information leading to the following conclusion; that in the elastic range of material response to dynamic loading, bare steel has lower levels of acceleration, velocity, peak displacement, and half-wavelength time than steel bars coated with a thin layer of polyurea. For the beneficial effects of polyurea coatings to appear, the mass ratio of polyurea to metal must be increased to the order of magnitude of one or higher. It was found that at higher mass ratios, the acceleration of cantilever beams and explosively loaded plates both show similar decreasing trends as the mass ratio of the polyurea to metal increases.

Finally, a very important conclusion was made with regard to coating thin-walled cylinders with polyurea. It was seen that at low acceleration levels, polyurea coated and uncoated cylinders both mitigate acceleration equally well even if the deformation of the coated cylinder was significantly less. This minimal deformation would result in a vehicle being structurally sound enough to drive away from an explosive event. In addition to this powerful fact, the data from a multitude of tests was used to logically come to the conclusion that as the explosive event becomes more violent, the polyurea coated cylinders can be expected to act to mitigate more of the acceleration.

7.2 Suggested Future Work

143

Throughout the course of the research, certain issues arose that were unable to be resolved in this paper. The first of these issues was highlighted by looking at the acceleration signals in the small-scale vehicle testing. It was noted that what appeared to be low-frequency plate vibration resulted in a high acceleration reading following the initial acceleration peak. How much of the peak acceleration resulted from frame vibration remains an area of interest.

Additionally, only cylindrical shapes were tested as a mitigation technique. It might be of some interest to determine if other geometric shapes might be able to offer similar or supplementary benefits to acceleration mitigation. Tube buckling was also identified in the preliminary tests as a promising means for acceleration mitigation. Buckling tubes as a stand-alone source for mitigation or as a combination to the crushing thin-walled cylinders might also warrant further study.

Finally, the tests for the mitigation were run at a single set of test conditions. It would be beneficial to develop a better understanding whether the mitigation techniques developed in this paper would prove as effective for a wide array of test variables such as depth of burial, stand-off distance, ejected media, and charge size. If shown that the mitigation of acceleration has a strong dependency on the previously mentioned variables, a study to optimize the thin-walled cylinder design could be undertaken.

Bibliography

[1]   Fiskum, G., Hazelton, J., Gullapalli, R., Fourney, W.L. "Animal Model of Mild Brain Injury Caused by Blast-Induced Hyper-Acceleration Relevant to IED-Targeted Military Vehicles."

[2]   Nelson, N.W., Lamberty, G.J., Sim, A.H., Doane, B.M. "Blast from the Past and Present: A Review of Blast-Related Injury in Military Personnel and Veterans." *Neuropsychological Practice with Veterans* (2012): 145.

[3]   Fourney, W. L., Leiste, U., Bonenberger, R., Goodings, D. J. "Mechanism of Loading on Plates Due to Explosive Detonation." Fragblast, Vol. 9, No. 4, December 2005.

[4]   Genson, K. (2006). "Vehicle Shaping for Mine Blast Damage Reduction." University of Maryland: College Park.

[5]   Benedetti, R., Fourney, W.L. (2010) "Mitigation of Loading on Floorboards in Light Armored Vehicles Subjected to Explosive Loading." University of Maryland: College Park.

[6]   Leiste, U. (2012). "Experimental Studies to Investigate Pressure Loading on Target Plates." University of Maryland: College Park.

[7]   Lamb, C., Schmidt, M., Fitzsimmons, B. "MRAPS, Irregular Warfare, and Pentagon Reform." Institute for National Strategic Studies National Defense University. Volume 6, June 2009.

[8]   Alghamdi, A.A.A. "Collapsible Impact Energy Absorbers: An Overview." Thin Walled Structures, Vol. 39, No. 2, February 2001.

[9]   Yuen, S.C., Nurick, G.N. "The Energy-Absorbing Characteristics of Tubular Structures with Geometric and Material Modifications: An Overview." Applied Mechanics, Vol. 69, No. 2, March 2008.

[10]   Gupta, N.K., Sekhon, G.S., Gupta, P.K. "Study of lateral compression of round metallic tubes." Thin Walled Structures, Vol. 43, No. 6, December 2005.

[11]   Shim, V.P.W, Stronge, W.J. "Lateral crushing in tightly packed arrays of thin-walled metal tubes." International Journal of Mechanical Science, Vol. 28, No. 10, June 1986.

[12]   Gupta, N.K., Velmurugan, R. "An analysis of axial crushing of composite tubes." Journal of Composite Materials, Vol. 31, No. 13, July 1997.

[13]   Palanivelu, S., Paepegem, W.V., Degrieck, J., Vantomme, J., Kakogiannis, D., Ackeren, J.V., Hemelrijck, D.V., Wastiels, J. "Comparison of the crushing performance of hollow and foam-filled small-scale composite tubes with different geometrical shapes for use in sacrificial cladding structures." Composites Part B: Engineering, Vol. 41, No. 6, September 2010.

[14]   Palanivelu, S., Van Paepegem, W., Degrieck, J., Van Ackeren, J., Kakogiannis, D., Van Hemelrijck, D., Wastiels, J., Vantomme, J. "Experimental study on the axial crushing behavior of pultruded composite tubes." Polymer Testing, Vol. 29, No. 2, April 2010.

[15]   Palanivelu, S., Van Paepegem, W., Degrieck, J., Reymen, B., Ndambi, J.M., Vantomme, J., Kakogiannis, D., Wastiels, J., Hemelrijck, D.V. "Close-range blast loading on empty recyclable metal beverage cans for use in sacrificial cladding structure." Engineering Structures, Vol. 33, No. 6, June 2011.

[16]   Theobald, M.D., Nurick, G.N. "Numerical investigation of the response of sandwich-type panels using thin-walled tubes subject to blast loads." International Journal of Impact Engineering. Vol. 34, No.1, January 2007.

[17]   Theobald, M.D., Nurick, G.N. "Experimental and numerical analysis of tube-core claddings under blast loads." International Journal of Impact Engineering. Vol. 37, No.3, March 2010.

[18]   Yi, J., Boyce, M.C., Lee, G.F., Balizer, E. "Large deformation rate-dependent stress-strain behavior of polyurea and polyurethanes." Polymer, Vol. 47, No.1, January 2006.

[19]   Roland, C.M., Twigg, J.N., Vu, Y., Mott, P.H. "High Strain Rate Mechanical Behavior of Polyurea." Polymer, Vol. 48, No.2, January 2007.

[20]   Tekalur, S.A., Shukla, A, Shivakumar, K. "Blast resistance of polyurea based layered composite materials." Composite Structures, Vol. 84, No.3, July 2008.

[21]   Ackland, K., Anderson, C., Ngo, T.D. "Deformation of Polyurea-Coated Steel Plates under Localized Blast Loading." Impact Engineering, Vol. 51, January 2013.

[22]   Brodrick, T.J. "Mitigation of Frame Acceleration Induced by a Buried Charge." Diss. 2010.

[23] Fourney, W. L., Leiste, U., Bonenberger, R., Goodings, D. J. "Explosive Impulse on Plates." Fragblast, Vol. 9, No. 1, December 2005.

[24] Taylor, L.C., Skaggs, R.R., Gault, W. "Vertical Impulse Measurement of Mines Buried in Saturated Sand." Fragblast, Vol. 9, No.1, March 2005.

[25] PCB Piezotronics, Shock ICP Model: 350B04. (2013). Retrieved August 20, 2013 from <http://www.pcb.com/products.aspx?m=350B04#.UhOiuZLVAsI>

[26] RP-501 Economy EBW Detonator. (2011). Retrieved August 20, 2013 from <http://www.teledynerisi.com/products/0products_1ebw_page28.asp>

[27] HM-VK Ultra high strength handmix polyurea elastomer. (2013). Retrieved August 26, 2013 from <http://www.specialty-products.com/pdf/tech-data/polyurea/HM-VK%20Preliminary.pdf>

[28] Plunkett, R. Lee, C.T. (1968) "Length Optimization for Constrained Viscoelastic Layer Damping." Minnesota University Minneapolis Department of Aeronautics and Engineering Mechanics: Minneapolis.